REMOTE SENSING BASED COAL FIRE STUDIES IN JHARIA COALFIELD, INDIA

Ph.D. THESIS

by

ASHWANI RAJU

DEPARTMENT OF EARTH SCIENCES
INDIAN INSTITUTE OF TECHNOLOGY ROORKEE
ROORKEE-247667 (INDIA)

MAY, 2015

REMOTE SENSING BASED COAL FIRE STUDIES IN JHARIA COALFIELD, INDIA

A THESIS

Submitted in partial fulfilment of the requirements for the award of the degree

of

DOCTOR OF PHILOSOPHY

in

DEPARTMENT OF EARTH SCIENCES

by

ASHWANI RAJU

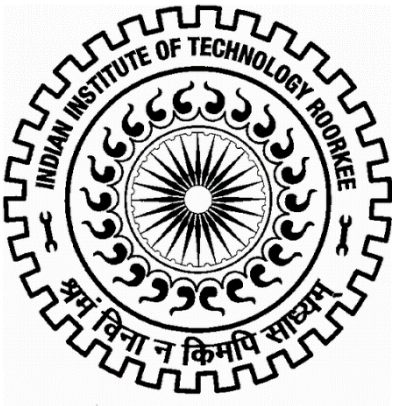

DEPARTMENT OF EARTH SCIENCES
INDIAN INSTITUTE OF TECHNOLOGY ROORKEE
ROORKEE-247667 (INDIA)

MAY, 2015

INDIAN INSTITUTE OF TECHNOLOGY ROORKEE
ROORKEE

CANDIDATE'S DECLARATION

I hereby certify that the work, which is being presented in the thesis entitled "**REMOTE SENSING BASED COAL FIRE STUDIES IN JHARIA COALFIELD, INDIA**" in partial fulfillment of the requirements for the award of the degree of Doctor of Philosophy and submitted in the Department of Earth Sciences, Indian Institute of Technology Roorkee, Roorkee, is an authentic record of my own work carried out during a period from July, 2009 to May, 2015 under the supervision of Dr. Pitambar Pati, Assistant Professor, Department of Earth Sciences, Indian Institute of Technology Roorkee.

The matter presented in this thesis has not been submitted by me for the award of any other degree of this or any other institute.

(ASHWANI RAJU)

This is to certify that the above statement made by the candidate is correct to the best of my knowledge.

(Pitambar Pati)
Supervisor

Date: 15th May, 2015

ACKNOWLEDGEMENTS

This thesis is the success of my endeavors that could have not been possible without the encouragement and support of my sympathizers. As a student, it was always pleasure for me to study in one of the finest technical institute of India. I am thankful to the administration of the Institute and Department of Earth Sciences for providing me an opportunity to study in IIT Roorkee. I appreciate the efforts of all those people who have made this thesis possible. Their efforts cannot be expressed in words but perhaps this attempt may extend my gratitude toward them.

Foremost, I would like to express my profound gratitude to my supervisor Dr. Pitambar Pati, Assistant Professor, Department of Earth Sciences, IIT Roorkee for providing his sound advice and unconditional help. I deeply appreciate his efforts for editing my thesis writing, and his immense support and critical reviews of my observations. I am fortunate to have him as a guide who support and helped me to overcome many crisis situations.

I also offer my sincere thanks to Dr. R. P. Gupta, Professor (Retd.), Department of Earth Sciences, IIT Roorkee who provided their precious guidance, valuable support, timely suggestions and necessary infrastructures for this research. Despite his busy schedule, he was always there for necessary discussions and direction. I am also grateful to him for his vigilant supervision through critical reviews, which was necessary during the different stages of my research. I am deeply grateful to Dr. Anupma Prakash, Professor, Geophysical Institute, Fairbanks, Alaska for the long discussions on practical issues and technical advices that helped me to understand my research area better.

I am also very grateful to Dr. G. J. Chakrapani, Professor, Department of Earth Sciences, IIT Roorkee (former Chairman, SRC/DRC), Dr. A. K. Sen, Professor, Department of Earth Sciences, IIT Roorkee (Internal expert) and Dr. Sudhir Kumar, Scientist-F, NIH, Roorkee (External Expert) for their immense support, critical reviews and valuable suggestions during the progress of this work.

I would like to acknowledge course coordinators Dr. M. K. Arora, Professors, Department of Civil Engineering, IIT Roorkee, Dr. P. K. Garg, Professors, Department of Civil Engineering, IIT Roorkee and Dr. A. K. Saraf, Professor, Department of Earth Sciences, IIT

Roorkee for their lectures on related topics that helped me to improve my knowledge in the field of remote sensing.

I warmly appreciate the generosity and the support given by Dr. S. P. Gupta, Deputy Director, IIT Roorkee at the time when I was at the crucial stage of my research. I will always be indebted to him for his kind help without which the existence of this research wasn't possible.

I am grateful to Dr. V. K. Singh, Head, Mine Fire Division, Central Institute of Mining and Fuel Research (CIMFR) and his staff for providing necessary support and guidance during field work in Jharia, Dhanbad. I would like to express my gratitude toward my organization, Geological Survey of India, for giving me permission to complete my research in part-time schedule. I am also thankful to Council of Scientific and Industrial Research (CSIR) for providing financial support to my research.

During my stay in IIT, I have got some very good friends to whom I am always indebted for help and belief in me. I deeply appreciate the help and support given by Ms. Anjali Singh, Research Scholar, Department of Earth Sciences, IIT Roorkee at every stage of completion of this work. I greatly appraise her friendship and owe my gratitude to her for motivational support. I also thank my fellow labmate Mr. Arvind Kumar Singh who have always helped me like my elder brother. I would like to acknowledge my colleagues Mr. Mohd Tabish Ansari, Mr. Narpat Singh Solanki and Mr. Rajendra Kumar of Geological Survey of India for the many valuable discussions and encouragement.

I am also grateful to Nair ji, Surendra and Sarvesh Ji for their administrative support. Their caring and familiar behavior always felt me like staying in home. I am thankful to the staff of IIT Roorkee and CIMFR, Dhanbad for their hospitality.

Last but not the least, this work would not have been possible without the patience and support of my family. I would like to my express my heart-felt gratitude to my mother and father, who were always there to encourage me with love and immense support. Finally, I thank to the almighty that provided strength and true spirit in me.

ABSTRACT

Jharia Coalfield (JCF) is known for one of the densest congregations of surface-subsurface coal fires in the world. It has witnessed numerous severe accidents and continuous loss of valuable coal reserves due to uncontrolled coal fires. Coal fire affected areas are often inaccessible and here can be precisely investigated by remote sensing techniques. In the present study, suitable methods for mapping and monitoring of coal fires have been developed and surface-subsurface coal fires have been systematically analyzed. The attempts made here are mainly emphasized on developing a novel approach for thresholding and mapping of surface coal fires, and monitoring spatial dynamics of coal fires in JCF through time and space.

Surface-subsurface coal fires are the typical characteristic of a coal mine area. Surface fires are common in coalfields where coal is exposed to sunlight for long durations of time. The heat energy emitted from these fires affects the signal recorded by sensors operating in the shortwave infrared regions of the electromagnetic spectrum. The Landsat TM/ETM+ band-7 is sensitive to solar reflected as well as emitted radiations from a target. The 'maximum solar reflection threshold' method proposed in this study uses the highest spectral radiance that can be attributed to solar reflection as the conservative threshold to segregate the pixels with emitted component from those with reflected component of the EM energy. Investigations with Landsat TM/ETM+ data indicate a reflectance value of 0.23-0.25 as the most representative highest reflectance (threshold) in coal mining areas. The method apparently has the advantage as it is based on the reflectance characteristics of materials (sandstone-shale mixtures) typically found in coal mining areas and is applicable in wide range of geographical setting.

To facilitate sustainable mining for industrial growth, temporal monitoring of coal fires has to be executed at regular interval. In the present approach, two ratio indices namely; 'Normalized Difference Coal Index (NDCI)' and 'Normalized Difference Coal-fire Index (NDCfI)' have been proposed to systematically map the coal seam fires using Advance Spaceborne Thermal Emission and Reflection Radiometer (ASTER). The adopted methodology has been implemented in Jharia Coalfield. Statistical thresholding of indices precisely segregate the pixels attributed to surface coal fires (high intensity coal seam surface fire and low intensity smoldering surface fire) and shows that the surface coal fires closely follow the pattern of the excavated coal seams. Surface fires are distributed mainly in the eastern and south-eastern part of the study area with a cumulative coverage of 3.93 km^2. Reliability of the obtained results has

been validated by computing an error matrix with overall accuracy of 87.7%. The adopted methodology precisely localized the surface coal fire affected areas and closely represents the actual scenario of surface coal fires in JCF. Beside its conservative and robust nature, the method introduced here is rapidly practicable and allows quick retrieval of surface coal fires.

Systematic investigation of actual scenario of coal fire is always been a critical issue for coal fire research community. ASTER provides data at high temporal and radiometric quantization level, and is unique in its ability to monitor the fluctuation in spatial extent of coal fire. Time series analysis of three consecutive sets of ASTER data evaluates the spatial dynamics and trend of coal fires propagation in Jharia.

Results indicated that the magnitude of coal fires in JCF have been fluctuated with time from 2000 to 2009. The area located around the Shatabdi opencast, Barora, Sijua opencast, Godhar colliery, Kusunda, Bokapahari, Kujama and Lodna are under intense coal fire. From 2000 to 2004, spatial extent of coal fire has shown a minor decrease of 6.74% and then shows a substantial increase of 11.93% between 2004 and 2009.

Coal fires are quite persistent in western part of the JCF from 2000 to 2004. However, between 2004 and 2009, considerable decrease of 1.157 km^2 of fire has been noticed in west and east Barora, Block II Project and Govindpur collieries located in western most part of the JCF.

It has been noticed that the west-central part of the JCF comprising Katras, Sijua, Western Jharia-II and Kusunda collieries are most affected. Since 2004, spatial extent of the fire exclusively in Kusunda colliery is increased by 1.122 km^2. This remarkable increase in spatial extent fire is due to the appearance of new surface fire site located south of Kusunda and north of Alkusha in 2009.

In south-eastern part of the JCF, fire is quite persistent from 2004 to 2009. However, minor increases in Kustor, Bastacolla and Lodna collieries have been noticed from 2004 to 2009.

Surface fires in JCF are highly sporadic and exhibits minor fluctuation in spatial extent between 2000 and 2008. It has increased by 8.6% since 2000 to 2004 and then decreased by 14.66% from 2004 to 2008, respectively. The increase in fire extent in 2008 has been marked by appearance of two new surface fires sites noticed near Kantapahari, in Katras colliery and north of Alkusha quarry in Katras colliery.

To evaluate the propagation of fire in JCF, coal fire maps of three consecutive years have been interpreted together with structural map on GIS platform. Systematic analysis of the obtained results reveals that the movement of fire is structurally controlled. Propagation of the fire has been well noticed in Kustor, Bastacolla and Lodna collieries. Fire appears to be moving toward Jharia. In 2009, it has been observed that the fire located east of Jharia, near Bokapahari (in Bastacolla colliery) is propagating towards NNW and fire located Jiyalgarh, Lodna is propagating northerly toward Jharia (in Lodna colliery). While fires located near Bokapahari and SE of Alkusha (in Kustor colliery) are propagating in south and SE direction heading toward Jharia. Both these fires have been observed to be moving along the strike of coal seam. Fire located SE of Alkusha (in Kustor colliery) may also under control of two NW-SE trending faults causing propagation of fire toward south and SE.

Coal fires in JCF causes tons of coal loss by burning and actively contributed to the instability in the area from safety point of view. Problem of coal fire in Jharia has long back history and is still persisting. Local villages and inhabitants lying in the vicinity of Jharia township are on the verge of major devastation. Status of the fire is demanding some firm measures to control them. Systematic investigations of coal fires are essentially required to facilitate plan sustainable mining and safety measurements for industrial growth on long term basis in Jharia.

TABLE OF CONTENTS

LIST OF TABLES

LIST OF FIGURES

LIST OF SYMBOLS AND ABBREVIATIONS

ASTER	Advanced Spaceborne Thermal Emission and Reflection Radiometer
BIRD	Bi-spectral Infra-Red Detection
CH_4	Methane
CIL	Coal India Limited
CIR	Color Infra-Red
CO	Carbon Monoxide
CO_2	Carbon Di-oxide
DEM	Digital Elevation Model
DN	Digital Number
EM	Electro Magnetic
ESE	East of South-East
ETM+	Enhanced Thematic Mapper Plus
FCC	False Color Composite
GDEM	Global Digital Elevation Model
GIS	Geographical Information System
GloVis	USGS Global Visualization Viewer
GPS	Global Positioning System
HDF	Hierarchical Data Format
IISCO	Indian Iron & Steel Company
ISAC	In-Scene Atmospheric Compensation
JCF	Jharia Coalfield
K	Kelvin
L1G	Level-1 G
LP DAAC	Land Processes Distributed Active Archive Center
LST	Land Surface Temperature
LULC	land-use/land-cover
MODIS	Moderate Resolution Imaging Spectro-radiometer
NASA	National Aeronautics Space Administration
NDCfI	Normalized Difference Coal fire Index
NDCI	Normalized Difference Coal Index

NDVI	Normalized Difference Vegetation Index
NDWI	Normalized Difference Water Index
NE	North-East
NF	No Fire
NNE	North of North-East
NO	Nitrogen Oxide
NOAA-AVHRR	National Oceanic and Atmospheric administration Advanced Very High Resolution Radiometer
NW	North-West
O^2	Oxygen
RCF	Ruqigou Coalfield
RMSE	Root Mean Square Error
SE	South-East
SO_2	Sulfur Di-oxide
SOI	Survey of India
SSW	South of South-West
SW	South-West
SWIR	Short Wave Infra-Red
T-1, 2, 3, 4	Terrace-1, 2, 3, 4
TES	Temperature-Emissivity Separation Algorithm
TIR	Thermal Infra-Red
TISCO	Tata Iron & Steel Company
TM	Thematic Mapper
TOA	Top of Atmosphere
USGS	United State Geological Surveys
UTM	Universal Transverse Mercator
VNIR	Visible Near Infra-Red
WGS-84	World Geodetic System-84
WNW	West of North-West
WSW	West of South-West

μm	Micrometers	
cm	Centimeters	
m	Meters	
km	Kilometers	
mt	Million Tons	
L_λ	Spectral radiance at the sensor's aperture	W $m^{-2}sr^{-1}\mu m^{-1}$
$Gain_\lambda$	Calibration gain coefficient of sensor	W $m^{-2}sr^{-1}\mu m^{-1}$
DN_λ	Digital number of a pixel in particular band	counts
$Bias_\lambda$	Calibration offset of sensor band	W $m^{-2}sr^{-1}\mu m^{-1}$
$DN_{MAX\lambda}$	Highest DN value in the scale	
$LMIN_\lambda$	Spectral at-sensor radiance that is scaled to $DN_{MIN\lambda}$	W m^{-2} sr^{-1} μm^{-1}
$LMAX_\lambda$	Spectral at-sensor radiance that is scaled to $DN_{MAX\lambda}$	W m^{-2} sr^{-1} μm^{-1}
$G_{rescale}$	Band-specific rescaling gain factor	W m^{-2} sr^{-1} μm^{-1} DN_λ^{-1}
$B_{rescale}$	Band-specific rescaling bias factor	W m^{-2} sr^{-1} μm^{-1}
UCC_λ	Unit conversion coefficient	
λ	Band / Wavelength	μm
$L_{\lambda C}$	Atmosherically corrected radiance	W m^{-2} sr^{-1} μm^{-1}
$L_{\lambda P}$	Path radiance per band	W m^{-2} sr^{-1} μm^{-1}
θ_s	Solar zenith angle	degree
π	Mathematical constant equal to ~3.14159	Unitless
ρ_λ	Planetary TOA reflectance	Unitless
B	Blackbody Radiance	W m^{-2} sr^{-1} μm^{-1}
C_1	1st radiation constant equal to $3.74x10^{-16}$	W m^2
C_2	2^{nd} radiation constant equal to 1.43876869×10^{-2}	m K
T	Temperature	K
h	Planck' constant equal to $6.63x10^{-34}$	W s^2
C	Speed of light equal to $2.99x10^8$	m s^{-1}
k	Boltzmann's constant equal to $1.38x10^{-23}$	W s K^{-1}

T_b	Effective at-sensor brightness temperature	K
K_1	Calibration constant 1	W m^{-2} sr^{-1} μm^{-1}
K_2	Calibration constant 2	K
ln	Natural logarithm	
T_k	Kinetic temperature or land surface temperature	K
$ESUN_\lambda$	Mean Exoatmospheric Solar Irradiance	W m^{-2} μm^{-1}
d	Earth Sun Distance	
Pv	Pixels attributed to vegetation	
Pw	Pixels attributed to water bodies	
ρB1, B2, B4, B8	Spectral Reflectance in band 1, 2, 4, 8	
Ɛ	Spectral emissivity	
$\bar{x}$	Mean	
σ	Standard Deviation	

CHAPTER 1

INTRODUCTION

1.1 BACKGROUND

Coal has significant contribution toward India's economic growth and feeds major percentage of industrial demand for energy production. Due to unavailability or inadequate supply of the other energy sources, coal is primarily used as fuel in the industries. More than 73% of the country's energy supply comes from the consumption of coal that self explains the necessity of coal for industrial development. Coal mining in India has a long history of nearly more than a century. India is the world's third largest producer of the coal following China and United States and ranks fifth in global coal reserves. In last few decades, demands for energy supply have been exponentially increased with growing economic activities. In spite of having enormous quantity of coal, the country still lags to accomplish the energy production for both domestic and industrial demand. High domestic and industrial requirement makes India one of the world's largest consumers of coal (Figure 1.1).

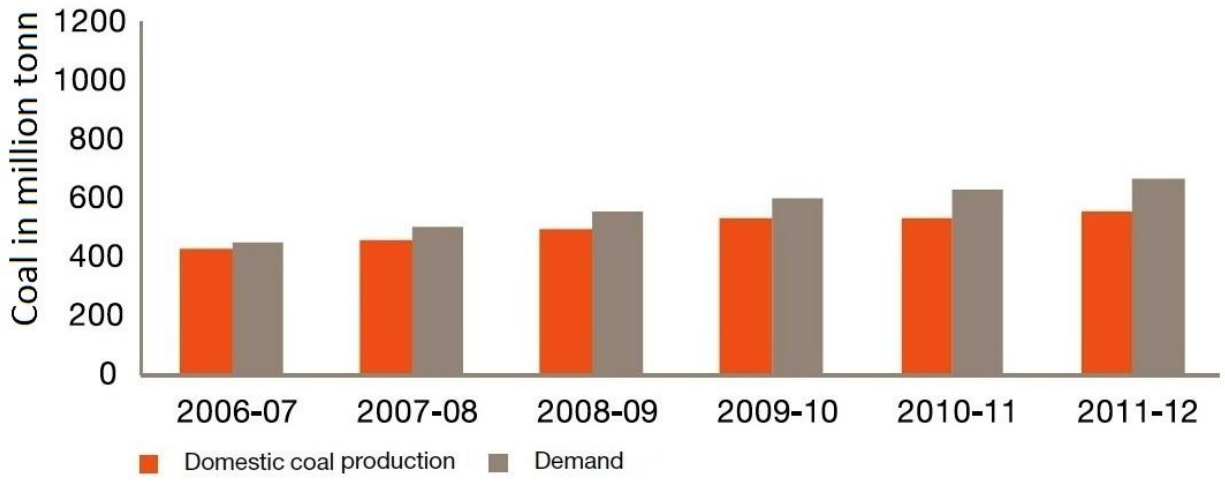

Figure 1.1 Demand and supply scenario of coal in India (ICC, 2012)

More than 90% of the coal available in India is confined to the Gondwana coalfields. The Gondwana coal is sub-bituminous to bituminous range having 50-65% of fixed carbon. Out of the total available resources, 88% of the coal is of non-coking type (GSI, 2004). Rest of the 12% coal is coking type that is exclusive contributed by Jharia Coalfield. Coking type of coal is an essential requirement of steel and cement industries. Limited availability of coking coal

indicates a huge gap between demand and indigenous supply. As a result, coking coal is now imported to meet the needs of industrial demand. Since 2004, the country's coal import has grown by 15% (till 2010-11). According to projections, country's coal import requirement will be more than 200 mt by the end of the 2016-17 (ICC, 2012).

Coal is a natural occurring solid substance formed by the vegetal matter that has been subjected to a variety of geological processes and has thereby undergone remarkable changes in physical properties as well as in chemical composition. Coal is chiefly composed of carbon. It is an inherent property of coal to self-ignite and undergo spontaneous combustion (Feng et al., 1973). Due to this fact, all known occurrences of high rank coal around the world are known to be invariably associated with the problem of **'coal fires'**. **'Coal fire'** is a term used for the natural occurring fire within in-situ coal seam or in stored coal. Fire can be burning or smouldering in nature located at the ground or beneath the ground.Coal fire can cause severe environmental and economic problems worldwide (Stratcher, 2004). It reduces valuable coal reserves and leads to the emission of gases that diffuse out into the atmospheric. These gases are actively contributing green house effect to the atmosphere. The smoke and windblown ash can plague the areas and cause significant environmental changes around coal fire affected areas. Spontaneous burning not only induces deleterious effect on the human health but also poses serious threat to the local inhabitants residing around the area.

To confront the exponential demands of energy supply for industrial growth, the haphazard coal mining activities are being intensely carried out in India especially by opencasts. Opencast activities reveal the burning coal seam to the exposed scenario and hence, accelerate combustion of coal in uncontrolled manner. Uncontrolled coal fires are highly dynamic and can propagate by feeding the coal seam. Fire in most cases also block the available coal resources and often make the area unapproachable causing tons of valuable coal loss every year. Thus, coal fires can be considered as a trio of social-economic and environmental problem that has worldwide influence at both local and global level.

As a problem, coal fires have drawn the attention of researchers, managers, miners, local residents and news media alike since last two decades. The goal of the researches is to precisely analyze and quantify the aspects of coal fires for sustainable socio-economic growth and environmental monitoring. In view of Indian scenario, Jharia Coalfield (JCF), the sole inventory of the prime coking coal is severely affected by coal fires. Since two decades remote sensing techniques based coal fire studies have been significantly carried out for mapping and

quantification of coal fires. In the present approach, an attempt has been made to further explore the potential of remote sensing data and novel techniques to study the various aspects of coal fires in Jharia Coalfield, India.

1.2 GLOBAL DISTRIBUTION OF COAL FIRES

Coal fires are the common problems associated with high rank coal bearing regions known worldwide, particularly from China, USA, Australia and India (Figure 1.2, Stracher and Taylor 2004; Whitehouse and Mulyana 2004; Gangopadhyay and Lahiri 2005; Kuenzer et al., 2007a; Kolker et al., 2009). In China, Xinjiang and Ningxia region located in the north-west and north-central part contain major coal reserves of the country. These reserves are of anthracite and bituminous type of coal forming the world densest congregation of the coal fires throughout the northern China. It has been estimated that these fires have consumed up to 200 million tons of coal per year (Rosema et al. 1995; Dijk, 1996) and annually contribute 2-3% atmospheric CO_2 to the environment (Zhang and Kroonenberg, 1996). In USA, coal production are mainly comes from Wyoming, West Virginia, Kentucky and Pennsylvania. Coal fire in USA was first reported during 1772 in Pennsylvania. Coal fires across Pennsylvania have destroyed floral and faunal habitats, induced land subsidence and yield acid rain in the state (Stracher and Taylor, 2004). In Australia, coal mines are not majorly affected by the spontaneous combustion. However, fires are mostly reported from opencast mines in many locations of Bowen basin and Hunter valley of New South Wales, Victoria and some parts of South Australia. Besides, from the world leading coal producing countries, coal fires are also known from Russia, Indonesia, Canada, Germany, South Africa and France.

1.3 COAL FIRE IN INDIA

In India, Jharia and Raniganj Coalfields located in the state of Jharkhand and West Bengal respectively are mainly affected by coal fires. These coal belts are the discrete sub-basin of the E-W trending Damodar River valley basin. In Raniganj, coal fire affected areas are localized and under geological control (Guha and Kumar, 2012). Fire occurred in relatively small extent from few meters to tens of meters (Gangopadhyay et al., 2006; Guha et al., 2008). However, coal fires of large spatial extent have been prominently noticed in Jambad and Ramnagar opencast (Martha et al., 2005). In Jharia, devastation due to coal fires are more pronounced as it is the sole occurrence of coking type of coal. History, distribution and characteristics of coal fires in Jharia have been discussed in detail in Chapter 3.

Figure 1.2 Worldwide occurrences of coal fires

1.4 SIGNIFICANCE OF THE COAL FIRE STUDIES

Coal fires have both local and global impact in different ways. Besides causing tons of coal loss every year, coal fires poses global threat by contributing harmful and toxic gases to the atmosphere. Coal fires degrade the vegetation land by removing moisture content of the soil. Burning coal seams at underground trigger land subsidence and damage infrastructure around the area. Thus, the detailed study and monitoring of coal fire is absolutely required due to its occurrence as major socio-economic and environmental problem. Significance of the coal fire studies in different areas are as follows:

(a) Management and planning for sustainable coal mining: Uncontrolled coal fire block up tons of coal. Inaccessibility to the area facilitates the continuous burning of blocked coal for years and hence leads to the loss of valuable resource. Mapping of coal fires allow to demarcate the fire affected area for sustainable mining.

(b) Coal fire related geo-hazards: Uncontrollable spread of underground fires causes volume reduction of the burning coal seam and triggers the overlying bed rocks to collapse. This abrupt collapsing is called coal fire induced 'land subsidence'. Land subsidence is the serious threat to the local inhabitants and mine workers. Coal fire affected areas are highly vulnerable to land subsidence. Precise mapping of the coal fires can help to mark the areas vulnerable to potential land subsidence.

(c) Mitigation and rehabilitation: Dynamics of coal fires poses serious hazard to the local resident. Temporal monitoring of coal fires can help to decipher the propagation or movement direction of the underground coal fires. This would further facilitate to plan (i) proper mitigation measures for controlling coal fires and (ii) rehabilitation measures for local residents.

1.5 SCOPE AND APPLICATION OF REMOTE SENSING IN COAL FIRE STUDIES

The study of coal fires is a difficult problem as the fire areas are often inaccessible and therefore, remote sensing techniques could provide very useful inputs in fire studies. Recent advances in remote sensing data products (like availability of multispectral TIR data) and techniques (like sub-pixel estimation, data fusion techniques etc.) extended enormous scopes for further advancement in coal fire related research (Dozier, 1981; Vekerdy et al., 1999a; Eckmann et al., 2009; Zhang, X. et al., 1997; Zhang, X. et al., 1999). Data are available at repetitive pass and at low or free cost. Moreover, large spatial extent of data coverage can allow precise analysis and quantification of coal fires in less time. Coal seams burning underneath

generate thermal anomalies at the surface. These thermal anomalies are the surface expression representing existence and outline of the coal fires. The thermal anomalies can be detected by thermal infrared sensors onboard airborne and space borne platforms. It can be used as an indicator for mapping and monitoring of magnitude, intensity, amount of coal loss and dynamics of coal fires. Beside, remote sensing data have also been used in environmental impact assessment of coal mining and quantification of coal fire related emissions (Chatterjee et al., 1994; Gangopadhyay 2007; Gangopadhyay et al., 2008; Kolker et al., 2009; Dijk et al., 2011).

1.6 RESEARCH GAPS

An extensive review of the literature reveals that the remote sensing techniques have wide range of application in monitoring thermal phenomenon such as, forest fires, volcano and coal fires etc. Study of these thermal processes was first started with aerial thermal scanner followed by advanced thermal imaging sensors (MODIS, ASTER, Landsat TM/ETM+, BIRD) operating today. In general, the prime motive of thermal remote sensing is to evaluate the temperature distribution and spatial extent of the hot feature. With time, different techniques for mapping have comes in light and potential of thermal remote sensing has been further enhanced to explore other related features associated with thermal phenomenon. Several research problems and gaps have been identified during literature survey that is given below in detail:

(a) Accurate mapping of coal fires is pre-requisite of remote sensing based coal fire related studies. However, mapping of the coal fires carried out worldwide including India is restricted only to the delineation of subsurface fires. No study or research specifically on delineation of surface fire has been observed.

(b) Thresholding is an eminent problem associated with mapping of coal fires. A threshold is the value assigned to an image to discriminate ‘anomalous region’ from ‘non-anomalous or background’. A slight miscalculation in setting a threshold can give erroneous results. Several researchers have introduced different methods of thresholding of coal fires (see Chapter 2, Section 2.4.1). However, all methods have been found to be only operable in TIR data and hence, restricted only for mapping of subsurface coal fires. No method has been specifically found to threshold SWIR band for mapping of high intensity surface coal fires.

(c) Surface fires are high temperature phenomenon that can be potentially detectable in SWIR range. However, SWIR is affected by both thermal emission and reflection component. Separate retrieval of both emission and reflection is a very complicated process. Although, ASTER has six SWIR channels but it's potential to map high intensity surface fire have not been fully explored before.

(d) Digital classification techniques have been widely used for mapping of various land cover classes. It requires precise selection of the spectral signatures to discriminate respective land cover classes. Fire is the processes of combustion of a matter (like coal or overburden dump) and there is no technique available for automatic classification of fires.

(e) Temporal monitoring and mapping of the coal fire affected areas are necessary to help plan sustainable mining and industrial remediation on long term basis. In Jharia particularly, dynamics of coal fires have been evaluated in recent past (Chatterjee et al. 2007; Martha et al., 2010). However, to decipher the change in spatial extent of coal fires affected areas and propagation of coal fires from 2000 to 2009 at colliery level have never been executed earlier.

(f) Fresh mine dumps located in the vicinity of the large opencasts are also affected by very low intensity smoldering fire. Such dump fires are perceived automatically by coarse resolution TIR satellite datasets and often misinterpreted and mapped as 'coal fire' in coal mining area. These 'misinterpreted coal fires' have to be carefully analyzed and must not be considered 'actual coal fire'.

1.7 OBJECTIVES

The main objective of the present research is to explore the potential of the short-wave and thermal remote sensing data (particularly ASTER) for precise mapping of surface-subsurface coal fires in Jharia Coalfield, India. The attempt is mainly emphasized on developing a novel approach for thresholding and mapping of surface coal fires. Besides, time series ASTER datasets have been also used to access the spatial dynamics of coal fires in JCF between 2000 and 2009. The objectives of the research have been achieved by routine and advanced processing of remote sensing datasets. The specific objectives of the present research are as follows:

(a) To propose a methodology of thresholding for delineation of 'surface coal fires'.

(b) To formulate new ratio indices for coal fire studies using ASTER satellite data and their implementation for mapping of surface coal fires in JCF.

(c) Temporal monitoring and mapping of coal fires in JCF with special emphasis on coal fire dynamics from 2000 to 2009 at colliery level.

1.8 SIGNIFICANCE AND INNOVATIONAL APPROACH OF THE RESEARCH

A review of the literature reveals that the previous coal fire studies are mainly restricted to the mapping of subsurface coal fires. No significant study strictly focused on the surface coal fires has been carried out. Hence, for the present research, the objectives have been set to study of surface coal fire. In the present study, two novel approach have been significantly introduced for delineation and mapping of surface coal fires using SWIR data. In first objective, the 'maximum solar reflection threshold' method has been proposed to set threshold for delineation of surface coal fire. Highest solar reflectance from fresh excavated dump is used as conservative threshold to isolate the pixels attributed to surface coal fires. To test the wider applicability of the technique adopted, the method has been also applied in different geographical setting. In second objective, spectral characteristics of the pixel attributed to surface fire have been analysed and two ratio indices have been formulated to discriminate the pixels attributed to surface coal fires. The approaches presented here significantly evaluate and improve the mapping of surface coal fire that may impart help in industrial management and planning.

1.9 ORGANIZATION OF THE THESIS

The thesis has been organized into eight chapters. An overview of the chapter wise distribution of the work is discussed below in detail:

(a) Chapter 1 discussed the necessity and purpose for the conducting research, scope and utility of remote sensing to accomplish the research, identification of the research gaps, setting the objectives and innovational approach to achieve the objectives.

(b) Chapter 2 discussed and summarizes the review on coal fire studies using remote sensing. This chapter gives the insight of coal fires, its causes and consequences followed by principle of thermal remote sensing and problem associated with coal fire studies. The chapter also discussed the potential of satellite data for mapping of coal

fires and quantification of coal related features with special emphasis on previous work in JCF.

(c) Chapter 3 gives the introduction to the physical and geographical attributes of the study area with special emphasis on the field based observations in JCF.

(d) Chapter 4 includes the details of the data used, pre-processing and processing of the remote sensing datasets. An overview of the methodology adopted in the present research has also portrayed in the present chapter.

(e) Chapter 5 gives an introduction to a novel method for thresholding of SWIR band to delineate coalfield surface fires and also discussed applicability of this method to wide range of geographical setting.

(f) Chapter 6 explain the formulation of ratio indices for mapping of surface coal fires. This chapter also deals with the estimation of spatial extent of high intensity and smouldering coal fires using obtained indices.

(g) Chapter 7 discussed the fluctuation in spatial extent of coal fires from 2000 to 2009 at colliery level in JCF.

(h) Chapter 8 presents the summary and conclusions for further studies.

CHAPTER 2

COAL FIRES STUDIES USING REMOTE SENSING: A REVIEW

2.1 INTRODUCTION

Coal fires are common problems associated with high rank coal bearing occurrences known worldwide and have great impact on both global and regional scale. Since last two decades, remote sensing techniques have been widely used for monitoring and mapping of coal fires. Over the years with recent advancement, the potentials and scope of satellite sensor techniques have been further extended to broad level in coal fire related studies. Regular and precise mapping of coal fires are important for sustainable industrial growth and environmental remediation on long term basis. In the present chapter a review of the literatures on coal fires have been discussed with special emphasis on recent researches around the world and in India. In this chapter, causes of coal fires and its social, economic and environmental consequences on both local and regional scale, principle and significance of the thermal remote sensing has been discussed. The focus has been primarily laid on to discuss the application and problem associated with thermal remote sensing data for coal fire studies. Besides, a brief discussion on the role of satellite sensor technology in monitoring and mapping of coal fires with reference to previous studies in Jharia Coalfield, India has been also given.

2.1.1 Causes of coal fire

Coal is highly combustible in nature and vulnerable to ignition by variety of processes. Spontaneous combustion of coal by self-ignition is the most obvious cause of the coal fires. In addition to the geological processes through time, anthropogenic activities are also the potential causes of coal fires. The causes of coal fires are briefly discussed below in details:

2.1.1.1 *Spontaneous combustion and self-ignition*

Self-ignition is the inherent property of coal. High rank (high degree of coalification), large particle size, large exposed surface area and low moisture content, coals are more prone to spontaneous combustion by self-ignition. It is initiated by the absorption of oxygen when a coal seams or coal dump is exposed to an open environment (Carras et al., 2009). Vents, cracks

or fractured rock surface above the coal seams act as a passage for oxygen influx that initiate oxidation in coal seams occurring beneath. With continuous absorption of oxygen at the coal surface, the oxidation reaction becomes strongly exothermic and temperature of the coal seams starts increasing.

$Coal + O_2 \rightarrow CO_2 + H_2O + Heat\ (393.5\ KJ)$

When the heat evolved by the oxidation of coal reaches above the threshold temperature, self-ignition in the coal seam begins. The threshold temperature to start self-ignition is about 50°C for lignites and 70-80°C for bituminous coals (Ackersberg, 2003). During the initial stage, the CO_2 evolved during the oxidation of coal got no route to escape and hence, reversible reaction starts.

$2CO + O_2 \leftarrow 2CO_2$

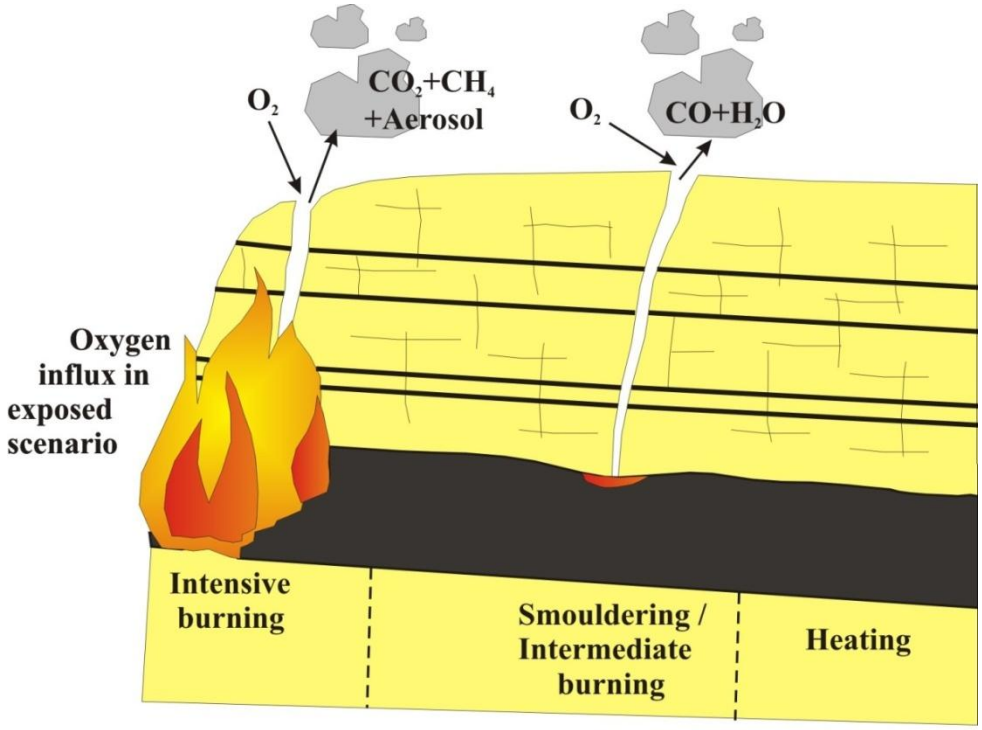

Figure 2.1 Schematic diagram showing phenomenon of coal combustion

During this reversible reaction, CO_2 starts releasing carbon-monoxide and oxygen. This oxygen acts as fuel for spontaneous combustion of coal. With continuous burning, volume reduction of the underlying coal seams results in the development of linear cracks and fissures over the surface that provide passage for uninterrupted inflow of oxygen. Once coal fire starts

in a coal seam, it burns for a long time by spreading along the seam (Schmal, 1987) (Figure 2.1).

2.1.1.2 *Igneous intrusion*

Igneous intrusions in coalfield basin are supposed to be the external ignition source that induced combustion in coal. Like in Jharia Coalfield, ignition of coal is also caused by dolerite and mica lamprophyre dykes and sills of Jurassic and tertiary age. The intrusions mainly occur at relatively greater depth and affect the central and eastern part of the JCF. Intrusion causes combustion of coal in the absence of the oxygen and induced baking effect in the affected section of the coal seam. However, combustion even in the absence of oxygen can cause reversible reaction to start and promote the process of self-ignition and spontaneous combustion. The process of combustion devolatized the affected part and transformed the entire seam section into 'burnt brick' called *Jhama* (Sengupta, 1980). External ignition together with self ignition and spontaneous combustion forms world densest congregation of coal mine fires in JCF.

2.1.1.3 *Coal mining and indirect processes*

Unplanned excavation and mining activities in opencasts expose coal seams to an open environment. In an exposed scenario, spontaneous combustion of coal is facilitated by the accelerated influx of oxygen. With continuous burning, fire starts moves along the direction of dipping coal seams. Combustion reduces the volume of the coal seam and results in the overlying bed rock to collapse. Hence, a complex system of fractures is developed over the surface that allows the frequent supply of oxygen for spontaneous combustion.

2.1.2 Consequences

Uncontrolled coal fires have significant environmental and economic impact at both local and global level. Spontaneous combustion can occur either within the underground coal seam or in piles of stored coal and spoiled dumps on the surface. Spontaneous combustion of coal actively contributes to the loss of valuable coal resources, poses serious threat to the coal mining and surrounding infrastructure, induce severe environmental hazard and ecological disturbances in and around the affected area. These impact and consequences are briefly discussed below:

2.1.2.1 *Socio-economic impact*

Uncontrolled coal fire occurring underground can block substantial reserves of valuable coal. It has been estimated that in JCF approximately 3 mt coal is lost every year due to coal fire (BCCL, 2008). Burning of coal seams not only consumes the coal but also induces inconveniences and difficulties in operating exploration, and fire controlling strategies in a coal mining area. Once ignited, fire propagates along the dip direction of the coal seam. While propagating, fire consumes the coal and causes volume reduction of the underlying coal seam. This results in the overlying bed rocks to collapse and induces unexpected sudden subsidence. Uncontrolled subsidence poses serious threat to the urban and human settlements in and around the affected area. Subsidence causes severe mine accidents, damage the infrastructure and stimulates danger to life of local inhabitants residing proximity to the fire area (Prakash et al., 2001). Lack of attention and limited financial support from the government and private sector deeply impact the social condition of the local residents. In JCF, due to poor socio-economic condition, local residents of several mining villages are also linked with small scale illegal mining activities. Precise mitigation and reclamation measures to reduce the consequences of this geo-hazard essentially require serious attention to raise the socio-economic condition of the affected area.

2.1.2.2 *Environmental hazard and ecological disturbance*

Coal fire causes severe environmental and ecological disturbance at both local and regional scale. Haphazard mining activities around the coal mine induce significant negative impact on the surrounding area. Mining operations cause deforestation and lowering of groundwater table. Coal seam fires occurring at subsurface level degrades the surface vegetation by removing the moisture content of the soil. Continuous heating also reduces the soil fertility by changing pH and chemical composition of the soil. Degradation of vegetation produces ecological disturbances around the area. Active coal fires lead to atmospheric pollution through the emission of diffused gases, such as sulphur dioxide (SO_2), nitrogen oxides (NO), carbon monoxide (CO), carbon dioxide (CO_2), and methane (CH_4) (Rosema et al. 1995; Kolker et al., 2009). Among these diffused gases, the contribution of CO_2 and CH_4 is significantly large. These gases actively contribute greenhouse effect to the surrounding environment and leads to global warming (Dijk van et al., 2011). The smoke and windblown ash also plague the areas around coal fires. Emission of these gaseous pollutants, particulate matters and toxic trace elements, such as arsenic, mercury and selenium also poses direct

hazard to human health. Fumerolic mineral formed along the gaseous vent and pits may also leached from encrusted surface to the water bodies and hence also cause indirect endangerment to the human health (Stracher et al., 2005). In recent years, significant efforts have been made on quantification of coal fires related emission on regional scale (Carras et al., 2009; Dijk et al., 2011; Engle et al., 2011). However, precise quantification of gaseous emission on regional scale is difficult to access and magnitude of impact in global scenario is little.

2.2 PRINCIPLE OF THERMAL REMOTE SENSING

Any object above absolute zero (0 K or -273.15 °C) emits radiation in SWIR and TIR of the spectrum. The amount of energy emitted by an object is the function of its thermal state and can be speculated by its emission spectra. The emission spectra of an object vary across the electromagnetic spectrum. The relationship between the emission responses of an object at different wavelengths is well explicated by Planck's radiance function.

In late 1800s, Planck derived the emission response curves across the different wavelengths for perfect black body at different temperature (Prakash and Gens, 2010; Figure 2.2). The curves obtained have suggested that the maximum emission response of an object having temperature close to 300 K (Earth ambient temperature) can be detected within 8-10 μm spectrum range (TIR). Similarly, the objects having temperature close to 1000 K can be detected within 2-3 μm (SWIR) spectrum range.

Likewise, the sensor onboard satellite platforms designed to operate within SWIR and TIR can measure the spectral emission response in respective spectral channel. Fires occurring at greater depth (subsurface coal fires) can produced the subtle thermal anomaly by increasing the ambient surface temperature range (300 K) up to 15°C (Prakash and Gens, 2010). This anomalous temperature can be potentially detectable within TIR range. High intensity surface fires in in-situ coal seams or in coal dumps having temperature over 1000 K can well suited for detectable within SWIR or NIR region of the spectrum. However, in nature, no object behaves like true black body (not perfect emitter or not perfect absorber). Thus, spectral emissivity (Ɛ) of the objects greatly varies from one other. It is the ratio of the amount of energy emitted by an object at certain temperature and wavelength to the amount of energy emitted by a black body at same temperature and wavelength. The emissivity of the most natural substances ranges from 0.7-0.96.

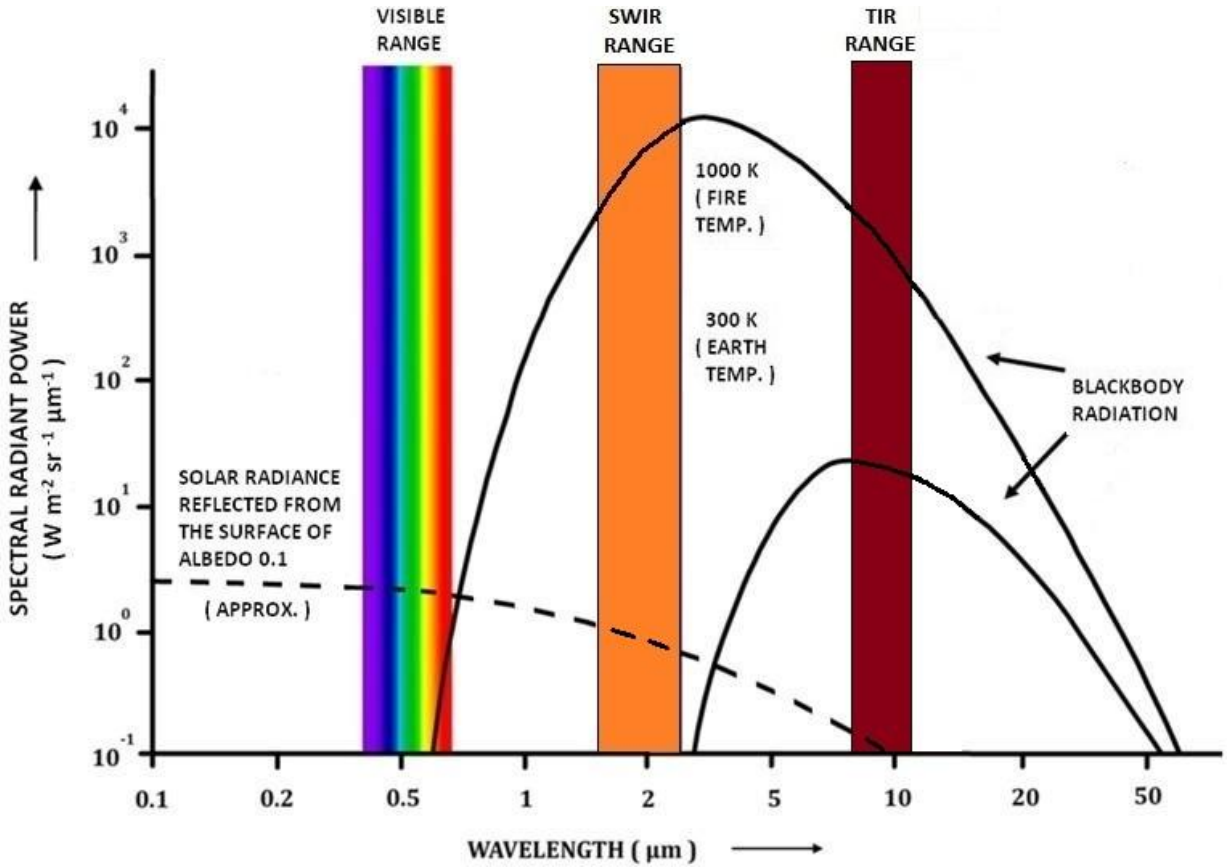

Figure 2.2 Emission spectra of the blackbodies at different temperature. The solar radiance reflected from a surface of albedo 0.1, and the spectral position of SWIR and TIR bands are also shown in the figure. SWIR bands are sensitive to both solar reflected radiation and blackbody radiation emitted by high intensity fire whereas TIR bands is sensitive to spectral response by subsurface coal fires producing subtle thermal anomaly

2.3 PROBLEMS ASSOCIATED WITH COAL FIRE STUDIES

Remote sensing based coal fire studies mainly focused on the effective mapping and monitoring of coal fires (Zhang, X., 1998). However, remote sensing also has certain limitations in terms of available techniques and data specifics. The common problem associated with the remote sensing sensor is the influence of atmosphere. Gaseous emanation and particulate matter in the atmosphere cause haziness in the image and hence cause hindrance in remote sensing based observations. Cloud cover, if exists, also conceal the area under observation up to some extent. Prolong burning heat up the surrounding area by atmospheric convection. Seasonal heating from March to September in tropical-subtropical regions also restrict to use the satellite data acquired during these seasons. Due to this reason, images obtained during cold season i.e. from November to February are preferably used for monitoring thermal phenomenon. Limited availability and coarse spatial resolution of the TIR sensors also

restrict the thermal analysis of coal fire. Besides, thresholding of spectral response and characteristics of coal fires are some technical issues that renders the problems associated with coal fire studies.

2.3.1 Thresholding of sensors response and extraction of thermal anomaly

Thresholding of sensor response is an important task to delineate the thermal anomaly. The techniques of thresholding allow to set a value for extracting the sensor response of the object of interest from the image. A precise threshold demarcates the pixels attributed to the favorable object from the rest of the image that corresponds to background. The pixel values above the threshold value is considered to be 'anomalous' and values below the threshold values are 'background'. In this way, the techniques of thresholding segment the image into binary output class and facilitate the further analysis of the anomalous class separately.

Coal fires are very restricted in spatial extent and radiate high energy heat flux that cause subtle thermal anomaly at the surface. Thermal anomalies detected over the surface are the function of size (dimension), depth and intensity of the coal fire. Low thermal conductivity of the overlying bed rocks such as shale and sandstone also control the thermal anomaly obtained at the surface. Fire of even low intensity if occurring at shallow depth may produce detectable thermal anomalies on the surface than high intensity fire occurring at greater depth. However, as mentioned earlier that coal fire is a complex phenomenon and thermal response due to coal fires received at the satellite sensor is controlled by data specifics and characteristics of coal fires. Precise estimation of the threshold value to delineate thermal anomaly associated with underground coal fires is a difficult task. Coal fires occur as very complex systems in different geographical setting around the world. Hence, different workers have proposed different techniques of thresholding to delineate fire from remote sensing data as no single method works accurately in all conditions.

In recent years, several algorithms and methods have been developed for thresholding and extract the coal fire related thermal anomalies from various remote sensing satellite data such as LANDSAT, ASTER, MODIS or NOAA-AVHRR. Among the various applicable methods of thresholding, density slicing technique based manual approach have been most widely used and applied in recent researches (Prakash et al., 1995b; 1997, Yang et al., 2005) for delineating coal fires. The technique involved to estimate a threshold digital number defined by the user based on 'trial and error method' to discriminate the pixels attributed to fire from non-fire pixel or background pixels. In trial and error method, geographical locations of some

coal fires are observed in field and their corresponding location on the thermal images are demarcated on Landsat TM band 6. Then, several spatial linear profiles (thermal profiles) are drawn on Landsat TM band 6 data passing through the anomalous hot pixels. DN value of each pixel lying along the profile has been computed on pixel-by-pixel basis and plotted against the distance. The DN values corresponding to hot pixels are shown high peaks than normal background. For different profiles, maximum value of background pixel slightly varies. A reasonable value of the maximum background pixel together with user's field based knowledge is considered as threshold to delineate the pixels attributed to coal fire from non-fire ones. Prakash et al., (1997) successfully applied this technique and set a reasonable best threshold DN value to 137/138 in TM band 6 to delineate the subsurface coal fire areas from normal background.

However, it is hardly possible that anomalous pixels area estimated using this technique match the fire outline derived from field surveys. The error may arises due to coarse resolution of TIR data, ignoring the atmospheric effects, non-uniform background temperature, ignoring lateral variation in spectral emissivity of the ground material (Zhang et al., 2004). Any misinterpretation in selecting a threshold may leads to the over or underestimation of spatial extent of coal fires. Hence, estimated threshold are corrected and checked frequently till it accurately discriminates the fire from non-fire area.

Density slicing technique based on trial and error method for threshold estimation has been widely used as it is easy to apply and close to the real scenario. However, automated methods for detection of thermal anomaly have been also applied for mapping of coal fires. Prakash et al., (1999a), used statistical parameters to set the threshold at standard deviation of two ($\bar{x}$+2σ) for discriminating coal fires, Rosema et al., (1999) identified the change in shape of the slope of histogram of the image and figure out its corresponding point in x-axis. Semi automated-automated algorithms have been recently proposed by Prakash and Vekerdy (2004) and Kuenzer et al., (2007c) for estimating threshold. The methods give more realistic information about the target which best meets the observed information derived from the field surveys. These methods automatically extract the thermally anomalous pixels from the non-anomalous ones. In the simplest case, threshold may be selected by trial-and-error as possibly guided by field data (Figure 2.2a). Alternatively, the threshold may be derived using a statistical parameter, e.g. standard deviation (Figure 2.2b), or on the basis of change in the slope of frequency diagram implying a change in type of objects (Figure 2.2c), or on the basis of bi-(multi-) modal character of the frequency diagram (Figure 2.2d).

Prakash and Vekerdy (2004) applied semi-automated techniques on small subsets of TIR images based on statistical parameters for managing and extraction of surface and subsurface coal fires in the Ruqigou Coalfield in north-west China using CoalMan prototype GIS. This semi-automated technique provides flexibility in setting up threshold and automatically changes thethreshold DN based on the spatial variability of the subset window. It gives more realistic estimates of the fire area but coarser resolution thermal data (Landsat TM band 6) makes it difficult to determine the actual location of fire spots. Kuenzer et al., (2007c) employed 'moving window algorithm' for separating thermally anomalous pixels from the normal background where raw satellite data occupying anomalous pixels were spatially subset into small windows of varying size. Histograms of each spatial subsets were statistically analyzed and threshold value was set at DN where first local minimum drop after the main maximum peak. DN values beyond first local minimum drop were considered as thermal anomalies. However, all pixels which declared as thermally anomalous using above approach may not represent coal fire. Such pixels were taken as 'error' and rectified again using statistical analysis based on detailed field knowledge. This automated approach to delineate the thermal anomaly is worked well for detection and monitoring of unknown coal fire using remote sensing satellite data over a large area but have same limitations like other techniques due to spatial dependency of thermal data.

2.3.2 Limitations of TIR remote sensing data

TIR data have coarse spatial resolution and exhibit their own limitation in detecting thermal phenomenon like coal fires. Total thermal emission of a unit TIR pixel is the contribution of membership value of each end members of that pixel along with coal fire. Hence, the emissivity and radiant temperature of a pixel containing fire depends on the contribution of different component within the pixel. Temperature obtained from the satellite data represents overall temperature of the pixel called 'pixel integrated land surface temperature' (LST) (Gupta, 2003). LST represents the average thermal flux emanating from both coal fire and non coal fire area. For example, in Landsat data, each TIR pixel constitutes an area of about 3600 m^2 and it is hardly possible that whole pixel contains fire. Even a very high temperature surface fire of small spatial extent present in 60x60 m^2 pixel can raise the pixel integrated LST of that pixel by few Kelvin against the normal background. Therefore, TIR can detect the anomalous hot pixel only if it contains fairly large coal fire body that is long enough to enhance the radiant temperature of that pixel than normal background. Coal fire

related anomalies are extremely weak anomalies and their surface manifestations are also intensely very low.

These factors facilitate the detection and analysis of coal fire very difficult. Hence, it is suggested that the remote sensing based coal fire estimation is the function of the size of pixels and the user defined preselected background temperature value.

TIR sensor receives the radiant energy response in proportion to its temperature (T) and emissivity (Ɛ) (Coll et al., 1994; Gillespie et al., 1998). Most natural substances show an emissivity value ranging from 0.7 to 0.97 (Prakash and Gens, 2010). Previous studies have used a constant emissivity of 0.95-0.96 to retrieve pixel integrated LST. Recent advancement in remote sensing techniques and availability of multispectral TIR sensors allow separate retrieval of land surface temperature and emissivity spectra. Gillespie et al., 1999 proposed temperature-emissivity separation (TES) algorithm that can estimate the precise surface temperatures and corresponding emissivity values of given pixel. It is reported that TES can recover temperatures within about ±1.5 K and emissivity within about ±0.015.Surface temperature values derived using TES algorithm are more close to the ground truth for all classes (Schmugge et al., 2002; Coll et al., 2007; Gangopadhyay et al., 2012). However, satellite data with single TIR band like Landsat has to use constant emissivity or field derived emissivity to compute land surface temperature.

2.4.3 Heat transfer and depth estimation of coal fire

Underground coal seam fires are the highly complex multi-variable dependent system. Precise analysis of subsurface components of coal fires requires an interdisciplinary approach. Thermal anomaly obtained at the surface is key to all remote sensing based measurements. Such surface observations can be implemented to model the subsurface component of the coal fires using simplified approach and several assumptions.

Depth estimation is an important component of subsurface coal fires studies. In recent years, different methods have been proposed to estimate the depth of coal fires. Saraf et al., (1995) proposed geometrical methodfor fire-depth estimation. Geometrical method involves (a) distance between surface thermal anomaly and exposed coal outcrop on the surface and (b) dip of the coal seam as input in trigonometric functions to determine the depth of coal fire.

Table 2.1 Brief review of the methods that have been implemented for thresholding remote sensing data to map coal fires

Previous Methods	Applied By	Brief Description	Advantages	Limitations
Density slicing technique based trial and error method	Prakash et al., 1995b; Prakash, 1996; Prakash et al., 1997; Yang et al., 2005	A threshold DN value is picked and set up for thresholding based on extensively defined field data (Fig. 2.3(a)).	Easy to apply and commonly used for delineating coal fires. Not strictly based on digital techniques for threshold estimation.	Anomalous pixels area estimated may or may not match the fire outline derived from field surveys. Method is subjective. Has user-bias as it depends on users field knowledge and image analysis skills.
Automated method based on statistical parameters	Prakash et al., 1999a	Statistical parameters used to set the threshold. A standard deviation of two ($\bar{x}$+2σ) is commonly used for discriminating coal fires (Fig. 2.3(b)).	Simplest automated method for threshold estimation.	Data utilized should be radiometrically corrected.
Histogram method	Rosema et al., 1999	Change in shape of the slope of histogram is identified A hypothetical uniform histogram slope is projected. The point (value) on x-axis where this projected slope intersects is taken as threshold (Fig. 2.3(c)).	Independent of radiometric information and statistical parameters.	Careful analysis of histogram is required.

Moving window algorithm	Kuenzer et al., 2007c	Histograms are statistically analyzed and threshold value is set at the DN value that represents the first local minimum drop after the main maximum DN peak (Fig. 2.3(d)).	Works well for detecting unknown coal fires and monitoring over a large area.	Algorithm tested only locally in Northern China. Wider applicability not tested. Algorithm is sensitive and may generate more false alarms for coal fires. To reduce false alarms the detected fire areas may need to be reanalyzed and rectified using statistical analysis based on detailed field knowledge
Semi automated methods	Verkerdy and Genderen, 1999b; Prakash and Vekerdy, 2004	Surface-subsurface coal fires extracted from the background based on statistical parameters using CoalMan prototype GIS	It provides flexibility in setting up threshold and automatically changes the threshold DN based on the spatial variability of the subset window. It gives more realistic estimates of the fire area.	Coarser resolution thermal data makes it difficult to determine the actual location of fire spots.

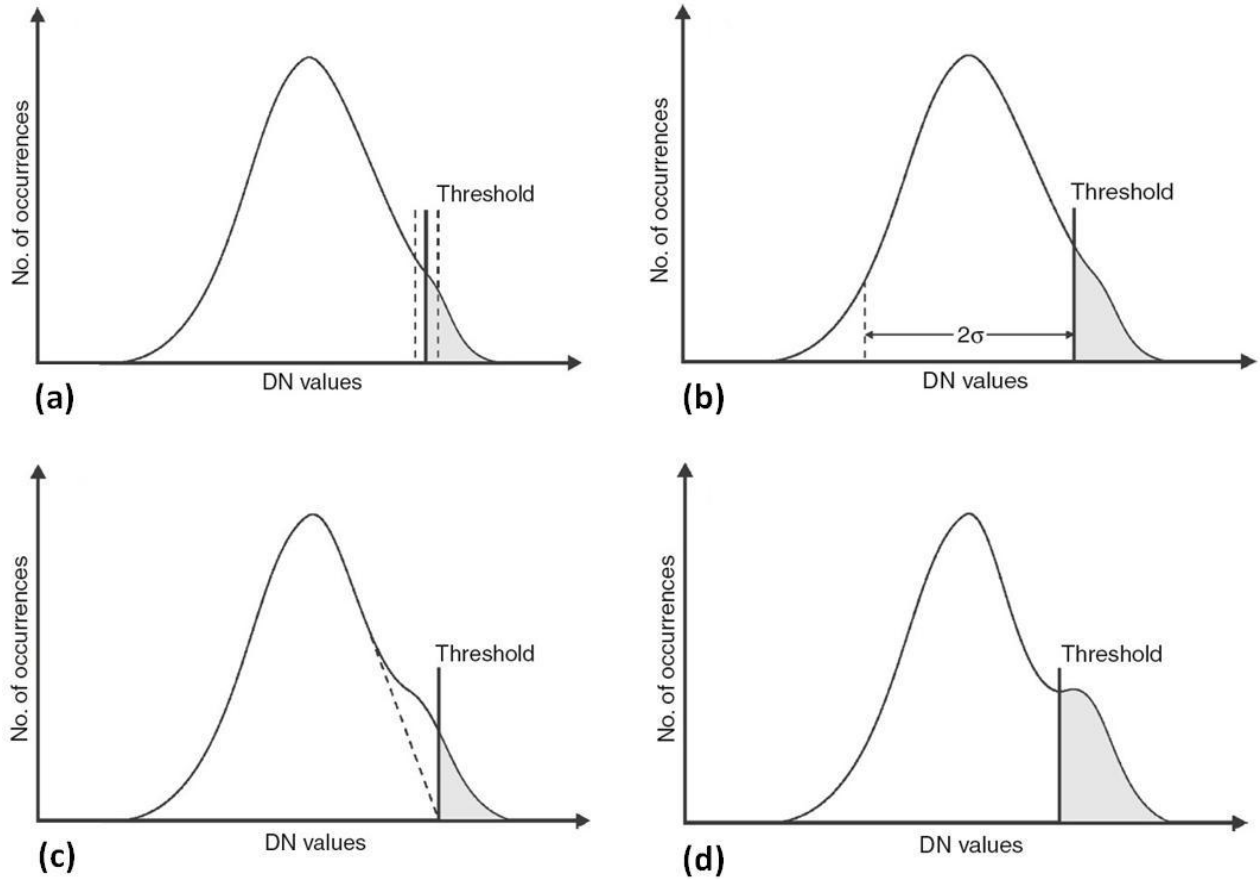

Figure 2.3 Various methods for thresholding Landsat TM/ETM band 6 data for delineating thermal anomalies associated with subsurface fires. Threshold is set by (a) density slicing based on trial-and error (b) using statistical parameters (c) analyzing slope of the histogram (d) detecting the first minimum DN value dip after a major DN value maxima. (Adapted from Prakash and Gens, 2010).

The method assumes that the thermal anomaly obtained on the surface is lying vertically above the burning coal seam and also requires desirable information from field surveys (Prakash and Gens, 2010). Geometrical method has been further improved by introducing geological component (stratigraphy and structural attributes) of the area to the model the depth of coal fires (Peng et al., 1997).

Review of literature reveals that the depth estimation of coal fires in recent researches are mainly focused on the numerical simulation using finite element method under steady state condition. The simulations are generally based on the conductive heat flow model to determine the depth function (Mukherjee et al., 1991; Prakash et al., 1995a; Genderen et al., 1996; Cassells, 1997; Prakash and Berthelote, 2007) and dynamic behavior of the coal seam fire

(Wessling et al., 2008b) from the information available from remote sensing data. Depth estimation of underground coal seam fire is the function of intensity and magnitude of the energy transmission. Energy transport is strongly influenced by the hydraulic and mechanical processes (Wessling et al., 2008a, 2008b). In mining area, interaction of the underground coal seam fire with exhaust gases and overlying system of fractured rock facilitate the energy transport by free convection (Huang et al., 1991; Huang et al., 2000; Wolf and Bruining, 2007). Excessive mining activity further exposes the coal seams to mechanical and thermal processes to accelerate the convective transfer. Due to these parameters, modeling for depth estimation based on free convection is very complex.

2.3.4 Coal mining induced variation in land use pattern and dynamics of coal fire

Coal mining is closely associated with temporal variation in land use pattern (Kuenzer et al., 2004; Kuenzer et al., 2005). In any coal mining area, land use patterns are significantly affected by both anthropogenic and natural activities. Continuous demand of energy supply for industrial growth leads to the haphazard mining activities in coal bearing area. Mining activities frequently expanded in spatial extent with time to enhance the coal production and hence, in turn temporally changes the surrounding topography of the area. Open cast mining, dumping of excavated coal and frequent accumulation of mine dumps (overburden dumps) are some of the anthropogenic activities that causes frequent change in the land-use pattern. Natural phenomenon such as land subsidence, surface and subsurface coal fires indirectly influences the land-use. Opencast activities also unveil the shallow subsurface coal seam fires. Exposure to an open environment accelerate the propagation of coal fire that further affects the land-use land cover of the area like vegetation, infrastructure etc. Therefore, temporal variations in land-use is closely associated with coal fire especially surface fire and cause hindrance in regular monitoring of surface coal fires around the affected area.

As mentioned, coal fires are highly dynamic in nature and vary frequently in their spatial extent. A single coal fire map may not be useful for long term basis. Hence, precise planning and mitigation measurements require temporal monitoring of coal fires. Spatial dynamics of coal fires can be accessed by repetitive satellite data. However, due to technical limitations like accurate pixel by pixel geometric co-registration, unavailability of satellite data of same season and handling large datasets cause difficulties in retrieving coal fire dynamic.

2.4 MAPPING AND MONITORING OF COAL FIRE USING SATELLITE DATA

Fires in coal fields are a common occurrence and have drawn the attention of researchers, managers, miners, local residents and news media alike due to the local and global threats they pose to the coal resource and the environment. Coal fires occur at the surface and underground and are reported from almost all coal bearing regions of the world, particularly from China, India, USA, Indonesia, Russia, South Africa and Australia (Walker, 1999; Stracher and Taylor, 2004; Whitehouse and Mulayana, 2004; Gangopadhyay et al., 2005; Kuenzer et al., 2007a, b; Kolker et al., 2009). Remote sensing technology has been used for coal fires studies for nearly five decades. Earlier studies were restricted to the air borne methods of detecting coal fires. Airborne remote sensing provides greater spatial detail for mapping coal fires (Fisher and Kunth, 1968; Knuth et al., 1968; Rabchexsky, 1972; Ellyett and Fleming, 1974). Though earliest studies were relied on the use of aerial thermal scanners, studies in the last two decades have been focused on the use of data from satellite sensors such as National Oceanic and Atmospheric Administrations Advanced Very High Resolution Radiometer (NOAA-AVHRR), Moderate Resolution Imaging Spectroradiometer (MODIS), Landsat Thematic Mapper (TM) and Enhanced Thematic Mapper (ETM+), Advanced Spaceborne Thermal Emission and Reflection Radiometer (ASTER), and experimental satellites such as the Bi-Spectral Infrared Detection (BIRD) (Mansor et al., 1994; Zhang and Kuenzer, 2007a, Zhang et al., 2007b; Prakash and Gupta, 1999a; Voigt et al., 2004; Zhang, X. et al., 2004a; Tetzlaff et al., 2005; Chatterjee et al., 2007; Gangopadhyay, 2007; Kuenzer et al., 2008; Quattrochi et al., 2009; Yaobao, 2010; Martha et al., 2010). Satellite remote sensing provides low-cost repeat data coverage over the fire areas that are very useful for fire monitoring. Multispectral data from satellite sensors such as the Landsat TM and ETM+, and ASTER have the additional advantage that they acquire data in both the thermal infrared (TIR) and the shortwave infrared (SWIR) parts of the spectrum. TIR data are used widely to delineate subtle surface thermal anomalies associated with underground coal fires, while SWIR data are used to isolate very high temperatures associated with surface fires (Dijk et al., 2004; Zhang et al., 2004).

China has the extensive reserves of valuable coal and ranked first in coal production. Coal fires in such large reserves are quite persistent and dated back to Pleistocene age in China (Zhang, X. et al., 2004b). Spontaneous combustion of coal in China have drawn serious attention of the various research groups to study the various aspects and characteristics of coal fires especially in northern China (Gielisch and Kuenzer, 2003; Dijk et al., 2003). Since 1980, multispectral and thermal infrared air borne and space borne scanners have been widely used

for monitoring of coal fires. Landsat datasets (Landsat TM/ETM+) have been sufficiently applied for detecting large surface fires and shallow subsurface fires in northern China. Zhang X. et al., (1995) proposed a method to evaluate the capability of landsat-5 TM band 6 data for sub-pixel coal fire detection. Satellite data with a coarser spatial resolution (like NOAA-AVHRR data) than that of Landsat-TM are rarely used for coal fire research. Due to low resolution, the temperature of the hot objects may not enough to exceed the pixel integrated LST than pixel integrated background temperature. Hence, satellite data based detection and mapping of the underground coal fires are more precisely governed by Landsat or ASTER data using different techniques of thresholding (Zhang, J. et al., 2004; Tetzlaff, 2004; Kuenzer, 2005; Yang et al., 2005). In recent years, advanced remote sensing techniques have been potentially applied in quantification of surface-subsurface fires and associated environmental problems (Guan, 1989; Dijk et al., 1994; Rosema et al., 1995; Genderen and Guan, 1997; Li-Ding, 1999). With time, the coal fire researches have been further extended to study various aspects of coal fires using advance modelling techniques of numerical simulation to (Gao et al., 2006; Chen et al., 2007) and quantification of coal fire related emissions (Kolker et al., 2009; Dijk et al., 2011; Gangopadhyay, 2007; Gangopadhyay et al., 2008).

2.5 PREVIOUS STUDIES IN JHARIA COALFIELD (JCF), INDIA

Mine fires in JCF have a long back history (Sinha, 1986). Coal fires in JCF have been well monitored from space using aerial scanner and satellite sensors since last two decades. Earlier coal fires related studies were restricted to the applicability of thermal scanner. Airborne thermal scanner produces inherent distortion in the scanned image but allow obtaining imagery with reasonable spatial and thermal resolution (Lillesand and Kiefer, 2000; Zhang, X. et al., 2003). Thermal anomalies are the function of coal fires. These anomalies have been potentially detected over the thermal images derived from airborne or space borne thermal scanners to map surface-subsurface coal fires. With time, the remote sensing based coal fire studies in JCF are not limited to mapping but further expanded to different aspects of coal fires some of which are described below in details:

2.5.1 Mapping and monitoring of coal fires in JCF

In 1990's, airborne thermal images were first used to detect and monitoring surface-subsurface coal mine fires in JCF (Bhattacharya et a. 1991, Bhattacharya and Reddy, 1994; Bhattacharya et al. 1996; NRSA, 1996). However, soon after the launch of Landsat-4 with Multispectral Scanning system (MSS) and thematic Mapper (TM) sensor aboard in 1982,

monitoring and mapping of coal fires was widely extended to an advance level. With availability of repetitive satellite data, coal fires in JCF were temporally monitored. Cracknell and Mansor (1992) analyzed the potential utility of Landsat-5 Thematic Mapper (TM) thermal infrared (band 6) and short wavelength infrared (bands 5 and 7) data for detecting and mapping of surface-subsurface coal fires in test site of JCF. The results obtained from the study was correlated with ground measurements and suggested that Landsat TM have significantly enabled the detection, mapping and quantifying of subsurface coal fires zones. Reddy et al. (1993) used the short-wave infrared region (SWIR) to detect the high temperature surface fire and related geo-environmental features in JCF. Prakash (1996) exclusively carried out remote sensing-GIS based studies of coalmine fires in JCF. The study broadly describes the various aspects and characteristics of coal fires using Landsat MSS and TM data. Landsat TM band 6 data was potentially used to detect the surface thermal anomaly associated with underground coal fires in JCF. The area corresponds to underground coal fires was precisely mapped by selecting a threshold DN value by employing trial-and-error method using the density slicing technique (Prakash et al., 1995b). In JCF, surface fires are sporadic in nature and relatively small in spatial extent. TM-6 is useful for mapping subsurface fires and TM-5 and TM-7 are useful for mapping surface fires (Prakash et al., 1997). Underground fire removes the moisture content of the soil which degrades the vegetation over the surface and turned the corresponding area into dry barren land. The barren show higher reflectance when observed on Landsat TM band 3-4. The regions of higher reflectance are called as' reflectance aureoles' that act as indicators of underground coal fires (Gupta and Prakash, 1998). Prakash and Gupta (1999a) briefly reviewed the potential of shortwave infrared (SWIR) bands in estimating temperatures of high-temperature objects and computed sub-pixel area with corresponding sub-pixel temperature using dual band approach (Landsat TM band 5 and 7). Mapping of coal fires have been periodically executed in JCF to detect subsurface fire using both novel and traditional approaches (Gautam et al., 2008; Mishra et al., 2011; Pandey et al., 2011).

2.5.2 Estimating depth of coal fires in JCF

Evaluation of possibilities and limitations of airborne and space borne remote sensing data to estimate the depth of sub-surface coal fires is a critical issue in coal fire studies. Mukherjee et al., (1991) detected and delineated the depth of subsurface coalmine fires using an airborne multispectral scanner in JCF. The method was based on conductive heat flow mechanism and assuming linear heat flow from subsurface to surface under steady state condition. Prakash et al., (1995a) has further extended method and proposed a conceptual

approach for estimating depth of hot buried features by accounting assumed convective component of heat transfer. The method required a prior knowledge of the heat source (like temperature and time of initiation of fire) and two sets of thermal infrared (IR) data of different time instances for the same anomalous area to compute depth of the buried heat source. Saraf et al., (1995) formulated geometrical method and used Landsat TM thermal infrared data to pinpoint the subsurface fire locations. The depth of the coal fires was computed using field derived information and located coal outcrops on TM visible and near infrared channels (Section 2.4.3).

2.5.3 Coal fire dynamics in JCF

Chatterjee et al., (2006) addressed the retrieval of true spectral radiance from raw digital data using scene-specific calibration coefficients of the detectors and thermal emissivity of surface materials to obtain pixel-integrated kinetic temperature at each ground resolution cell of Landsat TM thermal IR data. The methods also involve field-based modeling to observe lateral propagation of coal fires in JCF. Chatterjee et al., (2007) made an attempt to study the coal fire dynamics of Jharia Coalfield during the 1990s from medium resolution satellite thermal IR data such as Landsat-5 TM and Landsat-7 ETM+ data. The dynamics of coal fire was addressed on the following two aspects: (i) changes in the spatial extent of fire-affected areas, and (ii) propagation of coal fire during the 1990s. The results show a marked decrease in the spatial extent of fire-affected areas during the 1990s. The propagation of coal fire was found to be more erratic than regular in nature and propagate mainly toward south from 1992-1996 and towards north till 2001. Further studies reveal that area affected by the coal fires have been significantly increased by 0.51 km^2 from 2003 to 2006 (Martha et al., 2010). Mapping of coal fires suggests that the west-central and eastern part of the JCF is more affected by coal fires than the western part (Mishra et al., 2014).

2.5.4 Detecting change in land use pattern and land cover studies in JCF

Land use changes are closely associated with coal fires and intense mining activity in a coal mining area. Prakash and Gupta (1998) discussed different Landsat TM false colour composites of bands 4-3-2, 7-5-3 and 5-4-2 in R-G-B combination for identification of various land-use classes. The study also briefly described the time-sequential changes in land-use pattern of JCF from 1990 to 1994. It has been observed that since 1994, approximate 6.9% of the area around JCF has been occupied by mining-related activities that are potentially vulnerable to environmental degradation (Martha et al., 2010).

CHAPTER 3

STUDY AREA: JHARIA COALFIELD, INDIA

3.1 INTRODUCTION

Jharia coalfield (JCF) in India is the prime contributor to the country's economic growth. It has a long mining history and is also famous for the 'coalfield fire' that has been burning underground for nearly a century. This chapter briefly describes the formative aspects of the JCF and discusses its attributes in terms of the location, accessibility, physiography, climate and regional geological set up. Description also elaborates the mining history and current scenario of coal resources available in JCF.

The present chapter portrays the significance of the study area and introduces the insight of 'coalfield fire' as a substantial problem associated with it. The chapter has also laid emphasis on the description of field survey conducted to evaluate various aspects and characteristics of coal fires in JCF. Ground truth observation involves the collection of field data such as (a) thermal profiles measurements to obtain depth function of the coal fires and (b) field photographs showing panoramic view of the major land cover type and coal fire induced geomorphological features recognized in JCF. This chapter has been primarily focused on the description of the field observation that helps to establish a conceptual framework of the situation of coal fires in JCF discussed in the succeeding chapters.

3.2 LOCATION AND ACCESSIBILITY

Jharia coalfield (JCF) hosts the India's largest coal repository, located 260 km NW of Kolkata. The coalfield was named after the main mining centre situated around Jharia township in Dhanbad district of Jharkhand (Figure 3.1). The area is confined between latitude N 23° 38' to 23° 50' and longitude E 86° 08' to 86° 30' with an spatial coverage of 450 km^2 situated at 77m above mean sea level. JCF falls in parts of the Survey of India Toposheet No. 73I/05, 06, 09 and 10. The area is well approachable by the dense mesh network of metalled roads and eastern railway lines. National highway-32, Purulia-Dhanbad road and Dumra-Gomoh road connects the Dhanbad district with other districts of Jharkhand. Dhanbad is the nearest rail head situated about 8 km north of Jharia (Figure 3.2). Other important localities of the area are Baghmara, Katras, Kusunda, Lodna and Sudamdih. These are well connected by local roads

and state highways. The nearest air connectivity are from Birsa Munda Airport, Ranchi and Netaji Subhas Chandra Bose International Airport, Kolkata situated approximately 140 km and 270 km, respectively, from Dhanbad.

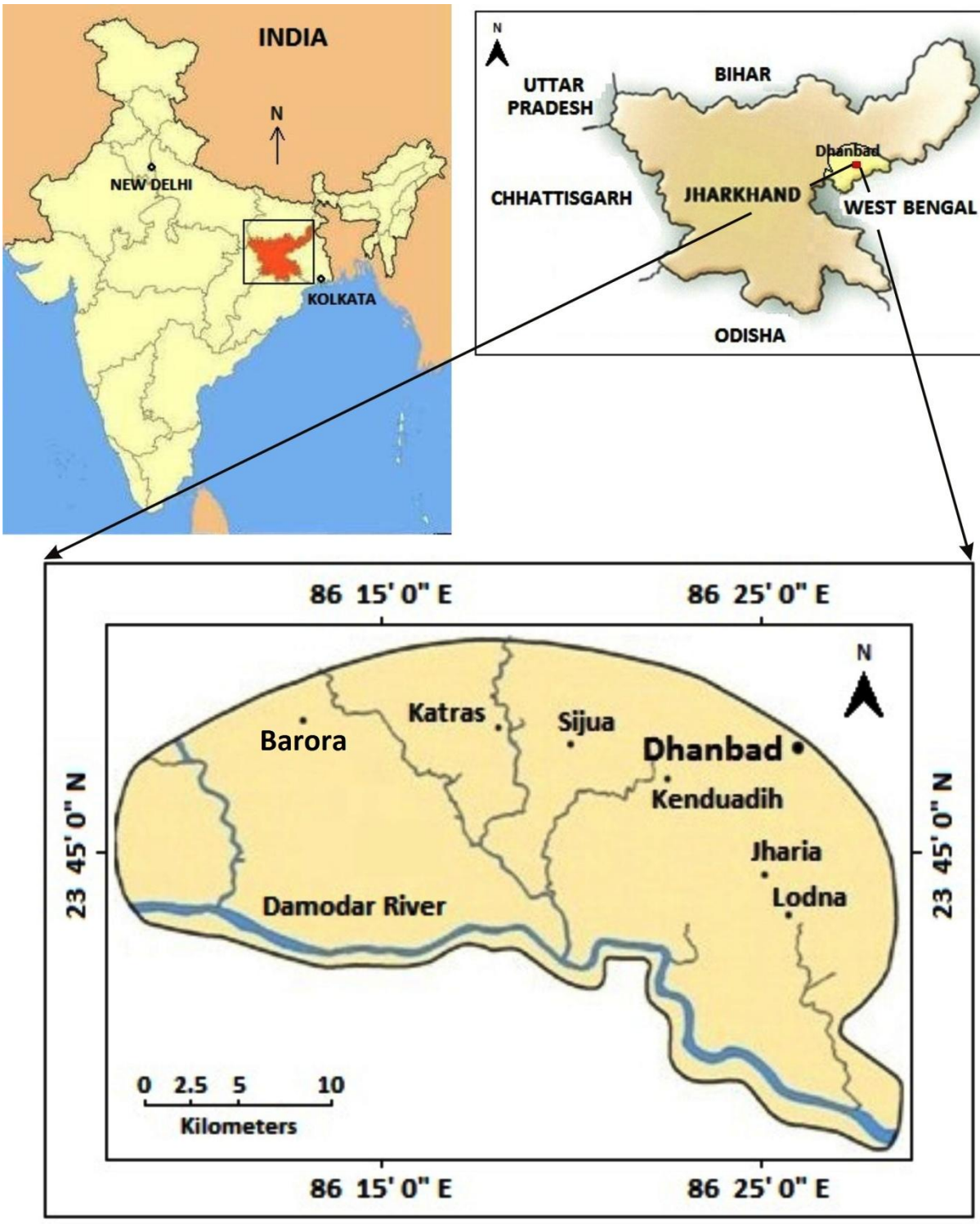

Figure 3.1 Location map ofJharia Coalfield, Dhanbad district, India

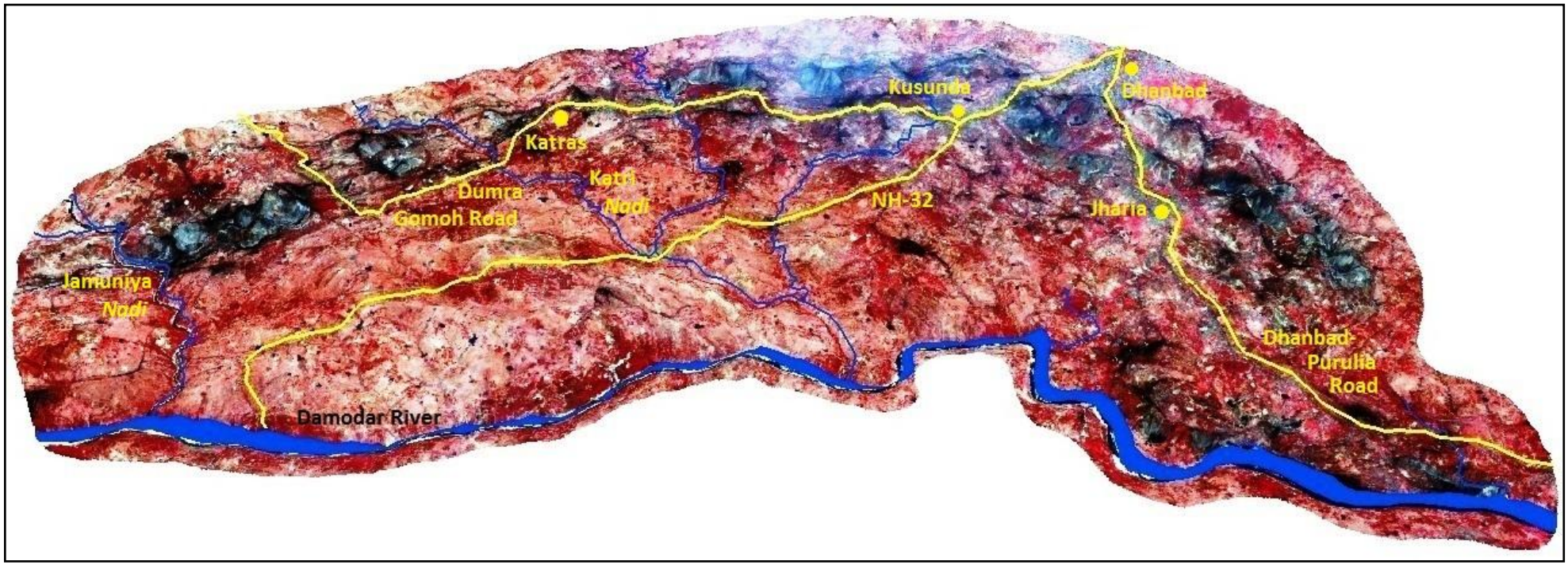

Figure 3.2: A synoptic view of the Jharia Coalfield showing accessibility to the major localities of the study area. The image is generated by draping a standard FCC with band combination 3-2-1 (= R-G-B where R is Near Infrared band, G and Red band, B is Green band) of ASTER image dated 5th February 2004 over the ASTER GDEM covering study area

3.3 PHYSIOGRAPHY AND CLIMATE

Physiographically, JCF extends about 38 km in east-west and 20 km north-south along WNW-ESE trending longest running axis (Chandra, 1992). The area fall under the territory of JCF is mainly occupied by relatively flat topography forming dissected pediplains with minor but consistent decrease in slope from north to south. The evenness in topography is well evident by the representative elevation contours of the area. The highest and lowest elevation of the area ranges between 220 m to 180 m, respectively. The highest elevation in topography has been recorded around Baghmara area located in the westernmost part of the JCF. Whereas, areas such as Bhowrah, Jamadadoba, Sudamdih and Patherdih located in southern and south-eastern part of the coalfield exhibit lowest topography forming relatively low ground. In Jharia, topographic variations are invariably associated with the mining activities. Majority of the opencasts and mine sites are located all along the northern fringe of the JCF. However, due to intense anthropogenic activity, the physiographic status of northern part of the JCF is highly dynamic that significantly changes from time to time.

Jharia coalfield belongs to the Jharia basin, a sub-basin of the Damodar River valley basin. The area is mainly drained by easterly flowing Damodar River and its tributaries namely, Jamuniya *nadi* (river) and Katri n*adi* originating from thenorthern hills of Parasnath and Tundi areas, respectively (CGWB, 2009). The Damodar River is under the control of WNW-ESE trending fault forming southern boundary of the JCF. Drainage in western most part of the JCF is mainly governed by N-S trending Jamuniya *Nadi* and its tributary *nala's* (small streams). Jamuniya n*adi* marks the western boundary of the JCF where it confluences with the Damodar River. Central portion of the JCF is drained by NW-SE and NE-SE trending Kudia *nadi* and Jirian *nala*, respectively. Both of these are the tributaries of NNE-SSW trending Katri *nadi* which joins the Damodar River at south-central part of the JCF. The Damodar together with its all tributaries forms dendritic drainage pattern (Figure 3.2).

Western part of the JCF located around Baghmara is characterized by barren and uncultivable waste covers. The area falls under sub-tropical to semi-arid climatic zone with pleasant weather from the month of July to September and fairly cold winters during November to February touching minimum temperature of 8°C-10°C. It experiences extreme hot climate from April to June reaching to maximum temperature of 42°C-48°C. The JCF receive fairly enough rainfall due to coal dust, which attracts clouds and brings rainfall to the area (CGWB,

2009). The area receives moderate to fairly high rainfall by southwest monsoon from July to September with an average rainfall of 120-140 cm annually.

3.4 REGIONAL GEOLOGICAL SET UP OF THE AREA

Jharia basin is an integral part of the east-west trending discrete Damodar basin. It is WNW-ESE trending slightly elongated basin bounded by a major fault running parallel to the longest axis of the basin toward south. The basin is characterized by a series of numerous intrabasinal faults trending NW-SE to NNE-SSW (Chakraborty et al. 2003). The stratigraphic and structural features of the JCF are briefly described below.

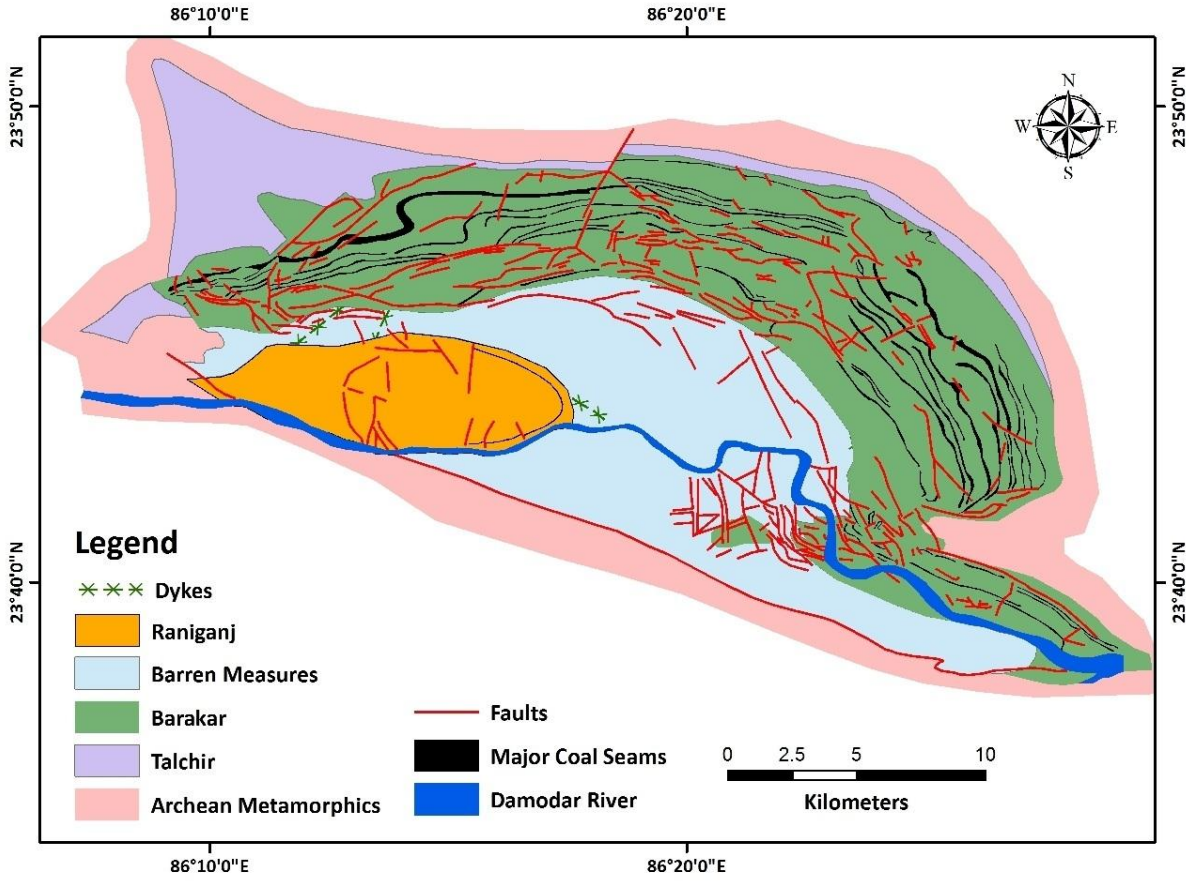

Figure 3.3 Geological map of Jharia Coalfield (CMPDIL, 1989)

3.4.1 Lithostratigraphy and structure

JCF comprises sedimentary litho-package belonging to Gondwana Supergroup of Permo-Carboniferous age. The package is composed of alternating sequence of sandstone and shale with interbedded coal seams of fluvial-lacustrine origin deposited in intra-cratonic archean gneissic basement. The sedimentary succession of the area is unconformably lying over the Archaean metamorphics. The succession comprises Talchir Formation at the base

successively followed upward by the Barakar, Barren Measures and Raniganj Formations. Talchir Formation is fluvio-glacial in origin and well exposed all along the margin of the JCF. Talchir Formation is followed upward by Barakar Formation by an erosion contact. Majority of the regional coal seams of the Jharia basin are restricted only to the Barakar Formation of lower Permian age. Barakar Formation is successive followed upward by Barren Measures which is devoid of any coal seam. Raniganj Formation of Upper Permian age forms the uppermost part of the JCF and occupies the south-western part of the Jharia sub-basin.A synoptic view of region geological set up of the JCF is shown in Figure 3.3. The detailed litho-stratigraphic succession of the Jharia Coalfield has been given in Table 3.1.

Structurally, the area has been deformed considerably to form broad gentle syncline plunging toward west with axis trending toward ESE-WSW. The deformations have modified the coalfield to occupy the shape of **'sickle'**. The contortions facilitate the regional and local scale folding and faulting in the strata. However, the area does not show any evidence of major tectonic deformation except normal faulting of varying magnitude (Ghosh and Mukhopadhyay, 1985). The lithounits exhibit regional east-west to NW-SE strike with shallow dip of about 3°-8° toward south (Figure 3.4).

Figure 3.4 Alternate bands of almost horizontal dipping sandstone and shale exposed due to mining near Sonardh, area, JCF

Table 3.1 Litho-straigraphic succession of the Jharia coalfield, India (Chandra, 1992)

Age	Formation	Litho-type	Maximum thickness
Jurassic / Tertiary		Dolerite dykes	
Lower Jurassic		Mica lamprophyre dykes and sills	
Upper Permian	**Raniganj**	Fine grained feldspathic sandstones, shales with minor coal seams	800 m
Middle Permian	**Barren Measures**	Sandstone, shale and carbonaceous shale	730 m
Lower Permian	**Barakar**	Medium to coarse grained feldspatic sandstone, shale, carbonaceous shale and coal seams	1250 m
Upper Carboniferous	**Talchir**	Boulder bed as base followed by fine grained sandstone and needle shale.	245 m
---------- Unconformity ----------			
Archaean	Metamorphics (gneisses, mica schist and amphibolites)		

3.4.2 Coal seams

In Jharia, 49 coal seams have been recognized of which 26 seams are impersistent and locally mineable (Sengupta, 1980). Rests of the coal seams are regional in extent and mainly confined to the Barakar Formation except three regional coal seams that are lying with in Raniganj Formation of the Jharia basin. Coal seams in JCF have been grouped into 18 major seams (I-XVIII) with individual thickness of 2-18 m (Paul and Chatterjee, 2011). However, the thickness of the coal seam in Raniganj Formation is greatly varied and restricted to less than 2 m in JCF (Chandra, 1992). Jharia coal belongs to medium to high volatile sub-bituminous to bituminous range coal containing 0.13% to 2.81% of moisture, 12.0% to 26.63% of ash, 6.93% to 28.40% of volatile matter and >60% of fixed carbon (Karmarkar et al., 2013).

3.5 MINING HISTORY AND CURRENT SCENARIO

Most of India's coal comes from Jharia. Qualitatively, Jharia coal mines produce bituminous coal and is India's most important storehouse of prime cooking coal that feeds major percentage of the industrial demands. The mining activities in these coalfields had started in 1894 and really got intensified in 1925. In Jharia, majority of coal resources are confined to the shallow depth (discussed in Section 3.6). Hence, because of significantly higher

productivity and less cost inputs, production of coal is majorly performed by opencast activities in JCF. Till 1970, there were many subsidiary coal mines in JCF where the exploration of the coal was dominantly operated by illegal mining sector. To stand up against the industrial crises happened during 1960's and illegal mining, all the subsidiary coal mines in India have been 'nationalized' in 1971 to 1973 and enterprise into the administrative control of 'Coal India Limited (CIL)'. In Jharia, particularly, since 1973, the mining is operated in twelve administrative blocks by 'Bharat Coking Coal Limited (BCCL)' a subsidiary of CIL (BCCL, 2008). Presently, BCCL mainly conduct coal production by large opencast mining due to persistent problem of coal fire associated with it (Figure 3.5). In addition to BCCL, Tata Iron & Steel Company (TISCO) and Indian Iron & Steel Company (IISCO) also operate coal mining in JCF.

Figure 3.5 Intense mining activity in the Moraidih opencast mine, Barora in the JCF

3.6 INVENTORY OF COAL RESOURCE IN JCF

JCF is potentially leading India's coal production as this coal field is the only contributor of the coking coal to meet the exponential demands of energy supply for industrial growth in the country. Out of the total 32,073.32 mt resource of coking coal available in India, the prime, medium and semi-coking types of coals are together contributed 5,313.06 mt, 25,053.13 mt and 1,707.13 m, respectively (GSI, 2004). In JCF, total resources of both coking and non-coking coal are confined within the depth of 1200 m. Out of which 73.1% (14212.42

mt) of the resource is confined to 0-600 m depth. In addition, depth-wise breakup of the total resource of coking coal reveals that about 75.1% (4039.41 mt) of proved resource of coking coal exists up to 0-600 m depth level (GSI, 2004). Total resources of different types of coal available in JCF are shown in Table 3.2.

Table 3.2 Total resources of different types of coal in Jharia coalfield, India (GSI, 2004)

Type of coal	Depth(m)	Proved	Indicated	Inferred	Total
Prime Coking	0-600	4039.41	4.01	0.00	4043.42
Prime Coking	600-1200	574.94	694.70	0.00	1269.64
Total Prime Coking	**0 - 1200**	**4614.35**	**698.71**	**0.00**	**5313.06**
Medium Coking	0-600	4064.18	2.82	0.00	4067.00
Medium Coking	600-1200	296.30	1800.70	0.00	2097.00
Total Medium Coking	**0 - 1200**	**4360.48**	**1803.52**	**0.00**	**6164.00**
Non Coking	0-600	5606.74	495.26	0.00	6102.00
Non Coking	600-1200	496.00	1355.00	0.00	1851.00
Total Non Coking	**0 - 1200**	**6102.74**	**1850.26**	**0.00**	**7953.00**
Total	**--**	**15077.57**	**4352.49**	**0.00**	**19430.06**

Uniqueness of the JCF can be determined in such a way that it is the only sole repository of the prime coking coal in India. When comparing it with worldwide occurrences of the coal deposits, this coalfield is relatively very limited in spatial extent but characterized by multiple closely spaced composite coal seams of up to 12-14 m in thickness causing it commercially appealing for mining (Prakash et al., 2013). Due to this reason, this coalfield was haphazardly exploited by illegal mining activities before nationalization. Impracticable and uncontrolled mining activities in Jharia over last more than hundred years left exposed coal seams susceptible to fire and hence making it one of the densest congregations of the coalfield fire in the world.

3.7 COAL FIRES IN JCF

Indian coal mining has been one of the most disaster prone industries which have witnessed numerous severe accidents leading to repeated loss of life and energy resources. Jharia has a long mining history but is also famous for coalfield fire that has been burning underground for nearly a century (Munshi, 1995; Michalski et al. 1997). It has hosted maximum number of known coal fires among all coalfields in India. The first incidence of fire

was reported from XIV seam of Bhowrah colliery in 1916 (BCCL, 2008). In 1972, it was estimated that, out of 158 known occurrences of coal fires in Indian coalfield, 96 are reported to occur in JCF (Sinha, 1986). Presently, coal fire has been reported to occur in all components of the coal mines including opencasts, underground mines and accumulated overburden coal dumps. In JCF, coal fire is occurring at both surface and shallow subsurface level. Fire is mainly confined to the coal seam X and XIV-XVIII and occurs up to maximum depth of 110-130 m (Chandra, 1992). At present, nearly 67 active fire sites have been reported from 23 large underground and nine large open cast mines in JCF. Status of the fire in different coal seams of JCF has shown in Table 3.3. It has been estimated that about 37 mt of good quality prime coking coal has been destroyed and about 1864 mt of coal has been locked up due to these fires (BCCL, 2008). BCCL (2008) published the map showing coal fire distribution in JCF (Figure 3.6). Fires is actively spreading over an area of app. 17.5 km^2 and hence considered to be the potential source of disaster in and around the area.

BCCL, the competent authority, has implemented several measures to control fire with some conventional methods in JCF. The efforts extinguished ten fires completely and frame nine fire sites at dormant stage (BCCL, 2008). Some common method practiced to control fire in JCF include total excavation and isolation by trenching, surface sealing by soil or dump, cooling by water of foam, gas injection and chemical treatment through borehole etc. (MINENVIS, 2001; Michalski, 2004; Figure 3.7).

3.7.1 Characteristics of coal fires and associated geomorphic features observed in JCF

The existences of surface and subsurface fires have both short and long term impacts on the environment. A typical coal mine area is apparently characterized by exposed coal seams, accumulated mine dumps and very importantly ‘surface-subsurface coal fires’. In JCF, such features are sporadic in spatial extent and vary in dimension from few meters to tens of meters. Distribution and dynamics of surface-subsurface coal fires are strictly controlled by the geology and orientation of the coal seam. Different workers have classified coal fires into different categories depending up on their positions, mode of occurrences, intensity, magnitude and burning state or state of combustion (Genderen and Guan, 1997; Singh, 2013). As mentioned earlier, in JCF more than 75% of the coking coal seams occur at very shallow depth. High carbon content, composite thickness of the coal seams and their exposure to the open environment allow them to catch fire by spontaneous combustion. Unplanned mining activities and excavations in opencasts unveil the burning coal seams in Jharia.

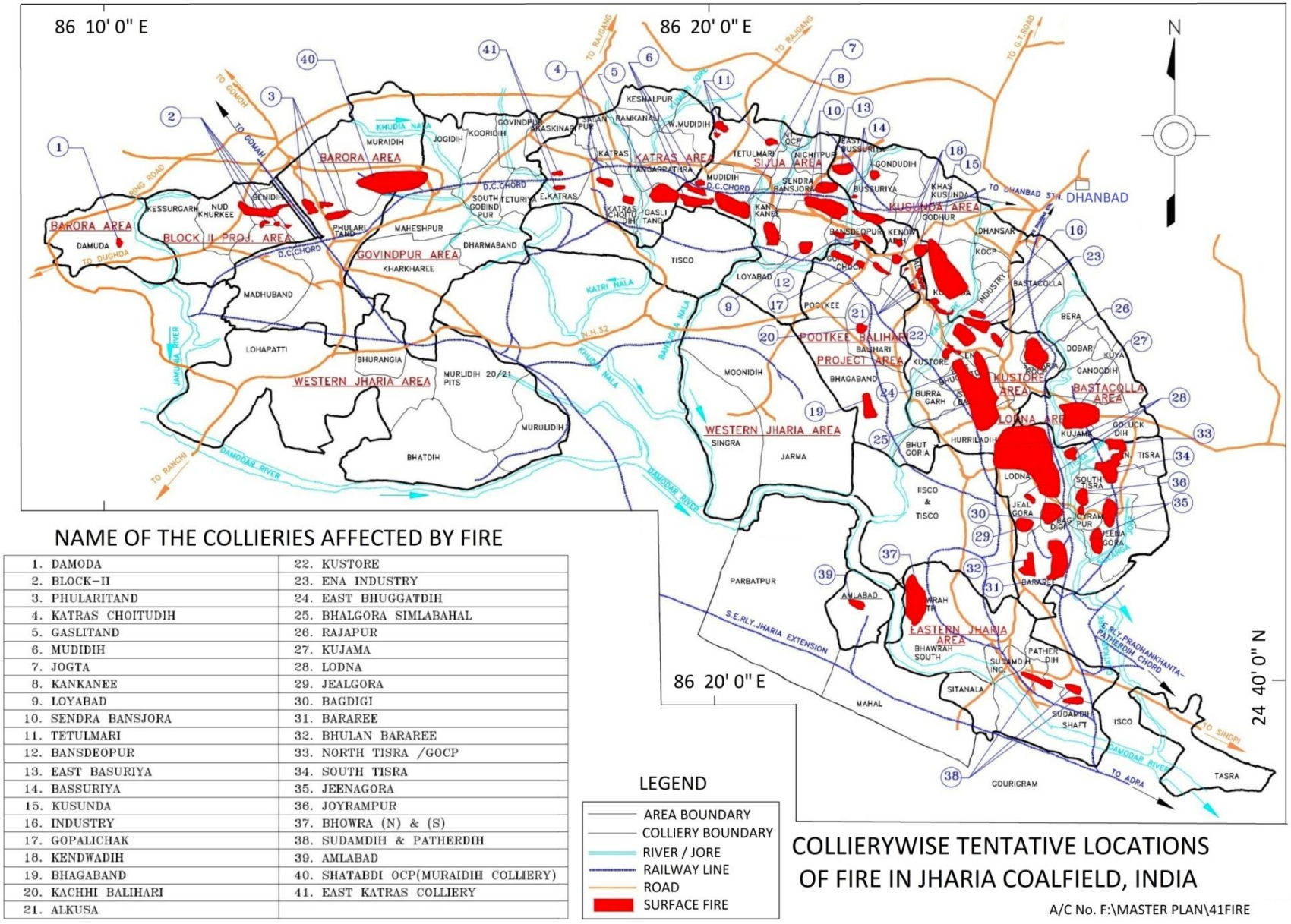

NAME OF THE COLLIERIES AFFECTED BY FIRE

1. DAMODA	22. KUSTORE
2. BLOCK–II	23. ENA INDUSTRY
3. PHULARITAND	24. EAST BHUGGATDIH
4. KATRAS CHOITUDIH	25. BHALGORA SIMLABAHAL
5. GASLITAND	26. RAJAPUR
6. MUDIDIH	27. KUJAMA
7. JOGTA	28. LODNA
8. KANKANEE	29. JEALGORA
9. LOYABAD	30. BAGDIGI
10. SENDRA BANSJORA	31. BARAREE
11. TETULMARI	32. BHULAN BARAREE
12. BANSDEOPUR	33. NORTH TISRA /GOCP
13. EAST BASURIYA	34. SOUTH TISRA
14. BASSURIYA	35. JEENAGORA
15. KUSUNDA	36. JOYRAMPUR
16. INDUSTRY	37. BHOWRA (N) & (S)
17. GOPALICHAK	38. SUDAMDIH & PATHERDIH
18. KENDWADIH	39. AMLABAD
19. BHAGABAND	40. SHATABDI OCP(MURAIDIH COLLIERY)
20. KACHHI BALIHARI	41. EAST KATRAS COLLIERY
21. ALKUSA	

LEGEND

- AREA BOUNDARY
- COLLIERY BOUNDARY
- RIVER / JORE
- RAILWAY LINE
- ROAD
- SURFACE FIRE

COLLIERYWISE TENTATIVE LOCATIONS OF FIRE IN JHARIA COALFIELD, INDIA

A/C No. F:\MASTER PLAN\41FIRE

Figure 3.6 Distribution of coal fires in Jharia Coalfield, India (BCCL, 2008)

Table 3.3 Status of the fire in coal seams distributed in different colliery block of Jharia coalfield, India (BCCL, 2008)

S. No.	Colliery Block	Name of fire	Total no. of fire	Status of the fire
1	Barora (West and East Barora)	Shatabdi V/VI/VII seam	5	Active
		Phularitand X, XI, XII seam fire		
		Damoda V, VI, VII seam fire	-	Dormant
2	Block-II Project	Block-II XII, XI/XII, X Spl. seam fire	1	Active
		Nudkhurkee X seam	-	Extinguished (Surface fire)
		Kessurgarh V/VI/VII seam		
3	Western Jharia-I and II	Moonidih XVII seam	-	Extinguished (Underground fire)
4	Govindpur	Jogidih X seam	-	Extinguished (Surface fire)
		Kooridih X seam		
5	Katras	Katras-Choitudih XIII, XIV, XV seam fire	4	Active
		East Katras XI, XIII, XIV seam fire		
		Gaslitand XVT, XVB seam fire		
		Angarpathra XII, XI, X, IX Spl. seam fire	-	Extinguished (Underground fire)
		East Katras XIV seam		Extinguished (Surface fire)
		West Mudidih IX / X seam		
		Mudidih fire	-	Dormant

6	Sijua	SendraBansjora XIV, XIII, XII, XI, X seam fire	11	Active
		Tetulmari IV, VI/VII seam fire		
		Ekra XI to XIV seam fire		
		Loyabad XV, XIV, XIII seam fire		
		Kankanee XIII, XIV seam fire		
		Bansdeopur XIV, XII seam fire		
		Kendwadih XIII, XIV seam fire	-	Dormant
7	Kusunda	Kusunda XII, XI seam fire	7	Active
		Bassuriya IX to XIV seam fire		
		East Bassuriya V/VI, VIII seam fire		
8	Pootkee-Balihari	Gopalichak XVI, XV, XIV, XIII, XII,XI seam fire	6	Active
		Bhaga XV seam fire		
		Pootkee XV seam fire	-	Extinguished (Underground fire)
9	Kustor	Baniahar XV, XIVA, XIV seam fire	12	Active
		Kustore XI,XII, XIII,XIV, seam fire		
		Alkusa XII, XIV seam fire		
		Ena XI, XII,XIV, XV seam fire		
		East Bhuggatdih XV, XIV seam fire		
		Bhalgora XIV, XV seam fire	-	Dormant
		Simlabahal XIV seam fire		

10	Bastacolla	Kujama IX, X, XI, XII seam fire	2	
		Pure Jharia X seam fire		
11	Lodna	N.S. Lodna XIII, XIIIA, XIV seam fire	14	Active
		BhulanBararee XIII, XIV, VV, XVI seam fire		
		North Tisra VII, VIII, IX, X seam fire		
		South Tisra VII, VIII, IX, X seam fire		
		Bagdigi XV, XIV, XIA seam fire		
		Joyrampur XI, XII, XIII seam fire		
		Jeenagora IX, X, XI,XII seam fire		
12	Eastern Jharia	Bhowra IX, X, XIII, XIV seam fire	5	Active
		Sudamdih IX to XIV seam fire		
		Patherdih IX to XIII seam fire		
		Sudamdih XV seam	-	Extinguished (Underground fire)
		Amlabad XIV seam fire	-	Dormant
		Total number of fire	67	

Figure 3.7 Coal extraction in the Sijua opencast mine in the JCF. Dousing the fire with water, excavating the burning seam and using the unburnt coal are popular means of keeping the coal fire under control (Prakash et al., 2013)

Depending up on their position, burning coal seams are more often categorized into the 'surface coal seam fires' and 'subsurface coal seam fires'. Surface coal seam fires are characterized by the intense and complex system of linear cracks and fissures developed on the surface. The rock units overlying the surface fire are baked, fractured and crumbled. Along these fractures and cracks, certain fumarolic minerals like Salmiac (NH_4Cl) are developed due to high temperature and gaseous influx (Zhang et al., 2004; Figure 3.8). In JCF, 'subsurface fire' occurs at shallow depth of 30-50 m. These may represent as 'shallow subsurface fires'. They are characterized by linear trenches, cracks, cavities and oval pits etc. of varying dimensions as shown in Figure 3.9. Surface manifestation or impression of the 'shallow subsurface fires' suggested that they may occur as disintegrated / discrete patches in the coal seams occurring at subsurface level. Fire not only exists in the in-situ coal seams but also occurs in the stored / piled coal or in overburden dumps. In-situ coal seam fire is characterized by their inherent association with opencasts, encroaching flames and baked overlying rock

units. Excavated overburden dumps may contain carbonaceous shale that may have also perceived fire in some cases (Figure 3.10).

Figure 3.8 Development of fumarolic minerals around gaseous vents (Lodna area, JCF)

Figure 3.9 Development of broad linear crack of approximately 4 m in length and 5-15 cm in width. Degradation of vegetation is also visible. Such features are the surface manifestation of subsurface coal fire occurring underground (Bokapahari, JCF)

Figure 3.10 Massive overburden of waste mine material dumped in and around Alkusa colliery, JCF. The overburden dump also has a lot of carbonaceous material that can catch fire (Prakash et al., 2013)

Subsurface coal fires can also be distinguished on the basis of their intensity which is a function of the depth of fire occurring at subsurface level. Field observations in JCF suggests that the coal fires may categorized into low intensity (when occurring at >40 m depth and having surface temperature less than 40°C), medium (when occurring between 20-40 m depth and having surface temperature less than 40°C-80°C) and high intensity (when occurring at <20 m depth and having surface temperature more than 80°C) depending up on the depth fire from the surface (Section 3.7.2). Active and smoldering fire in coal field may be distinguished on the basis of state of burning. Active coal fires are characterized by intense burning with high flames and smoldering fires are characterized by slow burning with no flame. A brief overview of the classification and characteristics of coal fires as observed in JCF is portrayed in Table 3.4.

Active coal fires are highly dynamic in spatial extent and have significantly modified the geomorphology of the area. These geomorphic features are the surface manifestation of the coal fire occurring underneath. Fire results in volume reduction of the underlying coal seam and leads to the development of intense system of linear cracks and fractures developed over the surface. With increasing intensity of burning, overlying bed rock is collapsed and form certain geomorphic features such as fractures, linear vent, pits etc. on the surface.

Table 3.4 Classification and characteristics of coal fires as observed in Jharia coalfield, India

	Basis of classification	Type of fire	Characteristics of coal fires
Coal fire	**Position**	**Surface coal seam fire**	Extremely high surface temperature.
			Sharp and distinct thermal anomaly across the surface.
			Manifested by intense and complex system of linear crack and fissures of varying dimension from few meters to tens of meters.
			Baked, fractured and crumbled overlying rock units.
			Development of fumarolic minerals along the cracks and fissures.
			Completely destroyed the infrastructure and formed rugged landscape.
			Evident by land subsidence.
			Surface is devoid of vegetation due to completely drying of soil moisture contents.
		Subsurface or shallow subsurface coal fire	Low to moderate surface temperature.
			May missed some minor thermal anomalies whose temperature lies in closed association with background temperature.
			Sparse vegetation on the surface.
			Manifested by smoke emitting linear trenches, cracks, cavities and oval pits of varying dimensions developed on the surface.
			Linear trenches, cracks, cavities and oval pits occur as discrete or disintegrated patches on the surface.

Coal fire	**Mode of occurrence**	**In-situ coal seam**	Visible and exposed only in longitudinal or bench section of an opencasts
			Coal seam burn with encroaching flames.
			Baked overlying rock units.
		In coal stock	Excavated coal is heap up together. It may catch fire due to high carbon content of coal.
		In overburden dumps	In freshly excavated material has been dumped in the vicinity of opencast. Overburden dump also has a lot of carbonaceous material that can also catch fire.
	Intensity, magnitude and depth	**Low intensity coal fire**	Occurring at depth of >40 m with surface temperature less than 40°C.
		Medium intensity coal fire	Occurring between 20-40 m depth with surface temperature less than 40°C-80°C.
		High intensity coal fires	Occurring at depth of <20 m with surface temperature more than 80°C.
	State of combustion and burning	**Active fire**	Commonly observed in exposed in-situ coal seams.
			Coal is burn with encroaching flame.
		Smouldering fire	Mainly in coal dump and subsurface coal seams.
			Slow burning with no flame.

These features have been well recognized in JCF. It has observed that collapsing of burning coal seams is closely associated with uncontrolled subsidence. Intensity of destruction can be well evident near, Bokapahari area in JCF where coal fires induce uncountable devastation by uncontrolled subsidence. Fire completely damaged the infrastructure (Figure 3.11) in and around the area by propagating along the dip of the coal seams. Numerous sympathetic cracks and fractures have been developed parallel to the strike of the coal seams. These cracks are varying in dimension from 40-100 m in length and only few inches to feet in thickness. This intense system of fractures had transformed the area into a rugged landscape (Figure 3.12) and closely reflects the impact by very shallow subsurface or surface fire occurring at 10-12 m depth.

Smoke emitting along the linear pits and oblong vents of varying dimensions are observed near Sijua area, JCF. Such features occur as discrete patches over the surface lying approximately 30 m above the burning coal seams. These features represent the characteristics of subsurface or shallow subsurface fire.

Figure 3.11 Shallow subsurface coal fires cause uncontrolled subsidence. The destabilization of land also causes damage to existing infrastructures. Here, massive cracks can be seen running through a main wall in the remains of a house. The longer crack is about 2.5 cm wide in most places (Prakash et al., 2013)

Figure 3.12 Rugged landscapes in the Bokapahari area, JCF, due to mining and coal fire-induced uncontrolled subsidence. The surface contains fissures of all dimensions. This photograph was taken looking south (Prakash et al., 2013)

3.7.2 Temperature measurements and ground based observations in JCF

Thermal anomalies are the surface expression of existing coal fire and may be reflected in thermal profiles measurement across certain geomorphic features mentioned in Section 3.8.1. These surface expressions are controlled by the temperature, depth and size of fire occurring beneath and hence, considered to be the prime function for analysis of dynamics, intensity and extent of fire (Prakash and Gupta, 1999a; Rosema et al., 1999). However, temperature measurement in a coalfield is also a difficult task as the areas are often inaccessible due to uncontrolled nature of coal fires. During field survey, thermal data and information about other feature classes were collected for validation of the results obtained from satellite data (Figure 3.13(a)-(c), Table 3.5).

Ground truth information of the coal fires in JCF was obtained from the field based observations using portable thermometer. Surface signals are actively contributed by the effect of solar heating. Due to this reason, field survey was conducted during the month of February and December, 2010 to enhance the compatibility for validation of the results obtained from satellite data and to minimize the probability of getting misleading results.

Figure 3.13(a)-(c) Temperature measurements using a portable field thermometer in the field (a) showing 34°C temperature on the surface, (b) 131°C temperature of smoldering fire in the crack (c) 396°C temperature of a burning coal seam (measured from approximately 30 m distance) (Photo courtesy by Ms. Varinder Saini, December, 2012)

To observe the coal seam fire in an exposed scenario, the field work was exclusively carried out in Sijua area of JCF. An approximately 30 m thick complete lithological section exposed in an opencast site near Sijua Colliery, Tetulmari (N 23° 48’ 21.1” / E 86° 19’ 53.76’’) was selected for thermal profile measurement. A schematic diagram and corresponding field photographs displaying the synoptic view of the Sijua opencast in an exposed scenario is shown in Figure 3.14 (a) and (b), respectively. The site selected was underground mine initially but later turned into an opencast due to uncontrolled subsurface coal seam fire.

Table 3.5 Details of field observations carried out in Jharia Coalfield, India

S. No.	Site	Latitude (N)	Longitude (E)	Surface temperature range (°C)	Land cover type
1	Bokapahari	23° 45' 9.2"	86° 25' 4.2"	43.6 - 71.2	Area of intense shallow subsurface fire with sparse vegetation. Linear cracks have developed parallel to the strike of coal seams. Destruction of nearby infrastructure.
2	Baghadih	23° 43' 50.2"	86° 24' 52.8"	22.7 - 39.5	Subsidence area with sparse vegetation.
3	Lodna	23° 42' 58.0"	86° 25' 17.5"	42.8 - 122.1	Overburden dump site. Anomalies are due to dump fire and subsurface fire with surface temperature ranges from 165.2°C - 332.4°C at places.
4	Sudamdih	23° 40' 1.5"	86° 25' 19.8"	32.2 - 42.2	Anomalies are due to subsurface fire. Open cracks and smoke emitting vents are well recognized around the area.
5	Bhowra	23° 41' 2.3"	86° 23' 29.9"	41.5 - 76.8	Overburden dump site. Anomalies are due to smoldering fire in dump.
6	Tetulmari, Sijua	23° 48' 24.8"	86° 19' 57.8"	39.8 - 85.4	Opencast mine. Anomalies are due to high intensity burning coal seam fire (217.0°C -254.5°C) exposed due to intense mining activity. Linear cracks, vents and sinkhole are developed on the surface.

7	Bansjora	23° 47' 41.8"	86° 20' 40.1"	24.3 - 26.4	Overburden dump site.
8	Kankani	23° 46' 42.2"	86° 20' 45.1"	32.5 - 101.3	Opencast mine. Minor thermal anomalies due deep subsurface fire.
9	Dhansar	23° 46' 29.8"	86° 24' 33.2"	27.4 - 30.9	Overburden dump site. Sparse vegetation.
10	Kusunda	23° 46' 57.2"	86° 23' 36.7"	32.5 - 59.0	Overburden dump site. Minor anomalies due deep subsurface fire. Surface fire also observed in and around the area.
11	Baseria	23° 47' 10.6"	86° 22' 30.2"	37.8 - 41.4	Overburden dump site.
12	Kenduadih	23° 46' 18.7"	86° 22' 27.3"	26.6 - 28.7	Underground mine. No subsurface fire.
13	Alkusha, Kustore	23° 45' 40.6"	86° 23' 26.3"	34.3 - 38.8	Overburden dump site.
14	Karkenda	23° 46' 12.1"	86° 22' 14.7"	32.3 - 33.1	Opencast and overburden dump site.
15	Murlidih, Baghmara	23° 43' 52.2"	86° 16' 22.2"	27.3 - 33.0	Underground mine. Relatively dense vegetation at the surface.
16	Phularitand	23° 46' 4.7"	86° 13' 53.7"	23.4 - 24.6	Opencast and overburden dump site.
17	Sunardih	23° 47' 46.7"	86° 15' 45.6"	36.7 - 42.1	Abandoned mine.
18	Barora	23° 47' 40.7"	86° 14' 46.7"	42.6 - 46.8	Opencast mine. Surface fire in in-situ coal seam. Smoldering fire in dump.

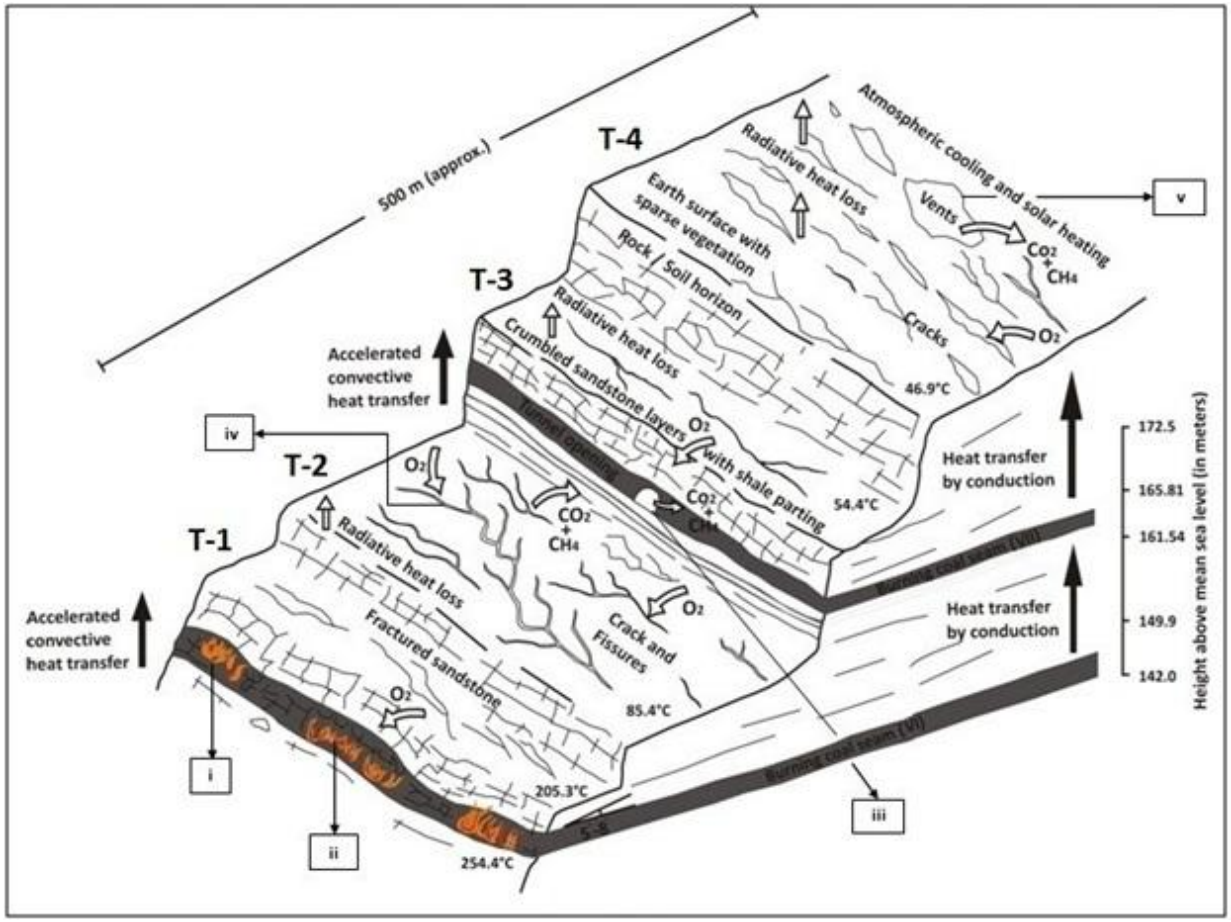

Figure 3.14(a) Schematic diagram showing synoptic view of the exposed underground coal seam fire in an opencast (Sijua opencast, Tetulamari, JCF)

Two interbedded coal seams (VI and VII from the surface) of approximately 2 m in thickness were recognized at 9.98 m and 30.52 m depth within sandstone striking N70°E-S70°W with 3°-5° very gentle dip toward SSE. Sandstone units above and below the coal seam VII are about 6.98 m and 18.54 m in thickness and capped by approx. 2 m thick pile of sandy soil at the top. Both coal seam VI and VII were observed under the intense and smoldering fire and showing temperature of more than >250°C and >80°C, respectively. Linear cracks, pits, vents and fracture system were intensely developed over the rock surface or terraces due to volume reduction of the underlying burning coal seam. Destruction due to underground coal fire is self evident around the area (Figure 3.15). Temperature measurements were taken at terraces T-4 (Figure 3.16, ground surface) and T-2 (Figure 3.17) using portable field thermometer and thermal profiles have been drawn to analyses the depth function of the thermal anomaly.

Figure 3.14(b) Corresponding field photographs of underground coal seam fire in Sijuaopencast, Tetulamari, JCF. Key: (i) and (ii) Burning coal seams (iii) Gas emanation from the tunnel opening complex system of fractured sandstone beds above the coal seam under fire (iv) Fragility of the landscape and the dangers of working in the area. The long, smoke-emitting linear cracks are clearly visible. (v) Gaseous emission from the vents developed at the surface due burning coal seam at underground

Figure 3.15 A view of a completely burnt outcrop of coal and collapsed strata in the Sijua opencast mine in the JCF. The destruction is self-evident. The horizontal field of view is about 80 m (Prakash et al., 2013)

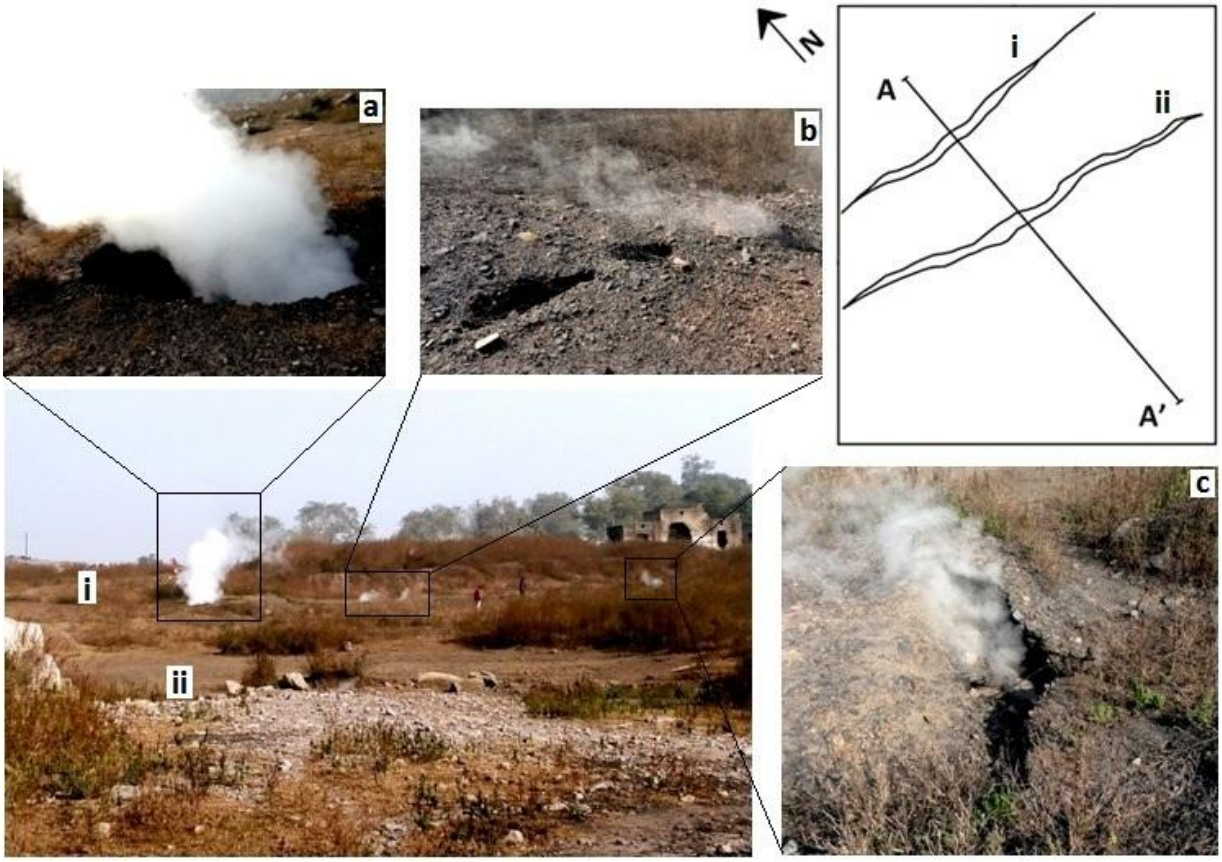

Figure 3.16 Thermal profiles A-A' running across the gas emitting vents and pits developed along the strike of the coal seam at T-4 (terrace 4, ground surface) located south of Sijua opencast, Tetulmari, JCF

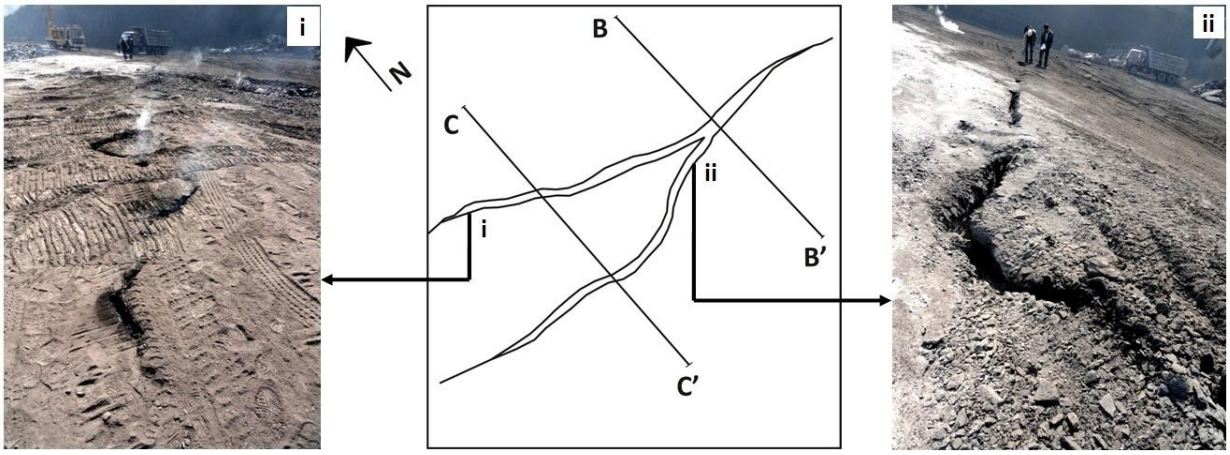

Figure 3.17 Thermal profiles B-B' and C-C' running across the burning coal seam at T-2 (terrace 2) of Sijua opencast, Tetulmari, JCF

It has been observed that the surface anomaly obtained is the function of depth. For a fire existing at 30 m depth, background temperature may lie close to 30°-35°C (Figure 3.18(a), Profile A-A'). But for a very shallow subsurface fire, it may be 50°-100°C (Figure 3.18(b) and (c), Profile B-B' and C-C'). This was certainly due to decrease in the intensity of heat dissipated from the burning coal seam.

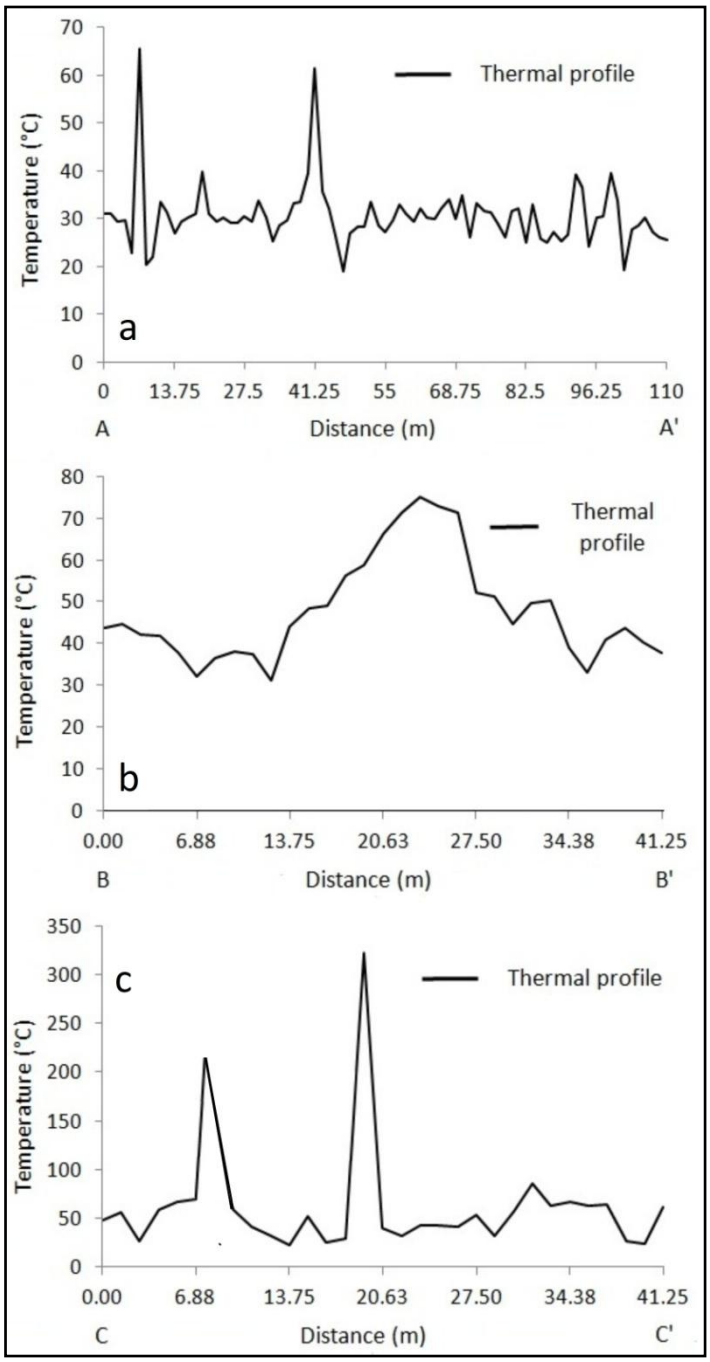

Figure 3.18(a)-(c) Temperature distribution along profile A-A', B-B' and C-C' showing relation between background temperature and thermal anomalies obtained at T-4 and T-2 (terrace 4 and 2)

3.8 CONCLUSION

In the present chapter, the attributes and mining scenario of the JCF have been discussed. Field work around JCF had been executed to observe the features associated with surface-subsurface coal fires. Area exposed around East Barora, Katras, Sijua, Kusunda, Kustor, Bokapahari, Bastacolla and Lodna collieries are significantly affected by fire. Surface or very shallow surface fires were precisely analyzed in JCF. The emphasis was mainly laid on to the collection of thermal data around Sijua and Bokapahari area. Observations suggest that the fires in coal seam occur as segregated patches and not extending in few meters to tens of meters in spatial extent. It has also been observed that the fire occurring at 10-12 m depth results in the development of fairly large elongated linear cracks on the surface. Coal fires occur at more than 30 m above the burning coal seams have been manifested only by small pits, cracks, sinkhole and likewise features. Magnitude of the burning coal seam, depth of the coal seam from the surface and intensity of the dissipated heat from it are the crucial factors that trigger the development of coal fire related features on the surface. Precise observation and recognition of such features may help to decipher the attributes of fire occurring beneath.

CHAPTER 4

DATA ACQUISITION, PROCESSING AND METHODOLOGY OVERVIEW

4.1 INTRODUCTION

This chapter gives an account of the different types of datasets used in the present study. The chapter provides an overview of processing of the satellite datasets and methodology adopted for the mapping of coal fires in Jharia Coalfield (JCF), India. The description of the datasets briefly discussed the specification details of the satellite data and their effectiveness being chosen in the present work. Processing of the satellite data is pre-requisite of remote sensing based studies. The chapter elaborates the processing techniques employed over the data for geometric and radiometric corrections and also discussed the quantitative method to calculate temperature distribution using sensor calibration. At last, a general overview of the methodology has also been portrayed. The aim of the chapter is to discuss how the datasets have been prepared for further analysis and interpretation as per the objective of the present work.

Table 4.1 Type of the data used in the present study

Remote sensing data	Ancillary data	Field data
Landsat TM/ETM+ (six sets temporal images)	Topographical maps of 1:50000 scale (73 I/1, 73 I/2, 73 I/5 and 73 I/6)	GPS data
ASTER (three sets of temporal images)	Geological map	Field Photographs
	Fire distribution map	Geological data
	GoogleEarth^{TM} reference image	Temperature measurement
	ASTER GDEM	
	Other published records etc.	

4.2 DATA SOURCES

In the present work, different types of the data have been procured and categorized into remote sensing data, ancillary data and field data (Table 4.1). Remote sensing data includes Landsat TM/ETM+ and ASTER images of the study area (Figure 4.1). Ancillary data used in the present work includes Survey of India (SOI) Toposheets nos. 73 I/1, 73 I/2, 73 I/5 and 73 I/6 on 1:50,000 scale, geological and fire distribution maps from different agencies and other

published records etc. Field data includes collection of the information about geology, land use-land cover and coal fires distribution around the area. However, emphasis has been mainly laid on to the temperature measurements and collection of field photographs of the coal fire related features. The data used in the present study have been further elaborated below in detail.

Table 4.2 Specifications of the remote sensing data sets used in the present study (Chander et al., 2009; Abrams et al., 1999)

Satellite / Sensors	Spectral Bands	Spectral interval (μm)	Central wavelength (μm)	Spatial Resolution	Radiometric Resolution
Landsat TM / ETM+	**Band 1**	0.452 - 0.514	0.483	30 m	8-bit
	Band 2	0.519 - 0.601	0.560		
	Band 3	0.63 - 0.692	0.662		
	Band 4	0.772 - 0.898	0.835		
	Band 5	1.547 - 1.748	1.648		
	Band 6	10.31 - 12.36	11.335	60 m	
	Band 7	2.065 - 2.346	2.206	30 m	
	Pan	0.515 - 0.896	0.706	15 m	
TERRA / ASTER	**Band 1**	0.52 - 0.60	0.56	15 m	8-bit
	Band 2	0.63 - 0.69	0.66		
	Band 3	0.76 - 0.86	0.81		
	Band 4	1.60 - 1.70	1.65	30 m	
	Band 5	2.145 - 2.185	2.165		
	Band 6	2.185 - 2.225	2.205		
	Band 7	2.235 - 2.285	2.260		
	Band 8	2.295 - 2.365	2.330		
	Band 9	2.360 - 2.430	2.395		
	Band 10	8.125 - 8.475	8.291	90 m	12-bit
	Band 11	8.475 - 8.825	8.634		
	Band 12	8.925 - 9.275	9.075		
	Band 13	10.25 - 10.95	10.657		
	Band 14	10.95 - 11.65	11.318		

4.2.1 Remote sensing data

Coal fires are the thermal phenomenon and hence can be potentially detectable in the thermal infrared region (TIR) of the electromagnetic (EM) spectrum. Hence, the present study has been exclusively focused on the thermal remote sensing data. Landsat TM/ETM+ and ASTER have been significantly used in the recent past for detecting thermal response and discussed earlier in detail (see section 2.5). Wide applicability and potential of the Landsat TM/ETM+ and ASTER sensors to receive emission response have made an obvious choice of

using them for mapping of coal fires in JCF. Specifications details of Landsat TM/ETM+ and ASTER sensors have been shown in Table 4.2. Details of the remote sensing datasets are discussed below:

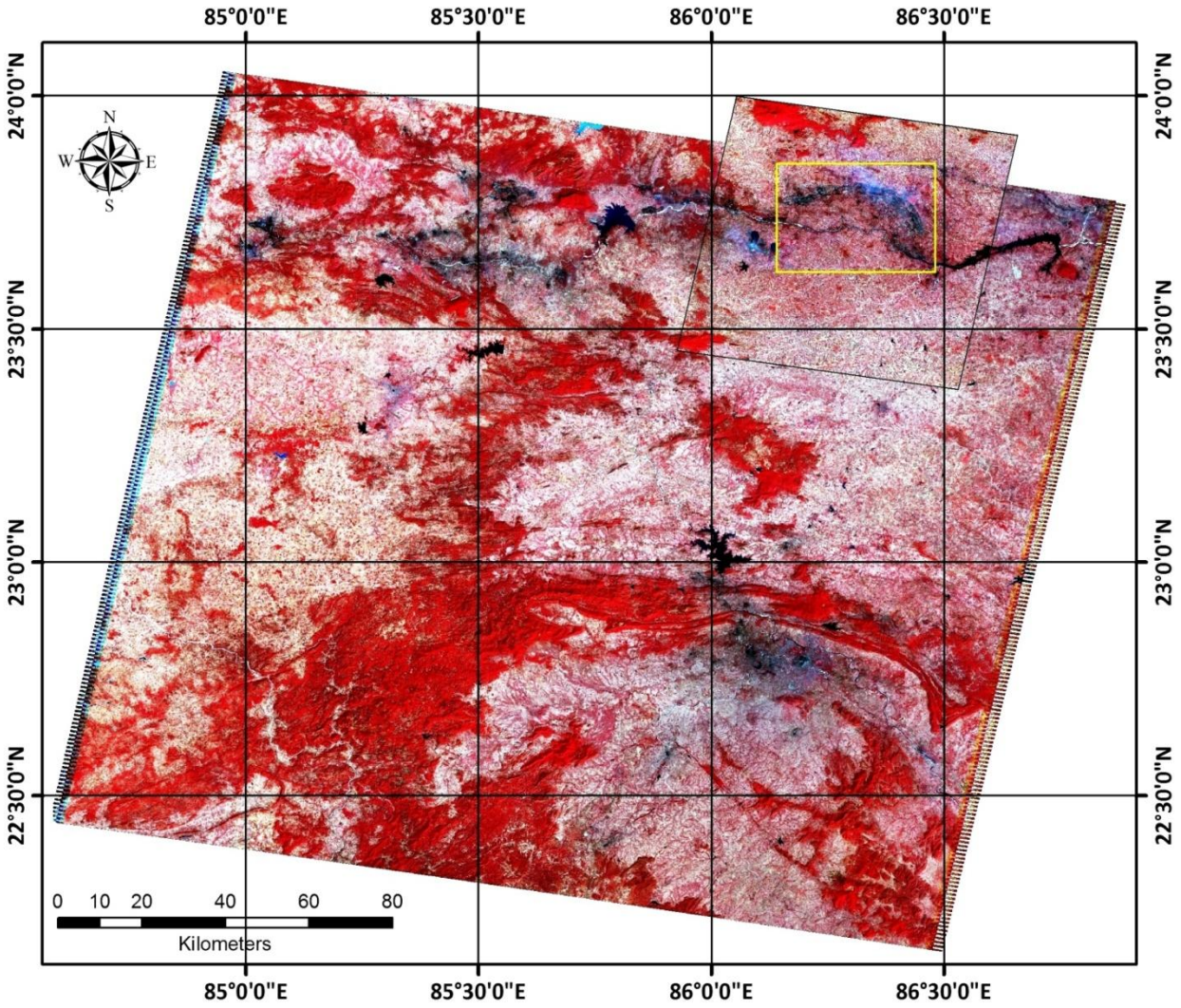

Figure 4.1 An overlay of the rectified ASTER images (60 km swath, 3-2-1 FCC) with Landsat ETM+ (183 km swath, 4-3-2 FCC) image covering JCF. The target area is marked under yellow square

4.2.1.1 *Landsat data*

Landsat satellite provides the longest repetitive coverage of the earth observation through TM/ETM+ sensors. The Landsat TM/ETM+ sensors on-board Landsat TM and ETM+ have spatial resolution of 30 m and 60 m for reflective bands and emission band, respectively, with 12-bits quantization level. Landsat ETM+ also has a panchromatic (pan) band of 15 m resolution (Table 4.1). Day time data have significant contribution by solar heat flux and considered less advantageous over night-time data (Prakash et al., 1999b). Due to unavailability

of the night-time data, six sets of cloud free day-time systematically corrected (geometrically and radiometrically corrected) Level-1G images from 2000 to 2010 covering the proposed study area have been procured from USGS Global Visualization Viewer (GloVis) archive (http://glovis.usgs.gov/data_access*)*. Beside, six Landsat data covering JCF, two sets have been also acquired covering Ruqigou Coalfield, Ningxia, China (discussed in Chapter 5). All images are geo-referenced to the Universal Transverse Mercator projection (UTM) system. The images acquired at predawn time between November to February months have been preferably selected (Table 4.3). In Indian subcontinent, these months are the coldest season and effect of the seasonal heating is considered to be minimum during this period. Moderate spatial resolution of Landsat thermal band and short revisit time potentially facilitate the temporal monitoring of fire in a coal fire affected area.

Table 4.3 Details of the scene ID and acquisition time of the data used in the present study

Study area	ASTER scene ID	Time	Acquisition date
Jharia Coal Field, India	L71140044_04420001217	Day	17th December 2000
	L71140044_04420011102	Day	02nd November 2001
	L71140044_04420021207	Day	07th December 2002
	L71140044_04420030329	Day	19th March 2003
	L5140044_04420091202	Day	02nd December 2009
	L5140044_04420100220	Day	20th February 2010
Ruqigou Coal Field, Ningxia, China	L71129033_03320001017	Day	17th October 2000
	L5129033_03320061010	Day	10th October 2006
Jharia Coal Field, India	AST_L1A_00311242000050737_04062003143049	Day	24th November 2000
	AST_L1A_00302052004045511_02162007095936	Day	05th February 2004
	AST_L1A_00303192008045415_04172009132739	Day	19th March 2008
	AST_L1A_00311820091632463_11250009543938	Day	18th November 2009 (only VNIR and TIR datasets are available)

4.2.1.2 *ASTER Data*

The Advanced Spaceborne Thermal Emission and Reflection Radiometer (ASTER) sensor is a collaborative campaign of NASA and Japan's Ministry of Economy. It is onboard the Terra satellite launched in December 1999 and has specifically designed to obtain information about emission and reflectance component of the surface features. Processed products of the ASTER datasets have been distributed by USGS Land Processes Distributed

Active Archive Center (LP DAAC) archive. ASTER registers the spectral response in three VNIR, six SWIR and five TIR channels functioning in 0.52 μm to 0.86 μm, 1.60 μm to 2.43 μm and 8.125μm to 11.65μm, respectively. The ASTER Level 1A data product is the raw unprocessed data. Level-1A data contain geometric and radiometric calibration coefficients. The ASTER Level-1B is the on demand at sensor registered radiance product that contains radiometrically calibrated and geometrically co-registered data produced by applying the radiometric calibration and geometric correction coefficients to the Level-1A (Abrams et al., 2009).

Specification detail of the ASTER has potentially suggested its wider applicability to the earth observation. ASTER VNIR and SWIR are calibrated on 8-bits quantized level. As compared to the other available land imaging sensors, TIR dataset of the ASTER has high spectral, moderate spatial resolution and high radiometric resolution with 12-bit quantification level. Moreover, fairly high spatial resolution of VNIR data can also be used in association TIR data to obtained information about different feature class. Such uniqueness has shown the superior capability of the ASTER data over other available multispectral sensor for land surface studies especially monitoring thermal phenomenon like coal fires. Thus, for present work, three sets of Level-1A cloud free, day time ASTER data covering proposed study area dated 2000, 2004 and 2008 have been acquired from the LP DAAC archive (https://lpdaac.usgs.gov/data_access) in HDF format (Table 4.3). Obtained datasets are *g*eometrically co-registered and radiometrically corrected. Both Landsat TM/ETM+ and ASTER images have been further processed and applied in estimating temperature distribution of coal fires in JCF through time.

4.2.2 Ancillary data

Ancillary data used in the present work constitute topographical maps of 1:50000 scale published by Survey of India (SOI) during 1978. The topographical maps published by SOI were based on Everest Datum and Polyconic Projection system. The area attributed to JCF falls in toposheets nos. 73 I/1, 73 I/2, 73 I/5 and 73 I/6. All topographical maps were precisely scanned, georeferenced and reprojected in Geographical Latitude / Longitude Coordinate System with World Geodatic System 1984 (WGS 84) datum. The maps were subsequently mosaicked and target area was subset to create a base map of the study area. However, as mentioned earlier that in the present work geometrically corrected satellite data (L1G Landsat TM/ETM+ and L1A ASTER datasets) have been used. The produced base map is paired with

handheld Global Positioning System (GPS) device, and used in field work for route planning and to obtained detailed information of the geographic location of the coal fires and other associated land cover features in JCF.

The present work is also supplemented with various thematic maps such as geological map (CMPDIL, 1989), fire and colliery distribution maps (BCCL, 2008) of the JCF. The study and interpretation of these thematic maps can significantly help to establish a brief overview of the various aspects of the JCF (discussed in Chapter 3, Section 3.7). Besides, auxiliary data such as GoogleEarth^{TM} image and ASTER derived digital elevation model (DEM) of the JCF have been also used (discussed in Chapter 5, Section 5.5). These datasets together with limited field observation helped to support the analysis and interpretation of the present work.

4.2.3 Field data

Collection of field data is an essential component of the remote sensing based studies. Field based observations not only help to validate the results obtained from the analysis of satellite data but also provide a synoptic view of the problem like coal fires at ground level. During present work, two field campaigns were planned in and around JCF. The first field survey was a reconnaissance survey carried out during February 2010 to visualize the severity and mark the geographic locations of the coal fires affected areas in JCF. Detailed informations about other feature classes recognized in JCF were also collected during field work.

Second survey was conducted during December 2010 emphasized mainly on to collect the temperature data for thermal profile measurements. During field surveys, two sites namely, Bokapahari and Sijua opencast, near Tetulmari area in JCF were found to be intensely affected by surface-subsurface coal fires. Photographs collected during the field work around Bokapahati area self explain the devastation due to coal fires. A complete depth wise vertical-log of the in-situ coal seam fire was found exposed in the Sijua opencast. This site has been preferably selected for thermal profile measurements. Actual scenario and ground based observations of various aspects of the coal fires in JCF along with field photographs have been precisely discussed in Chapter 3, Section 3.7.

4.3 SOFTWARE USED

Processing of the satellite datasets have been done using available image processing software packages like ERDAS Imagine^{TM} 9.3, 2010, ENVI^{TM} 4.7, and ESRI ArcGIS 10. Landsat datasets have been exclusively processed using ERDAS Imagine^{TM}. Reprojection of

the datasets, digital enhancement and other image processing operation has been carried out using 'Data Preparation' and 'Interpreter tool'. Mathematical computations used in the present work have been specifically formulated and solved using 'Moduler' tool given in ERDAS Imagine^{TM}. Similarly, processing of ASTER datasets have been exclusively carried out using Basic Tools' given in ENVI^{TM}. 'Pre-processing' and 'Band Math' operations have been used for necessary correction and processing of the ASTER data. Thematic maps used and portrayed in the present work have been prepared in ArcGIS. Other GIS based operations have also executed in ArcGIS. Besides, CorelDRAW Graphic Suite 13 and Microsoft Office Package have used for editing figures and manuscript.

4.4 METHODOLOGY OVERVIEW

The methodology scheme followed in this research involves acquisition and processing of the satellite data followed by analysis and interpretation of the data for coal fire related studies. The datasets have been processed as per the objectives of the research and described with relevant methodology flowcharts in succeeding chapters. However, a brief overview of the methodology adopted in the present work is as follows:

(a) Extensive literature review on remote sensing and its application in coal fires related studies to identify research gaps and objectives with special reference to JCF.
(b) Procurement of remote sensing and other ancillary datasets.
(c) Pre-processing of remote sensing data involving co-registration of the images followed by the removal of atmospheric contribution to the measured radiant intensity of the image.
(d) Conversion of corrected VNIR and SWIR data to surface reflectance and TIR data to temperature image.
(e) Collection of field data (field photographs and temperature measurements for thermal profile) to observe the characteristics and actual scenario of coal fire in JCF.
(f) Pre-processing followed by the processing and analysis of the remote sensing data.
(g) Based on the research gap, it has observed that there is no method of thresholding has been earlier proposed for delineation of surface coal fire. In the present study, a **'Maximum Reflectance Threshold Method'** has been proposed for delineation of surface coal fire. For this, temporal datasets of Landsat TM/ETM+ band 7 has been extracted and analyzed using several spatial profiles drawn over image subset.
(h) Beside, a novel approach for mapping of surface coal fires using ASTER data has been also proposed in the present study. Spectral reflectance curves for various land cover

features have been drawn and two new normalized ratio indices namely, **Normalized Difference Coal Index (NDCI) and Normalized Difference Coal fire Index (NDCfI)** have been developed for delineation of the pixels attributed to surface coal fires. The approach has been implemented over JCF as test site for mapping of surface coal fire.

(i) Utility of ASTER time series data for temporal monitoring and dynamics of coal fires in JCF has been also investigated during present work. To observe and evaluate the dynamics, coal fire distribution maps for three consecutive years have been prepared. Thermal anomalies due to coal fire have been delineated and mapped using precise thresholding of land surface temperature image.

(j) Finally, interpretations of the results obtained have been carried out and conclusion about of the present scenario of coal fires in JCF has drawn.

4.5 PRE-PROCESSING

Pre-processing of the satellite data is the fundamental requirement of the remote sensing based studies. Pre-processing techniques remove the geometric and radiometric errors from the data for precise analysis of the images. In addition, pre-processing also constitute conversion of the data to physical parameters like reflectance and brightness temperature using sensors calibration. The steps followed during pre-processing are defined by the type of the data used. An overview of the steps followed in pre-processing of the data is shown in figure 4.2.

4.5.1 Geometric correction and co-registration

Digital images recorded by the sensors are generally comprises systematic or non-systematic geometrical distortions. Systematic errors can be compensated by modifying sensors characteristics. Non-systematic distortions are caused by the altitude variation of sensors platform. These errors can be corrected by georeferencing or geo-registration using Ground Control Points (GCPs) where geographical coordinate of a point is assigned to the same point on the image. Georeferencing is the pre-requisite of the image processing and allows the interpretation of the data in same reference system.

As mentioned in Section 4.2.1, here in the present study six sets of systematically corrected L1G Landsat and three sets of L1A ASTER data have been used. Each multi-spectral band of the individual Landsat or ASTER data are geometrically co-registered with each other. However, for temporal monitoring of land surface features like coal fires, such time series

datasets (Landsat or ASTER datasets) of different time and season must be precisely co-registered with each other for better comparison and analysis.

Topographical maps of the JCF were published during 1978. Due to intense mining activity, land cover features around JCF are highly uncertain and suspected to have been changed temporally. Hence, all Landsat datasets (Table 4.1) have been co-registered with reference to the geometrically corrected Landsat 2010 image (base image). For co-registration, first the spatial subsets of the images covering JCF have been extracted. Features like, railway crossings, road convergence or divergences, bridges or platform over river have been carefully observed and selected as control points. In each Landsat data, 37 well distributed GCPs have been picked out and applied for image to image registration using second-degree polynomial transformation. Accuracy of the transformation is defined by root mean square error (RMSE) which has obtained less than 0.23 of a pixel. Finally, co-registered Landsat datasets have been generated using nearest-neighborhood resampling method. Output maps have been reprojected in Geographical Latitude / Longitude Coordinate System with WGS 84 datum and resampled to 30 m spatial resolution.

Similarly, all ASTER datasets used in the present study have been also co-registered with reference to the geometrically corrected ASTER 2008 image (base image). The co-registered ASTER datasets (SWIR and TIR data) have been resampled to 30 m spatial resolution for temporal monitoring of coal fires in JCF (discussed in Chapter 7). The accuracy of the co-registration has been visualized by swiping georeferenced images over corresponding reference base image (Landsat 2010 and ASTER 2008 images). A fair co-registration has been marked by precise spatial matching of the selected feature in all datasets.

4.5.2 Radiometric corrections

Signals received at the satellite sensors are affected by unwanted noise. These noises are induced by sensors sensitivity, topographic relief and atmospheric effects (absorption, scattering, path radiance, decrement of received light). These effects are needed to be removed from the data for the precise extraction of the true spectral response of the feature of interest. Absolute radiometric correction requires information of sensors calibration, topographical characteristics and atmospheric parameters (transmittance and upwelling radiance). Detailed description of the radiometric pre-processing of the datasets is given below.

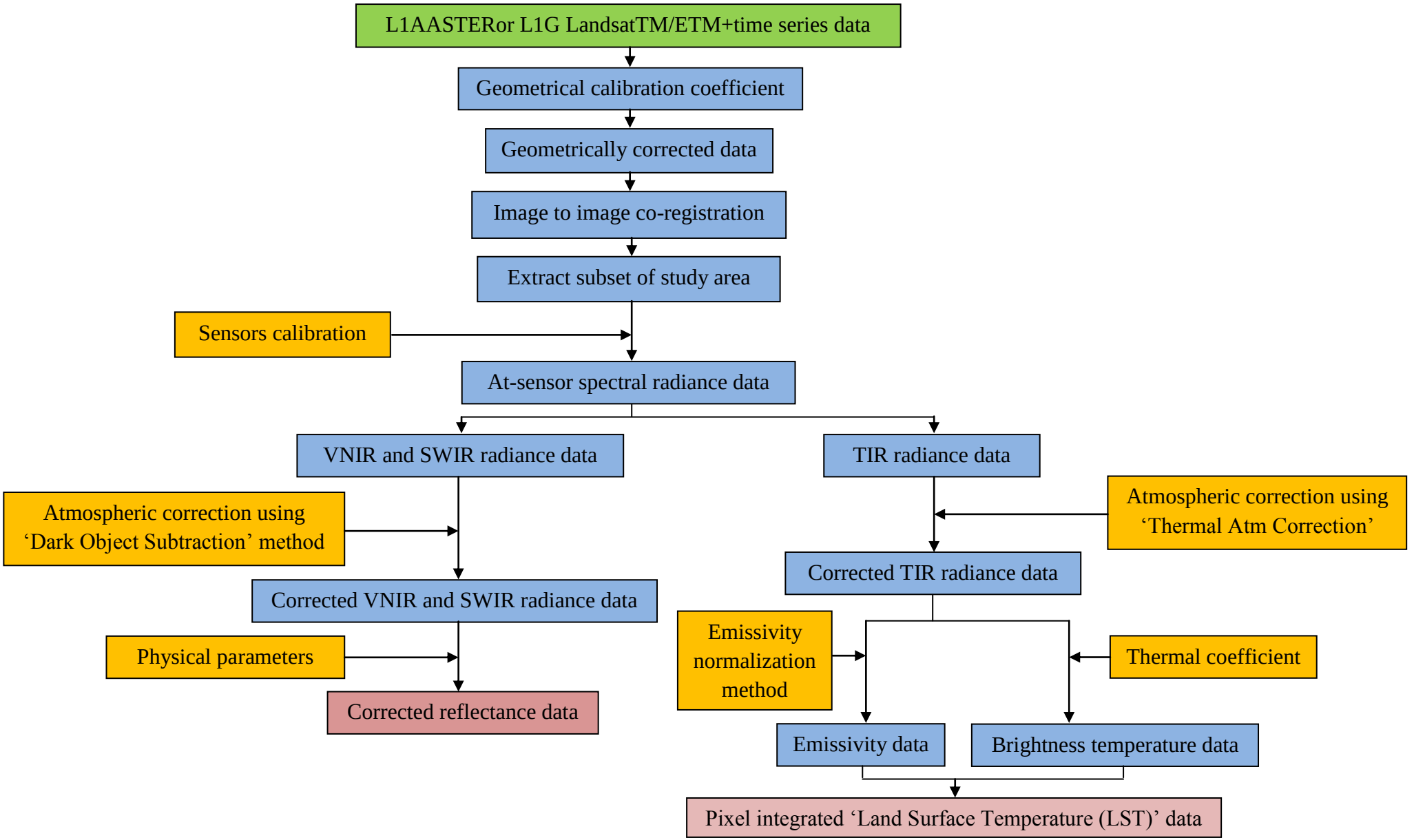

Figure 4.2 Flowchart showing an overview of the methodology adopted for pre-processing of the remote sensing datasets

4.5.2.1 *Sensors calibration and computation of spectral radiance*

Data values recorded by the sensors represent no physical connotations and hence, converted into spectral radiance value using sensors calibration for correcting sensor gain and offset. Calculation of at-sensor spectral radiance is the first step to convert image data from multiple sensors and platforms to a physically meaningful common radiometric scale *(*Chander et al. 2009*)*. The process of converting image digital number (DN) values to radiance is same for both thermal and optical data. To allow comparison of the datasets, the satellite images have been first converted into at sensor spectral radiance image by sensor calibration. The general formula for converting Landsat (eq. 4.1 to 4.3) and ASTER data (eq. 4.4) are different.

For Landsat data, spectral radiance at the sensor's aperture (L_λ) is given by,

$$L_\lambda = Gain_\lambda \times DN_\lambda + Bias_\lambda \quad (4.1)$$

where, $Gain_\lambda$ = calibration gain coefficient of sensor (W $m^{-2}sr^{-1}\mu m^{-1}$)

DN_λ = digital number of a pixel in particular band (counts)

$Bias_\lambda$ = calibration offset of sensor band (W $m^{-2}sr^{-1}\mu m^{-1}$)

The above equation can be expresses as L_λ that can be calculated easily using the following general formula (Chander et al. 2009):

$$L_\lambda = \frac{(L_{MAX\ \lambda} - L_{MIN\ \lambda})DN_\lambda}{DN_{MAX\ \lambda}} + L_{MIN\,\lambda} \quad (4.2)$$

or

$$L_\lambda = G_{rescale}\ x\ DN_\lambda + B_{rescale} \quad (4.3)$$

Where, $G_{rescale} = \frac{(L_{MAX\ \lambda} - L_{MIN\ \lambda})}{DN_{MAX\ \lambda}}$

$B_{rescale} = L_{MIN\,\lambda}$

L_λ = Spectral radiance at the sensor's aperture (W m^{-2} sr^{-1} μm^{-1})

DN_λ = Quantized calibrated pixel value in the band (counts)

$DN_{MAX\lambda}$ = Highest DN value in the scale

$LMIN_\lambda$ = Spectral at-sensor radiance that is scaled to $DN_{MIN\lambda}$ i.e. = 0 (W m^{-2} sr^{-1} μm^{-1})

$LMAX_\lambda$ = Spectral at-sensor radiance that is scaled to $DN_{MAX\lambda}$ (W m^{-2} sr^{-1} μm^{-1})

$G_{rescale}$ = Band-specific rescaling gain factor (W m^{-2} sr^{-1} μm^{-1} DN_{λ}^{-1})

$B_{rescale}$ = Band-specific rescaling bias factor (W m^{-2} sr^{-1} μm^{-1})

In the present research, only band 7 image of the Landsat TM/ETM+ time series data have been used. The sensor calibration to compute radiant intensity response of Landsat TM/ETM+ band 7 is given in Table 4.4.

Table 4.4 Details of gain and bias factors for Landsat TM/ETM+ band 7 to compute at-sensor spectral radiance (Chander et al., 2009)

Landsat Sensor ID	**$LMIN_{\lambda}$ (W m^{-2} sr^{-1} μm^{-1})**	**$LMAX_{\lambda}$ (W m^{-2} sr^{-1} μm^{-1})**	**$G_{rescale}$ (W m^{-2} sr^{-1} μm^{-1} DN_{λ}^{-1})**	**$B_{rescale}$ (W m^{-2} sr^{-1} μm^{-1})**
ETM+ Band 7	-0.35	16.54	0.066496	-0.42
TM Band 7	-0.15	16.5	0.065551	-0.22

ASTER data used in the present study is L1A data that is processed using radiometrically calibration coefficient to obtained scaled radiance. At-sensor spectral radiance for ASTER data can be obtained using following formula:

$$L_{\lambda} = (DN_{\lambda} - 1) \times UCC_{\lambda} \quad (4.4)$$

Where, L_{λ} is ASTER spectral radiance at the sensor's aperture measured in a band (λ) and UCC_{λ} is the Unit Conversion Coefficient (W m^{-2} sr^{-1} μm^{-1}) given in Table 4.5.Metadata file of each ASTER dataset indicated all ASTER data has been acquired in normal gain setting except band 1 and 2 that are of high gain. The maximum radiance allocated for ASTER VNIR, SWIR and TIR bands are bands are determined by quantization level of the data and have shown in Table 4.6.

4.5.2.2 *Atmospheric correction*

As mentioned earlier, the spectral radiance received at the satellite sensor is commonly affected by molecular scattering and atmospheric absorption. Atmospheric conditions have considerably varied seasonally and temporally. In the area like coalfield, intense mining activity and coal burning have significantly contributed aerosol and particulate matter to the atmosphere. Solar radiation have been scattered by these atmospheric particles. Hence, sensor not only received true radiance but also scattered radiance or 'path radiance'. Path radiance induced haziness in the image. Intensity of the path radiance is significantly varied with the wavelength. It is high for shorter wavelength and subsequently decreases with increasing wavelength. Thus, atmospheric error in the VNIR and SWIR bands are

mainly governed by additive path radiance. Atmospheric absorption of the spectral radiance due to water vapour in VNIR band is quite impersistent and has been ignored.

Table 4.5 Unit conversion coefficient for ASTER data (Abrams et al., 1999)

Band	Unit Conversion Coefficient (W m^{-2} sr^{-1} μm^{-1})			
	High gain	Normal Gain	Low Gain 1	Low gain 2
1	0.676	1.688	2.25	N/A
2	0.708	1.415	1.89	
3N	0.423	0.862	1.15	
3B	0.423	0.862	1.15	
4	0.1087	0.2174	0.290	0.290
5	0.0348	0.0696	0.0925	0.409
6	0.0313	0.0625	0.0830	0.390
7	0.0299	0.0597	0.0795	0.332
8	0.0209	0.0417	0.0556	0.245
9	0.0159	0.0318	0.0424	0.265
10	N/A	0.006822	N/A	N/A
11		0.006780		
12		0.006590		
13		0.005693		
14		0.005225		

Table 4.6 Maximum detectable radiances response for all ASTER bands in different gain settings (ASTER L1 data processing, Ver. 3.0)

Band	Maximum Radiance (W m^{-2} sr^{-1} μm^{-1})			
	High gain	Normal Gain	Low Gain 1	Low gain 2
1	170.8	427	569	N/A
2	179.0	358	477	
3N	106.8	218	290	
3B	106.8	218	290	
4	27.5	55.0	73.3	73.3
5	8.8	17.6	23.4	103.5
6	7.9	15.8	21.0	98.7
7	7.55	15.1	20.1	83.8
8	5.27	10.55	14.06	62.0
9	4.02	8.04	10.72	67.0
10	N/A	28.17	N/A	N/A
11		27.75		
12		26.97		
13		23.30		
14		21.38		

To compensate atmospheric error due to path radiance, 'Dark Object Subtraction (DOS)'method given in ENVI^{TM} 4.7 has been applied to the images to obtain true radiance of ground features. The method involves the subtraction of radiance value of the darkest pixel from the data. The value of the darkest pixel should have zero. However, due to scattering, the dark pixels show 'non-zero value'. So, the maximum radiance value among the dark pixels has been considered as path radiance and subtracted from the at-sensor radiance image. In the present study, 2008 ASTER data has been specifically used for mapping and detection of surface coal fires (discussed in Chapter 6).While analysis, two dark pixels have been observed in 2008 ASTER SWIR bands (Figure 4.3). The path radiance value for 2008 ASTER SWIR band is determined (Table 4.7) and used in correcting the data using eq. 4.5:

$$L_{\lambda C} = L_{\lambda} - L_{\lambda P} \quad (4.5)$$

Where,

$L_{\lambda C}$ = Atmosherically corrected radiance

L_{λ} = At-sensor spectral radiance (uncorrected radiance)

$L_{\lambda P}$ = Path radiance per band.

Table 4.7 Observed path radiance value in ASTER SWIR bands

ASTER SWIR Bands (19th March 2008)	**Path Radiance ($L_{\lambda P}$) (W m^{-2} sr^{-1} µm^{-1})**
B4	1.23
B2	0.91
B3	0.83
B4	0.78
B5	0.71
B6	0.55

As mentioned earlier that the magnitude of the atmospheric scattering decreases with higher wavelength. Hence, atmospheric errors in TIR data is chiefly govern by atmospheric absorption (Bartolucci et al., 1988; Barsi et al., 2005). Absorption in mainly induced by water molecules and decrease the radiant intensity of the emitted radiance received at the sensors. Atmospheric parameters for ASTER TIR bands have been derived from the metadata and corrected individually from the measured radiant intensity of each ASTER TIR band (Thome et al., 1998). Precise correction allows the evaluation of true emitted radiance received at the sensor.

Table 4.8 Specification and details of the physical parameters used to compute TOA spectral reflectance

Study area	Acquisition date	Sensor ID	Earth Sun Distance (d) (astronomical units) (Chander et al. 2009)	$ESUN_{\lambda}$(Mean Exoatmospheric Solar Irradiance) (W m^{-2} μm^{-1}) (Chander et al. 2009) (Thome et al. 2001)	Solar Elevation Angle (Degree)
Jharia Coal Field, India	17th December 2000	ETM+ Band 7	0.98407	84.90	52.3793
	02nd November 2001	ETM+ Band 7	0.99228	84.90	43.6863
	07th December 2002	ETM+ Band 7	0.98519	84.90	51.4129
	19th March 2003	ETM+ Band 7	0.99840	84.90	33.2352
	02nd December 2009	TM Band 7	0.98592	83.44	50.3889
	20th February 2010	TM Band 7	0.98877	83.44	44.4370
Ruqigou Coal Field, Ningxia, China	17th October 2000	ETM+ Band 7	0.99662	84.90	38.6014
	10th October 2006	TM Band 7	0.99861	83.44	41.3893
Jharia Coal Field, India	19th March 2008	Band 1	0.99584	1848	32.443356
		Band 2		1549	
		Band 3		1114	
		Band 4		225.4	
		Band 5		86.63	
		Band 6		81.85	
		Band 7		74.85	
		Band 8		66.49	
		Band 9		59.85	

In the present approach, atmospheric correction of the ASTER TIR bands have been carried out using 'Thermal Atm Correction' module given in 'Preprocessing' tool of ENVI^{TM} 4.7. The algorithm for 'Thermal Atm Correction' is similar to the In-Scene Atmospheric Compensation (ISAC) algorithm. The algorithm performs the correction with assumptions of (a) considering uniform and single layer atmosphere over the data scene, (b) an occurrence of a near-near-blackbody surface within the scene and (c) no reflected downwelling radiance.

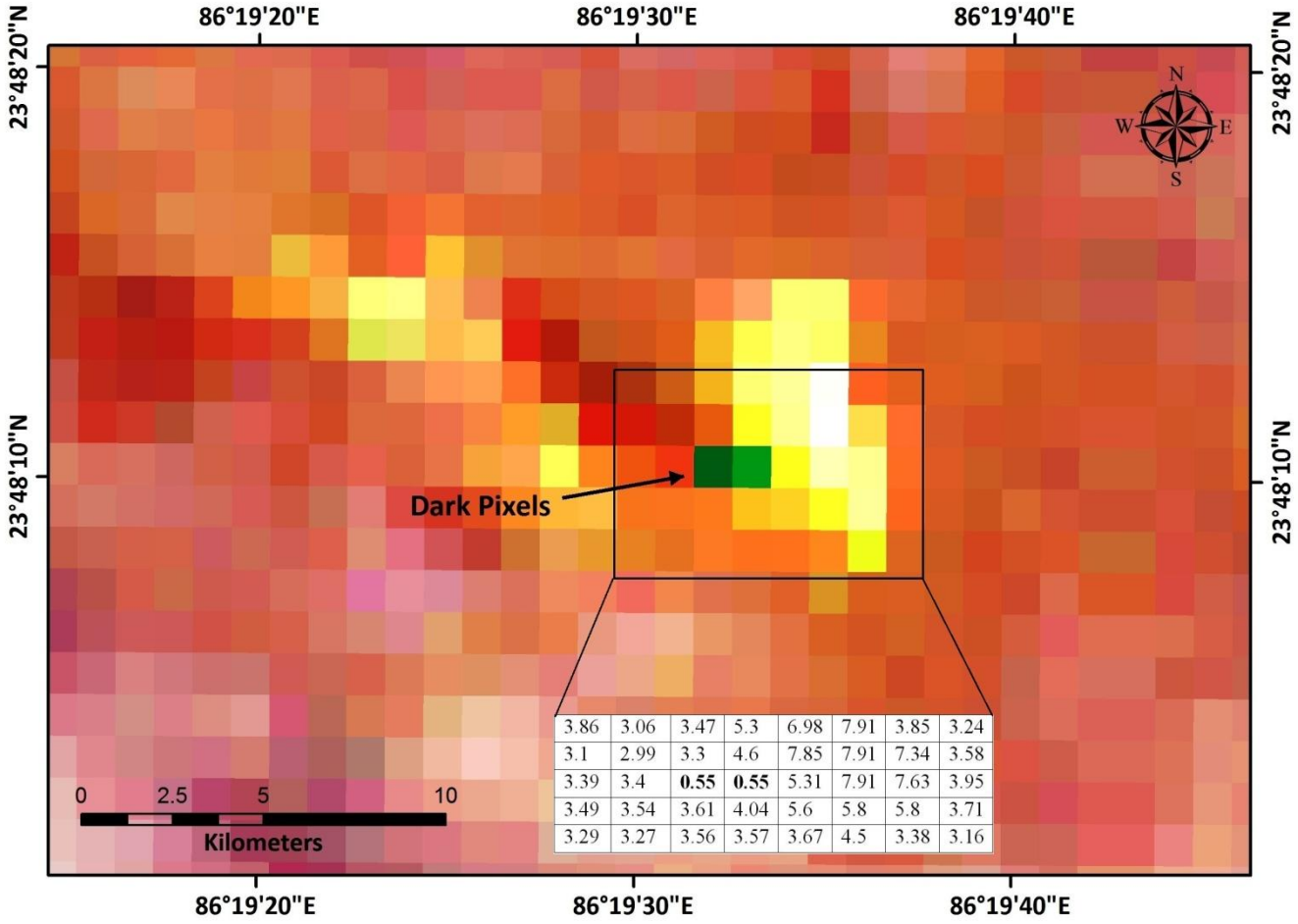

Figure 4.3 A small subset of the ASTER 8-6-4 CIR composite of 2008 covering Sijua area, JCF. The anomalous pixels showing in bright yellow color are attributed to the surface fire. Two dark pixels (appearing green) have shown 0.55 radiance value. These are the pixels with no value but have shown a minor value of 0.55 which is due to path radiance induced by scattering

The algorithm first determines the wavelength that most often exhibits the maximum brightness temperature. This wavelength is then used as the reference wavelength. Only spectra that have their brightest temperature at this wavelength are used to calculate the atmospheric compensation. At this point, for each wavelength, the reference blackbody radiance values are plotted against the measured radiances. A line is fitted to the highest points in these plotted data and the fit is weighted to assign

more weight to regions with denser sampling. The compensation for this band is then applied as the slope and offset derived from the linear regression of these data with their computed blackbody radiances at the reference wavelength. The 'Thermal Atm Correction' module also provides an account of upwelling atmospheric radiance ($L_{\lambda P}$) and atmospheric transmission (τ) for individual ASTER TIR band. The upwelling atmospheric radiance and atmospheric transmission has been evaluated by the regression analysis of the scatter plot of radiance vs. approximated brightness temperature derived from using the Planck's function and assumed emissivity of 1 (ENVI User's Guide, 2009).

As here, it has been observed that the ASTER band 13 (10.25-10.95 μm) has maximum atmospheric transmittance and minimum upwelling radiance among rest of the ASTER TIR bands (Figure 4.4). Hence, effective at-sensor spectral radiance of ASTER band 13 has been preferably chosen and further applied to calculate pixel wise distribution of radiant or brightness temperature of the area using eq.2. The generated thermal image has been used further for delineating subtle surface thermal anomaly associated with underground coal seam fires (discussed in Section 7.4).

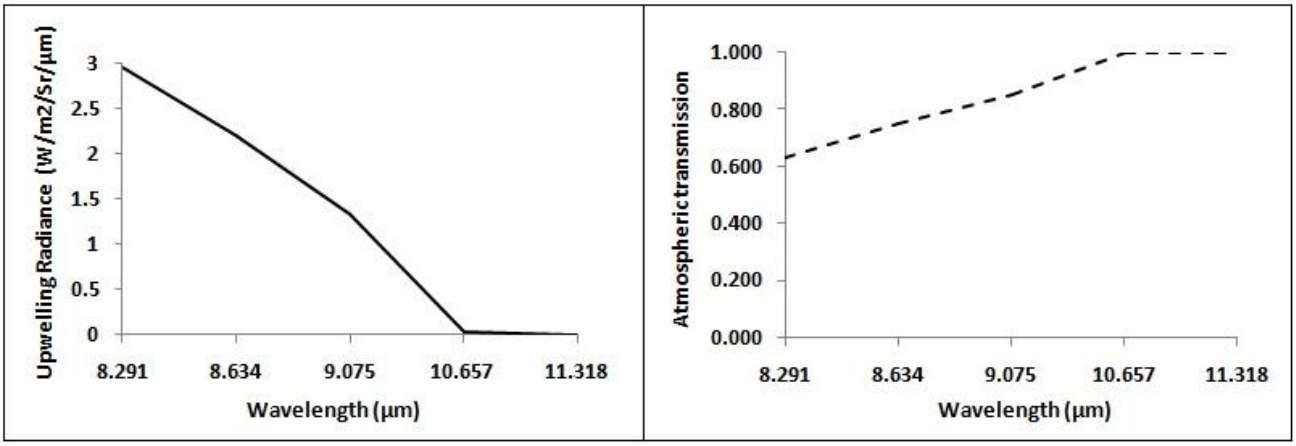

Figure 4.4 Atmospheric transmittance and minimum upwelling radiance profile of the ASTER 2009 TIR bands

4.5.2.3 *Computation of spectral reflectance*

Spectral reflectance received at the sensor is the fraction of solar radiation reflected from the surface to the radiation incident on the surface. The quantity of the solar irradiance is the function of the topography of the surface. As mentioned in Chapter 3, Section 3.3, JCF exhibits relatively flat topography and topographic correction to the image can be safely ignored. However, to reduce scene-to-scene variability, it is better to convert the corrected spectral radiance to top of atmosphere (TOA) reflectance as it removes the cosine effect of different solar zenith angles due to the time difference between data acquisitions. TOA reflectance compensates for different values of the exoatmospheric

solar irradiance arising from spectral band differences and it also corrects for the variation in the Earth-Sun distance between different data acquisition dates (Chander et al., 2009). The above variations may have significant impact on image data. However, actual retrieval of land surface reflectance from the SWIR data is complicated because of integrated effect of both emission and reflectance response from the ground. The TOA reflectance of the Earth is computed by applying physical parameters using eq.4.6 (Chander et al., 2009):

$$\rho_\lambda = \frac{(\pi . L_{\lambda C} . d^2)}{ESUN_\lambda . \cos \theta_s} \quad (4.6)$$

Where,

ρ_λ = Planetary TOA reflectance (unitless)
π = Mathematical constant equal to ~3.14159 (unitless)
$L_{\lambda C}$ = Effective spectral radiance at the sensor's aperture (W m^{-2} sr^{-1} μm^{-1})
d = Earth–Sun distance (astronomical units)
$ESUN_\lambda$ = Mean exoatmospheric solar irradiance (W m^{-2} μm^{-1})
θ_s = Solar zenith angle (degree) (equal to sine of the solar elevation angle)

4.5.3 Computation of brightness temperature

As mentioned in section 4.5.2.2, the effective at-sensor spectral radiance ($L_{\lambda C}$) can be further used to compute brightness temperature image. The brightness temperature image provide per pixel radiant temperature distribution of the area. According to Planck's radiance function, the temperature of black body is the function of the radiant intensity of the emitted radiance and can be computed using following formula (eq. 4.7, Gillespie et. al., 1999),

$$B_\lambda = \frac{C_1}{\pi \lambda^5} \left[\frac{1}{e^{\left(\frac{C_2}{\lambda T_b} - 1\right)}} \right] \quad (4.7)$$

Where,

B = blackbody radiance (W m^{-2} sr^{-1} μm^{-1})
λ = wavelength (μm)
$C_1 = 2\pi hc^2$ (3.74×10^{-16} W m^2; 1st radiation constant)
T = temperature (K)
h = 6.63×10^{-34} W s^2 (Planck's constant)

$c = 2.99x10^{8}$ m s^{-1} (speed of light)

$C_2 = hc/k$ (1.43876869×10^{-2} m K; 2nd radiation constant)

$k = 1.38x10^{-23}$ W s K^{-1} (Boltzmann's constant)

The above equation (eq. 4.7) can be reform as follows (eq. 4.8) by inverting Plank's radiance function (Gupta, 2003),

$$T_b = \frac{{}^{C_2}/_{\lambda}}{ln\left(\frac{C_1}{\pi\lambda^5 B_\lambda}+1\right)} \quad (4.8)$$

Where, $B_\lambda(T)$ is the measured radiant intensity response of a blackbody radiance obtained from a satellite sensor and it can be expresses as $L_{\lambda C}$ that has been earlier calculated for ASTER TIR data (see section 4.5.2.2). $C_1/\pi\lambda^5$ and C_2/λ (in eq. 4.8) are the coefficient determined by effective wavelength of a satellite sensor (Table 4.6) and can be expresses as K_1 and K_2 respectively (eq. 4.9). K_1 and K_2 calculated for the ASTER SWIR and TIR are given in Table 4.9. These values of K_1 and K_2 are then used to calculate effective at sensor brightness temperature using the following formula:

$$T_b = \frac{K_2}{ln\left(\frac{K_1}{L_\lambda}+1\right)} \quad (4.9)$$

Where,

T_b = Effective at-sensor brightness temperature (K)

K_1 = Calibration constant 1 (W m^{-2} sr^{-1} μm^{-1})

K_2 = Calibration constant 2 (K)

L_λ = Spectral radiance at the sensor's aperture (W m^{-2} sr^{-1} μm^{-1})

ln = Natural logarithm

4.5.3.1 *Computation of emissivity and 'pixel integrated land surface temperature (LST)'*

Thermal emissivity of the common land cover features are ranges from 0.7-0.97 (Prakash and Gens, 2010). Satellite data derived emissivity has been previously used by several workers for temperature estimation of the coal fire (Chatterjee, 2006). Van de Griend and Owe (1993) derived an empirical relationship between NDVI and field based thermal emissivity values. However, emissivity image obtained from ASTER NDVI has 15 m spatial resolution that cannot be extrapolated for calculating temperature from low resolution TIR data.

As discussed, multispectral TIR bands have potentially exhibits emissivity information of the different land cover classes. The emissivity for different TIR bands can be evaluated using temperature-emissivity separation (TES) algorithm (Gillispie et al. 1998). ASTER multispectral TIR bands have effectively retrieved the pixel integrated 'land surface temperature' and emissivity (Gillispie et al. 1999; Schmugge et al. 2002; Coll et al. 2007; Gangopadhya et al. 2012). In the present study, ASTER TIR band 13 emissivity has been used to derive LST estimates for temporal monitoring of surface-subsurface coal fires. Effective at-sensor brightness temperature computed above has been then converted into estimated kinetic temperature or 'pixel integrated land surface temperature (LST)' using the following general formula (eq. 4.10),

$$T_k = \frac{T_b}{\varepsilon^{1/4}} \tag{4.10}$$

Where,

T_k = Kinetic temperature or land surface temperature (K)

T_b = Effective at-sensor brightness temperature (K)

ε = ASTER TIR band 13 emissivity

Table 4.9 Calibration constants K_1 and K_2 for ASTER SWIR and TIR bands (ASTER L1B Manual Ver. 3.0)

ASTER SWIR and TIR Bands	**K_1 (W m^{-2} µm^{-1})**	**K_2 (K)**
4	9738855.547	8719.810242
5	2504022.009	6645.582864
6	2284991.959	6525.028073
7	2020158.52	6366.233142
8	1734395.109	6174.972918
9	1511471.827	6007.384927
10	3040.136402	1735.337945
11	2482.375199	1666.398761
12	1935.060183	1585.420044
13	866.468575	1350.069147
14	641.326517	1271.221673

4.5.4 Removal of 'false alarms'

Thermal anomalies obtained at LST image may constitute some 'false alarms'. These false alarms may generated due to heat source at industrial unit, high reflectance due to river sand, barren land etc. The high radiant intensity response due to such features have often perceived automatically by the TIR sensor. These may give error in mapping of coal fires. To compensate this problem, visual interpretation of ASTER VNIR (15 m spatial resolution) bands have been used to remove such false pixels. It has been estimated that the anomalous pixels attributed to the coal fire (whether in coal dump or coal seam) are closely associated with opencast mine. In JCF, no industrial heat source is available in the vicinity of the mining area. Seams are dipping southerly and if burning, can only produce very subtle thermal anomaly at the surface that may not be detected by moderate resolution ASTER TIR sensor (90 m). Hence, in the southern part of the JCF, anomalies are mainly due to high reflectance caused by barren land or river sand. These pixels have been carefully observed and subsequently removed from the LST images.

4.6 PROCESSING

Pre-processing techniques discussed above have been succeeded further by image processing for feature extraction. Processing techniques facilitate the interpretation of the image by digital enhancement, band combination, band ratioing, digital classifications, data computation, thresholding etc. to detect and extract the feature of interest from the image. The techniques followed in processing of the data used in the present study have been elaborated below in detail:

4.6.1 Contrast stretching

Contrast stretching induced digital enhancement of the grey image by linearly expanding digital values of the histogram into a new distribution. Contrast enhancement facilitates the precise recognition of the target feature by modifying the range of image tone. Coal fires appear as segregated patches of bright pixels over the grey scale image. Membership value of the fire in a pixel defines the brightness value of the pixel. Low membership value of a fire gives grey tone to the corresponding pixel. In this respect, contrast enhancement expands the narrow range of brightness values of the images and facilitates the interpretation of surface coal fire.

4.6.2 Band combination

Multispectral image allows the visualization and interpretation of the ground features in various band combinations. A band combination is a composite of three individual bands forming a color

composite image. The combination for composite image is user specified. However, a best combination can be defined by the spectral characteristic of the target of interest. The resulting composite image is called 'false color composite (FCC)'. In JCF, textural and spectral characteristics of the common land use / land cover features have been recognized in ASTER VNIR bands. Surface coal fires shows highest reflectance in SWIR bands and appears as pale to bright yellow patches on 8-6-4 ASTER color composites.

4.6.2.1 *Textural and spectral characteristics of different ground features observed in JCF*

During field work, there were seven broad land use / land cover (LULC) classes recognized in the study area. On the basis of field observations, these classes have been described below in detail. Criteria for identifying these LULC classes on the Landsat TM/ETM+ 4-3-2 and ASTER 3-2-1 color infrared (CIR) composite based on the spectral and textural characteristics are shown in Table 4.10.

a) Coal: Dark black color coal beds and dumps exhibiting very low reflectance are prominently observed and are well distributed in the entire JCF.

b) Sparse vegetation: Sparse vegetation comprises of small bushes and shrubs. In the vicinity of the coal fire affected area, the sparse vegetation is mainly dry

c) Dense vegetation: Dense vegetation is scarce and appears dense bushes and canopy.

d) Water body: Water bodies found in the study area are natural stagnant water ponds with irregular outline.

e) Barren land: Patches of land with rocky outcrop or devoid of vegetation.

f) Settlement: Generally marked by the populated colonies, dense railway and road networks.

g) Overburden dump: Bare and dumps of loose soil / rocks dumps after excavation are frequently found near the open cast mines; they exhibit somewhat wavy outline.

h) Coal fire: Coal fire is a high temperature phenomenon. Textural and spectral attributes of the fire is depends on the occurrence and type of coal fire. Different spectral and textural response of the coal fire has been observed on the CIR composites of ASTER data and their characteristics for identification are discussed in Chapter 6.

Table 4.10 Spectral and textural characteristics of the various Land use / Land cover type observed in Landsat TM/ETM+ and ASTER datasets

Land use / Land cover type	Coal	Vegetation	Water bodies	Barren land	Settlement	Overburden dump
Textural characteristics (on standard FCC)	Appears in form of exposed bedded layers in opencast and exist in close association with overburden dump	Vegetation comprises of dense canopy of perennial wood plants, small bushes and shrubs	Water bodies are natural stagnant small scale water ponds with irregular outline.	Patches of rocky outcrop and devoid of vegetation, exhibits high reflectance	Mainly characterized by blocky texture	Freshly excavated mine wastes dumped in the vicinity of opencasts mainly characterized by loose soil and fragmented rock mass
	Dark black in VNIR	Deep red to pinkish to light red in VNIR	Shades of blue. Very dark in SWIR and TIR	Pale to faint white in visible region	Light cyan to cyan in VNIR	Shades of light grey with smooth wavy outline pattern.
Detectable sensors response in different spectral channel	Very low to low visible reflectance	High NIR reflectance	No or minor reflectance in SWIR	High visible-NIR reflectance	Moderate visible reflectance	High visible reflectance

4.6.3 Normalized indices and band ratioing

Normalized indices and band ratio are also the technique of digital enhancement where the spectral contrast of a particular feature class has been enhanced. Band ratio involves the division of one band from another band. The selection of bands for ratio is defined by the distribution of the spectral reflectance values of a feature class in different spectral bands (spectral reflectance curve). Usually the bands with maximum and minimum spectral reflectance are preferably chosen for ratioing. Normalized difference ratio index is bit different from simple band ratio. It is the ratio of difference and sum of maximum and minimum reflectance of a particular feature class in specific spectral channels. In the present study normalized difference ratio indices have been used for mapping of surface coal fires and discussed in detail in Chapter 6.

4.6.4 Thresholding

Threshold determination is an important task in image processing, and is very useful to target recognition. A precise threshold is a spectral value or a range of value that can define the attributes of a specific feature. A slight error in the evaluation of threshold may give misleading results. In the present study, techniques and utility of thresholding have been discussed in detail in Chapter 2, Section 2.4.1. Besides, a new method of thresholding for delineation of surface coal fires in JCF has been proposed and discussed in Chapter 5.

4.7 SUMMARY

The present chapter described the type, characteristics and specification detail of the remote sensing, ancillary and field data used in the present study. Remote sensing data constitute time series L1G Landsat TM/ETM+ and L1A ASTER data. Analysis of the remote sensing datasets is aided together with ancillary (thematic maps and GoogleEarth^{TM} imagery) and field data for interpretation. Prior to the analysis, all sets of the remote sensing data have been pre-processed for necessary corrections using sensors calibration. The effects of atmospheric contributions have been removed from the measured radiant intensity of the images. The obtained corrected VNIR and SWIR bands have been converted into reflectance image. The corrected TIR bands have been applied to compute brightness temperature image using Planck's radiance function. Brightness temperature image has been then further converted into pixel integrated 'Land Surface Temperature' image using ASTER derived emissivity. Pre-processing of the satellite data has been followed by image processing. The type of the processing technique used is defined by the objective of the present work and it has

governed mainly by deciding band combinations, preparing normalized indices and applying precise threshold to the image.

CHAPTER 5

THRESHOLDING OF SWIR BAND TO DELINEATE COALFIELD SURFACE FIRES

5.1 INTRODUCTION

Surface fires are common in Coalfields where coal is being mined or exposed to sunlight for long durations. The heat energy emitted from these fires affects the signal recorded by the sensors operating in the shortwave infrared regions (SWIR) of the electromagnetic (EM) spectrum. SWIR bands hence, are sensitive to solar reflected radiation as well as emitted radiation from a target. With this theoretical background, an attempt has been made to propose a method based on maximum background reflectance for thresholding of Landsat TM/ETM+ band-7 operable in SWIR to segregate the pixels attributed to Coalfield surface fire. The **'Maximum Solar Reflection Threshold'** method proposed in the present approach uses the highest spectral radiance that can be attributed to solar reflection as the conservative threshold to segregate the pixels with emitted component from those with reflected component of the EM energy.

The present chapter illustrates a brief overview of the methodology adopted for thresholding of Landsat TM/ETM+ band-7 to delineate the pixels having Coalfield surface fires. First, a spatial subset of the Coalfield under active surface fire was selected using visual interpretation of false colour composite of Landsat TM/ETM+ 7-5-3 band combination. Several spatial profiles passes through active 'hot pixels' representing surface fires and barren material were prepared on temporal Landsat TM/ETM+ band-7 datasets. These profiles were analyzed and then compared. The results obtained from this method indicate that the maximum background reflectance evaluated is the most representative reflectance threshold to isolate the pixels of surface fire in a coal mining areas. The method has been systematically implemented over two different coal mine sites (in India and China) with different physiographic settings to test its broader applicability.

At the end of the chapter, a comparison of considering digital number (DN) values and maximum background reflectance as threshold for both test sites has shown and advantages of

using ‘maximum background reflectance’ as threshold to delineate Coalfield surface fire have been discussed.

5.2 COALFIELD SURFACE FIRES: PROBLEM AND CONCEPTUAL APPROACH

Landsat TM/ETM+ data have been widely used in coal mining and coal fire studies (Prakash et al., 2005; Saraf et al., 2005; Prakash et al., 1997; Zhang et al., 2004). These studies address a wide spectrum of related applications, including but not limited to mapping and monitoring the areal distribution of surface and underground coal fires (Zhang and Kuenzer, 2007a; Zhang et al., 2007b), land cover and land use change detection (Prakash and Gupta, 1998), effect of fires on local vegetation and soils (Gupta and Prakash, 1998), mutual relationship of the surface and subsurface fires (Prakash et al. 1997), fire temperature estimation (Gangopadhyay and Lahiri, 2005; Prakash et al., 2005; Gangopadhyay et al., 2005), depth estimation of subsurface fire (Saraf et al., 1995) and environmental impacts of coal fires (Chapter 2, Section 2.4 and 2.5).

Multispectral data from satellite sensors, such as the Landsat TM/ ETM+ and ASTER, have the additional advantage that they acquire data in both the thermal infrared (TIR) and the shortwave infrared (SWIR) parts of the spectrum. The TIR data are used widely to delineate subtle surface thermal anomalies associated with underground coal fires (Deng et al., 2001), while SWIR data are used to isolate very high temperatures associated with surface fires (Prakash and Gupta, 1999a). Delineation of thermal anomalies associated with both underground and surface fires requires a certain threshold value be defined on the TIR and SWIR data, respectively, to classify the area under investigation as ‘fire area’ or ‘non-fire area’ (Prakash and Gens, 2010).

This study focuses on day-time SWIR data processing and establishing a robust criterion for selecting a threshold to map surface coal fires, specifically using band-7 of the Landsat TM/ETM+ sensors. The focus on Landsat data is logical and significant as the Landsat series of satellites has provided the longest reliable uninterrupted archive of free or low-cost medium resolution satellite data and covers all the major coal fields in the world.

A review of the literature reveals that almost all the previous studies have dealt with TIR data (TM band-6) for thresholding of the sensor response to identify coal fire areas. No study recognized specifically involving TM/ETM+ SWIR bands in which thresholding have been implemented. Chapter 2, Section 2.4.1 gives a brief review of the methods that have been

implemented for thresholding of ETM+/TM band-6 (TIR) data by various researchers to isolate thermal anomaly of subsurface fires from the background (Prakash and Gens, 2010).

As such, the TM/ETM+ band-7 responds to solar radiation reflected by background objects and also emitted radiation by fire. Therefore, it is important to threshold or segment the sensor response so that the response of the background objects can be segregated vis-a-vis the response of fire (hot objects) (Figure 5.1). This study specifically focuses on the TM/ETM+ band-7 for thresholding of spectral response.

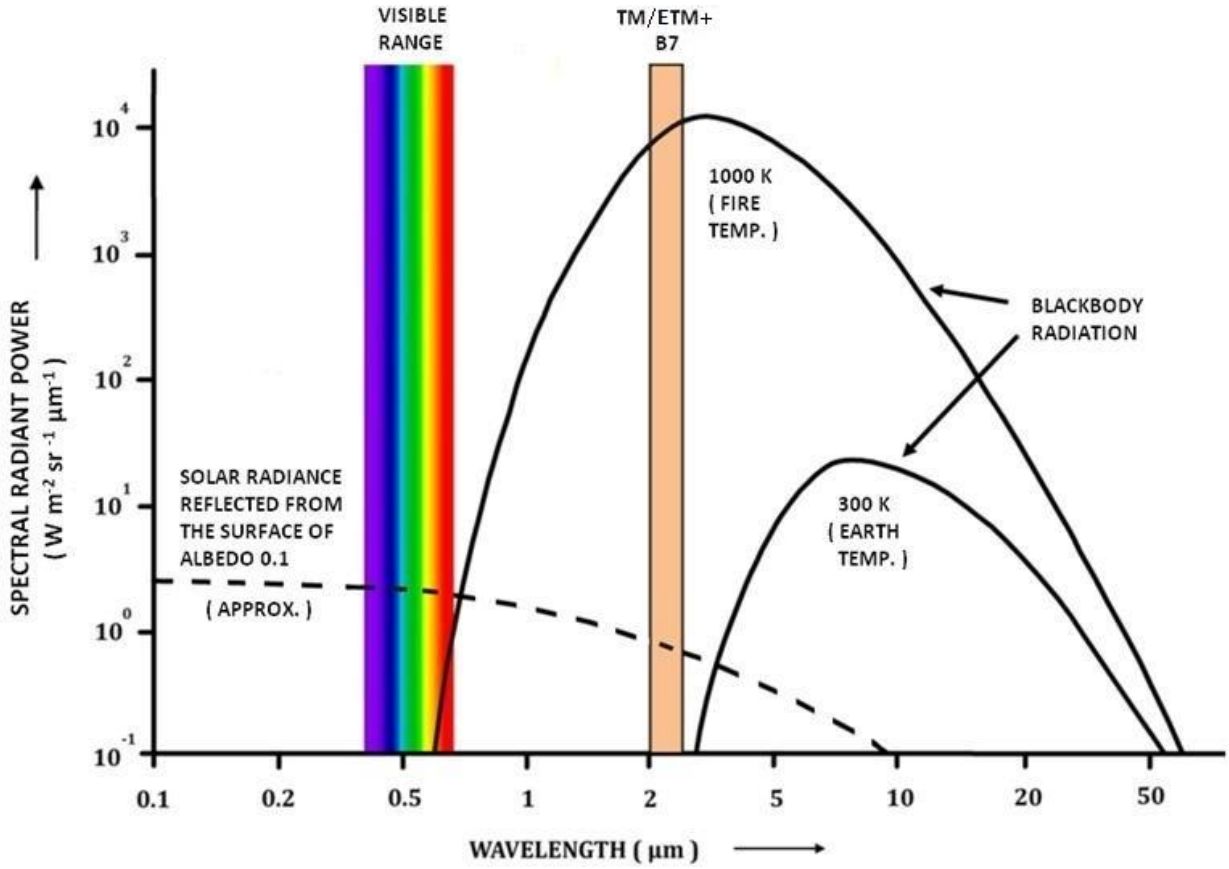

Figure 5.1 Blackbody emitted radiation curve for ambient earth temperature (300 K) and fire (1000 K). The solar radiance reflected from the surface of albedo 0.1 and the spectral position of Landsat TM-Band 7. Note that the Band 7 sensitive to both solar reflected radiation and blackbody radiation emitted by fire

5.3 METHODOLOGY

As mentioned earlier that the data from repetitive passes of Landsat TM/ETM+ spanning a decade have been exclusively used for the analysis. This study has utilized several temporal coverages of Landsat TM/ETM+ band 7. This has facilitated a comparative study of the data sets in various months/seasons spread over a time from December 2000 to February 2010. The methodology has been commenced with the acquisition of time series Landsat TM/ETM+ data subsequently followed by the extraction of band-7 and spatial subsetting of the study area. The datasets have been pre-processed using sensor calibrations as per the methodology discussed in Chapter 4, Section 4.5.

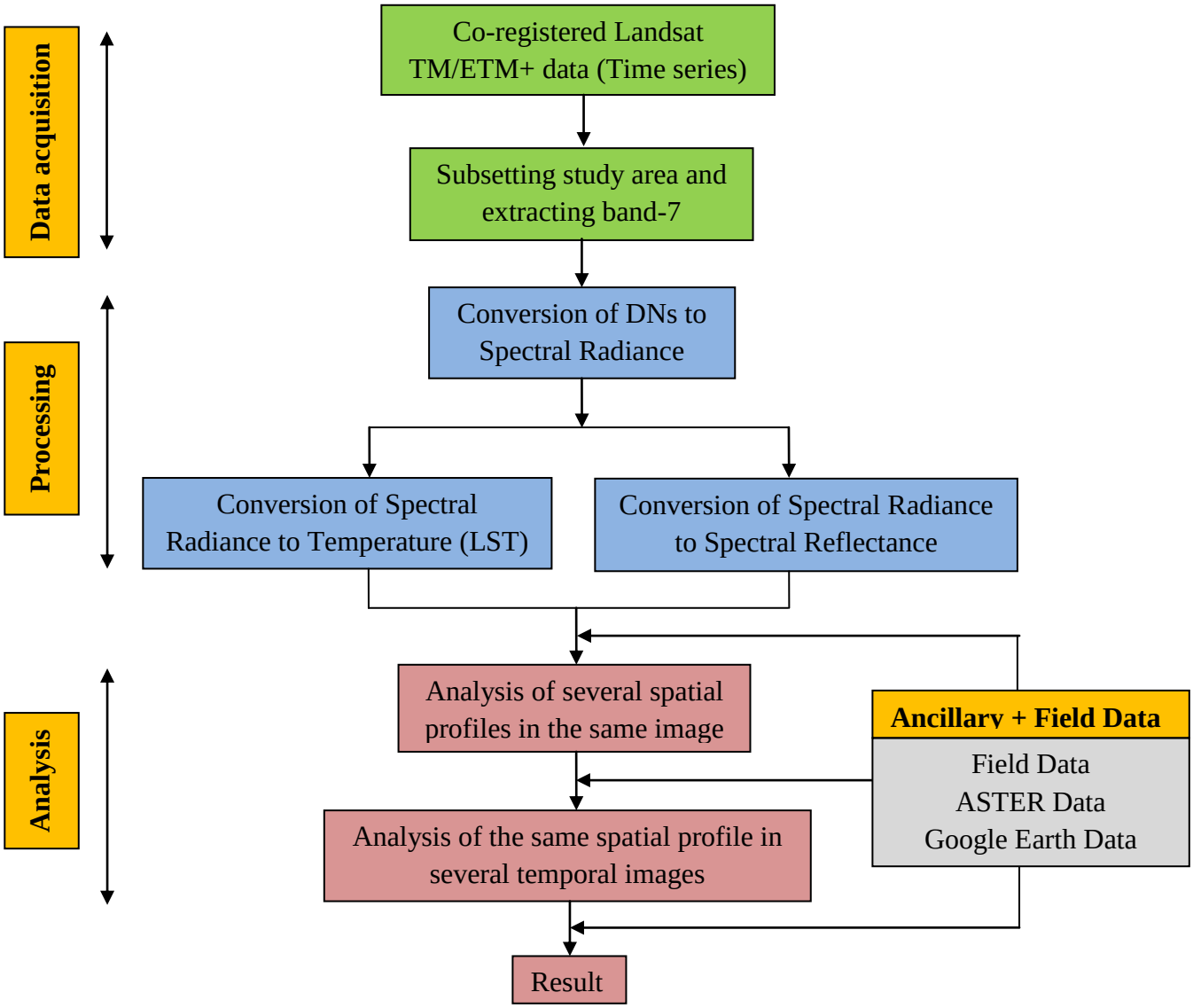

Figure 5.2 Schematic diagram showing the data processing and methodology adopted in the present work

Analysis of the datasets involves pixel-wise profile analysis of several spatial profile lines in a selected image followed by pixel wise analysis of a selected spatial profile in different temporal images. Auxiliary image datasets of ASTER and Google Earth^{TM} image together with field data have been used to support the analysis and interpretation. The overall processing scheme followed in the present approach is shown in Figure 5.2.

5.4 THE 'MAXIMUM REFLECTANCE THRESHOLD METHOD'

Opencast mining activities often lead to large exposures of fresh rock surfaces and production of bulk volume of mining wastes. The nature of soil and type of rock material is dependent on the geological characteristics of the underlying rocks. The mining wastes are the rock fragments of the host rocks and overlying soil material, piled up together in the vicinity of opencast mining area. In a coal-bearing sedimentary regime, these materials are commonly sandstone-shale surfaces and their chunks and fragments, often with no vegetation.

The fresh rock surfaces and overburden dumps provide surfaces of highest ground reflectance in the area. However, the spectral radiance due to emitted radiation from surface fires is still higher in comparison to that from the ground reflectance. This study deals with finding a threshold to differentiate between the two.

To determine the appropriate threshold for TM-7, first, several spatial profiles that pass through barren exposed materials and surface coal fires were selected on one Landsat TM scene using false colour composites composed of 4,3,2 and 7,5,3 band combinations. The spectral radiance values along these profiles were analysed on a pixel-by-pixel basis. In the next step, preselected spatial profiles were traced on all images of the temporal data stack. Again, spectral radiance values were analysed on a pixel-by-pixel basis for the spatial profile on each date image. This detailed analysis helped to determine the range of spectral radiance values and the corresponding maximum reflectance value associated with overburden dump material in the coal mining area. Auxiliary datasets such as the higher spatial resolution images of the study area available on GoogleEarth^{TM}, ASTER-derived digital elevation models and limited field data together helped to support the analysis and interpretation. The spectral radiance corresponding to the maximum reflectance value found in the study area associated with the exposed material was then set as the threshold value and any value higher than this threshold value was attributed to the presence of surface fires.

The above method was applied on selected parts of two coal fields with different geographic and climatic settings: (a) the Jharia Coalfield (JCF), India, that represents a tropical,

low altitude coal field occurring in relatively flat terrain with tropical monsoon dominated climate, and (b) the Ruqigou Coalfield (RCF), Ningxia, China, that represents a mid-latitude, high-altitude coal field occurring in an undulating terrain with semi-arid to arid climate. Calculation of at-sensor spectral radiance is the first step to convert image data from multiple sensors and platforms to a physically meaningful common radiometric scale (Gupta, 2003). The Landsat digital numbers (DN) were converted to spectral radiance and then to top of atmosphere (TOA) reflectance values (Chander et al., 2009). Spectral parameters and sensors calibration Landsat TM/ETM+ band 7 data used in the processing of the datasets is given in Table 5.1.

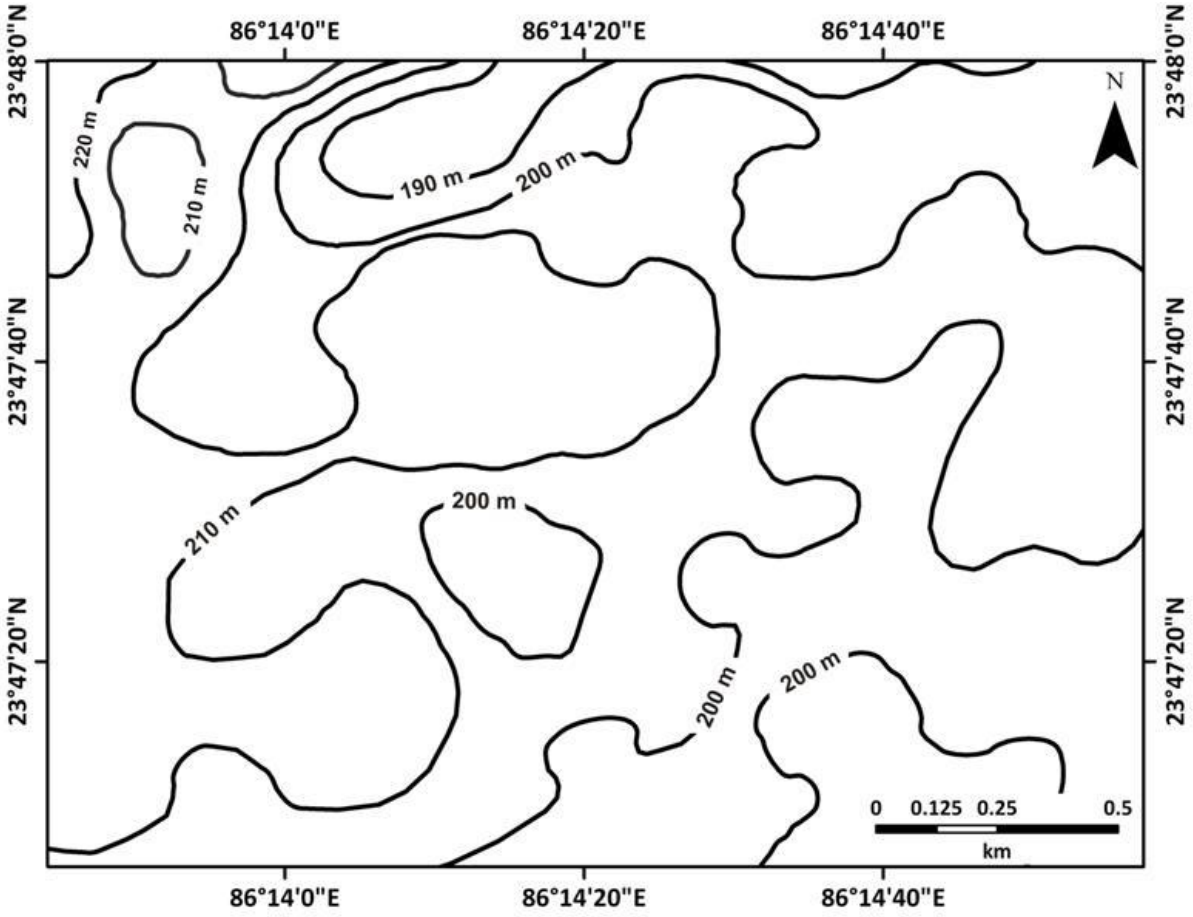

Figure 5.3 The contour map of the Shatabdi coal mine area, Barora, JCF derived from the 30 m spatial resolution ASTER global Digital Elevation Model product. The contours reveal that the JCF is generally flat lying with elevations varying from approximately 190-220 m

Table 5.1 Specification and details of the Landsat TM/ETM+ band 7 data used in the present study and parameters for TOA reflectance computation

Study area	Landsat scene ID	Acquisition date	Sensor ID	Earth Sun Distance (d) (astronomical units)	Mean Exoatmospheric Solar Irradiance ($ESUN_\lambda$) ($W\ m^{-2}\ \mu m^{-1}$)	Solar Elevation Angle (Degree)
Jharia Coal Field, India	L71140044_04420001217	17-12-2000	ETM+	0.98407	84.90	52.3793
	L71140044_04420011102	02-11-2001	ETM+	0.99228	84.90	43.6863
	L71140044_04420021207	07-12-2002	ETM+	0.98519	84.90	51.4129
	L71140044_04420030329	29-03-2003	ETM+	0.99840	84.90	33.2352
	L5140044_04420091202	02-12-2009	TM	0.98592	83.44	50.3889
	L5140044_04420100220	20-02-2010	TM	0.98877	83.44	44.4370
Ruqigou Coal Field, Ningxia, China	L71129033_03320001017	17-10-2000	ETM+	0.99662	84.90	38.6014
	L5129033_03320061010	10-10-2006	TM	0.99861	83.44	41.3893

Note: All Landsat datasets are systematically corrected L1G product.

5.5 DATA ANALYSIS IN TEST SITE 1: JHARIA COALFIELD (JCF), INDIA

5.5.1 Jharia Coalfield (JCF), India

Physiographical and geological attributes of the Jharia Coalfield (JCF), India have been already discussed in Chapter 3. Shatabdi coal mine, Barora a site proposed for the present study is an integral part of the JCF confined between N 23° 47’ 00” - N 23° 48’ 00” and E 86° 13’ 40’’ - E 86° 15’ 00’’ at 77 m above mean sea level (see Figure 3.1 in Chapter 3). Intense opencast activities in the Barora area unveil the shallow subsurface burning coal seam to an exposed scenario. Seams V/VI/VII in Shatabdi opencast are strongly affected by surface fires. Fire control measures in Shatabdi opencast are mainly deal by excavation and back filling methods (BCCL, 2008). Freshly excavated materials of the overlying rocks in Shatabdi coal mine are dump in the close vicinity of opencast.

The elevation contours prepared from the ASTER DEM of JCF with pixel size 30 m are shown in Figure 5.3. The contours reveal that the area is relatively flat with only minor topographic variation ranging from 190 to 220 m. Field observations suggested that the area can be potentially used as a test site for applying methodology of the present work.

Based on the spectral and textural characteristics on Landsat TM/ETM+ colour infrared (CIR 4-3-2) composites, various land-use/land-cover (LULC) classes were identified in the study area. These classes were also validated in the field. Spectral and textural characteristics of different ground features have been already discussed in Chapter 4 Section 4.2.6.1.

Field investigations for temperature measurements of thermal anomalies, distribution of coal fires (both surface fires and subsurface fires) and land use/land cover changes associated with mining activities were carried out in the JCF during February and December 2010 and described in detail in Chapter 3, Section 3.7. For this particular study, the overburden dumps were specifically studied and were found to be composed of sandstone-shale fragments in various proportions, the highest reflective regions being devoid of vegetation.

5.5.2 Data used in JCF

In this study, six sets of Level 1G (geometrically and systematically corrected) cloud free Landsat TM-7 day time data from December 2000 to February 2010 were used to apply the proposed maximum reflectance threshold technique and delineate surface coal fires in the JCF.

All sets of Landsat data were obtained from the US Geological Survey Landsat archive (http://glovis.usgs.gov) and processed using ENVI™ 4.7 and ERDAS Imagine™ 10. General information about the dataset and other specifications have already discussed in Chapter 4, Section 4.2.1.1 and are given in Table 5.1.

5.5.3 Analysis and interpretation in JCF

Temporal datasets of Landsat TM/ETM+ band 7 from December 2000 to February 2010 facilitated a decade-long comparative study accounting for season and inter-annual variations in surface reflectance and fire temperatures in the JCF. The JCF data were processed following the method described in detail in Section 5.3. Following are the data processing results and analyses.

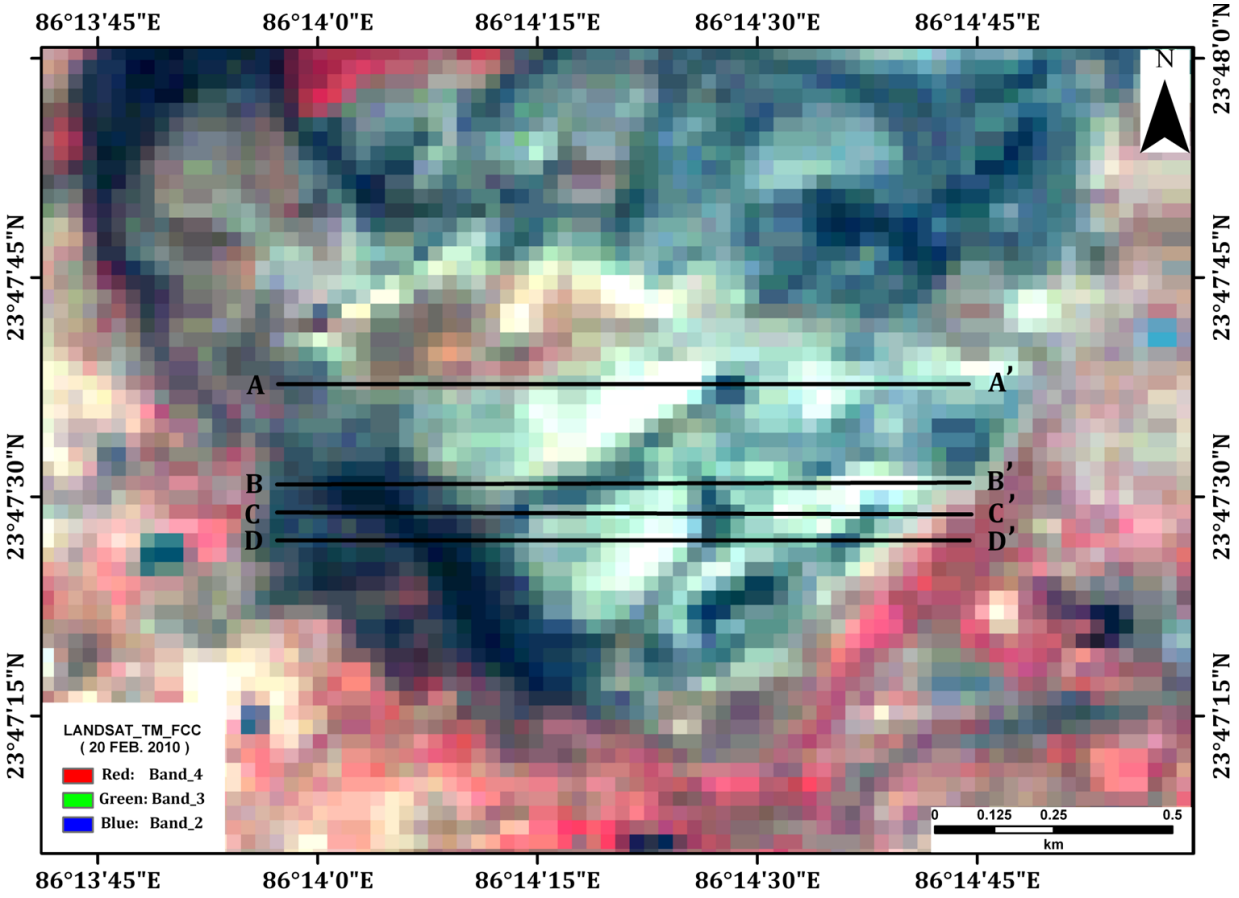

Figure 5.4 Location of spatial profiles A-A', B-B', C-C' and D-D' shown on a February 2010 on standard color composite on JCF

5.5.3.1 *Analysis of different spatial profiles in the same image*

For this study, field work in the JCF was carried out from December 2010 through January 2011. Selecting a Landsat scene closest to the field work time, several spatial profiles A-A', B-B', C-C' and D-D' were drawn crossing barren exposed materials on the February 2010 image (Figure 5.4).

Figure 5.5 shows (i) the location of profile D-D'. on the February 2010 Landsat TM-7 image; (ii) shows the pixel-wise DN values and computed spectral radiance values along the same profile D-D'; (iii) shows the corresponding Google Earth^{TM} image; (iv) and (v) show field photographs of points a and b, marked in (iii), and show surface fire and overburden dump, respectively. For all the spatial profiles (A-A', B-B', C-C' and D-D'), the DN values along the profile and their corresponding computed spectral radiance value are shown on the left along the Y-axis (Figure 5.6(a)-(d)).

In this open-cast mine area, the various ground features of concern are coal bed, coal dump, water body, overburden dumps and surface fires. Out of these features, the overburden dump possesses the highest ground reflectance. Therefore, in various profiles, pixels corresponding to the overburden dumps were first sought and marked with the support from Google Earth^{TM}, Landsat VNIR images and field data. These pixels have spectral radiance in the range of 4.2-4.8 $Wm^{-2}sr^{-1}\mu m^{-1}$ corresponding to the reflectance values from 0.23 to 0.25. Spectral radiance higher than this must be undoubtedly due to the thermal emission from surface fires.

5.5.3.2 *Analysis of same spatial profile in the multi-temporal images*

A detailed pixel-wise analysis of the DN values and spectral radiance of the same spatial profile (D-D') was carried out in different temporal images. The DN values and spectral radiance along the profile D-D' in different temporal images (17 December 2000, 2 November 2001, 7 December 2002, 29 March 2003, 2 December 2009 and 10 February 2010) are shown in Figure 5.7(a)-(f). Using the technique adopted for analysis in Figure 5.7, overburden dumps were sought and marked using the Landsat VNIR bands. Threshold in terms of DN values, spectral radiance and reflectance for different image datasets was established. The points or peaks corresponding to the maximum ground reflectance are marked in Figure 5.7(a)-(f). It is obvious that in general, the highest reflectance threshold is around 0.25, though in some seldom extreme cases it can be 0.27.

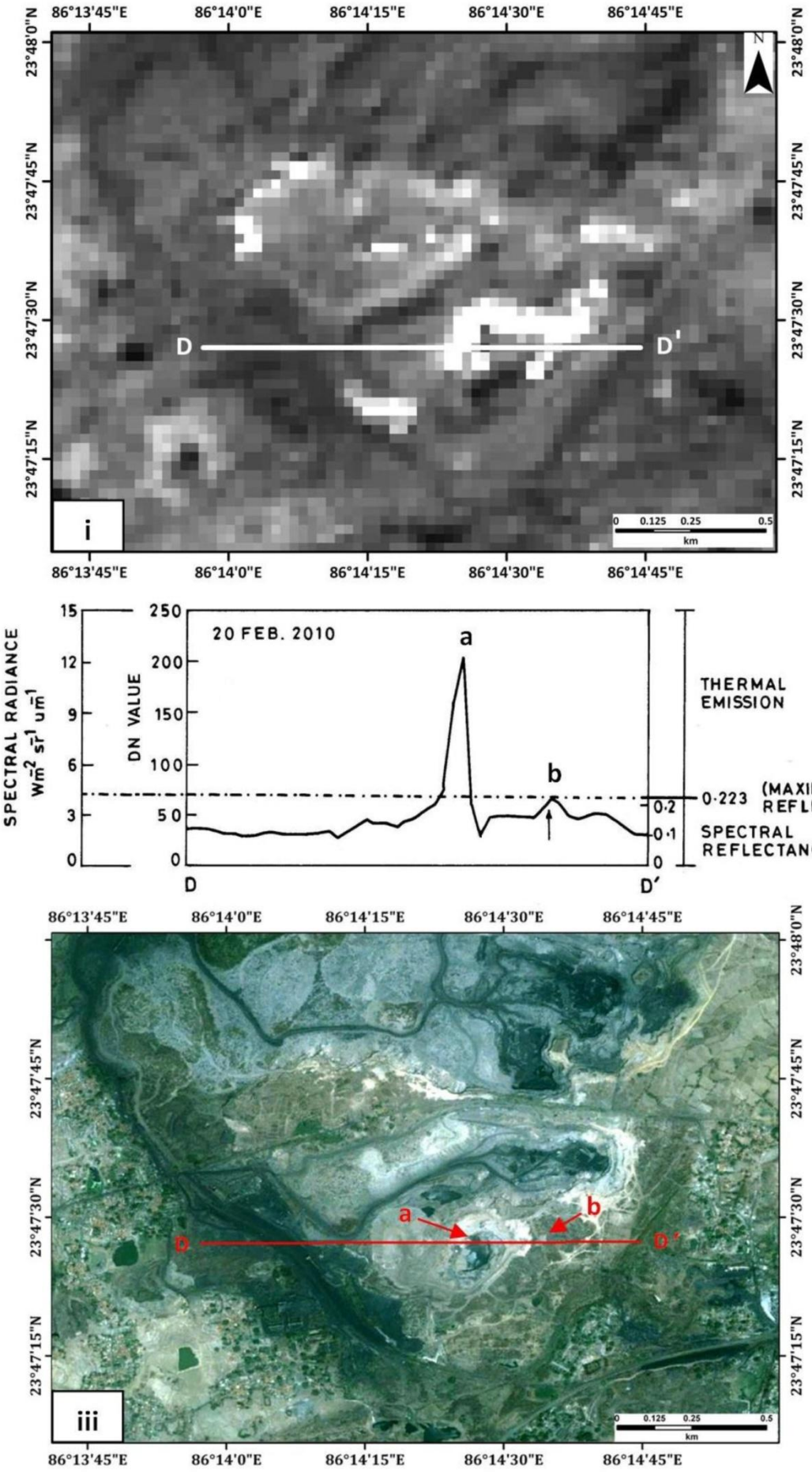
86°13'45"E
86°14'0"E
86°14'15"E
86°14'30"E
86°14'45"E
23°48'0"N
23°47'45"N
23°47'30"N
23°47'15"N
N
D
D'
i
0 0.125 0.25 0.5
km
SPECTRAL RADIANCE
Wm⁻² sr⁻¹ um⁻¹
DN VALUE
20 FEB. 2010
a
b
THERMAL EMISSION
0·223 (MAXIMUM REFLECTANCE)
SPECTRAL REFLECTANCE
ii
iii

Figure 5.5 Methodology followed in the study is presented here using the JCF as an example. Key: (i) the location of the selected profile line D-D' on Landsat TM band-7 image of February 2010, (ii) DN values, spectral radiance and maximum reflectance along profile line D-D', (iii) surface fire location a and overburden dump location b, along the selected profile line are shown as a reference on a high spatial resolution Google Earth^{TM} background image, (iv) field photograph of a coal fire at location (iiia) and (v) field photograph of an overburden dump at location (iiib)

5.6 DATA ANALYSIS IN TEST SITE 2: RUQIGOU COALFIELD (RCF), NINGXIA, CHINA

5.6.1 Ruqigou Coalfield (RCF), Ningxia, China

The Ruqigou Coalfield (RCF) is located in the northern part of the Helan mountains, approximately 100 km from Yinchuan city, capital of Ningxia Hui, autonomous region centered at approximately N 39° 04' and E 106° 08' (Figure 5.8). This Coalfield represents mid-latitude, high-altitude (1400-2640 m above sea level) and semi-arid to arid climate and shows large diurnal and seasonal temperature variations and a sparse vegetation cover dominated by dry desert shrubs. Both underground and open-cast mining practices have shaped the landscape of the area.

The approximately 80 km^2 RCF lies within a Jurassic syncline (Kuenzer et al., 2007b). It contains high rank coal, mostly anthracite. Like many other coal fields in China, the RCF coal was also deposited in a fluvial-lacustrine environment and is interbedded with mudstones, siltstones, sandstones and conglomerates in the Triassic Yanchang and Jurassic Zhiluo formations (Chen, 1997). Subsequent uplift and erosion of this basin exposed the coal. There

are about 10 major coal seams in the RCF of which three coal seams (locally numbered 1, 2 and 3) are prominently exposed in the study area.

5.6.2 Data used in RCF

Two sets of Level 1G cloud-free Landsat TM-7 day time data of 10 October 2000 and 17 October 2006 were selected for RCF (Table 5.1). A 5 m spatial resolution digital elevation model, derived using traditional photogrammetric techniques applied to aerial stereo-photographs, provides spatial details of the uneven topography in the study area (Prakash et al., 1999).

5.6.3 Analysis and interpretation in RCF

One of the objectives of this study was to determine a TM-7 threshold technique and threshold value that would have minimal dependencies on local conditions. Given the local extents of fires and exposed overburden rocks, variations in slope are insignificant to the analysis. Elevation and aspect can arguably influence the reflectance (Engle et al., 2011).

In the RCF, almost all the fires are located on the South, SE and SW facing slopes as these areas are exposed to more sunlight and are more vulnerable to heating and combustion. To check the broadest applicability of the maximum reflectance threshold techniques, profiles were, therefore, selected at different elevations and slopes without carrying out any topographic normalization. The results and analyses of selected profiles are presented here.

5.6.3.1 *Analysis of different spatial profiles in the multi-temporal images the same image*

A false-colour composite generated by coding TM bands of 7-5-3 in red-green-blue, respectively for both images was used for identifying the locations of thermally radiant surface fire pixels. Three profiles (E-E', F-F' and G-G') were selected in the RCF. As the fire in this study area was active, the associated thermal anomaly shows a shift in pixel location on the 2006 image with respect to 2000 image.

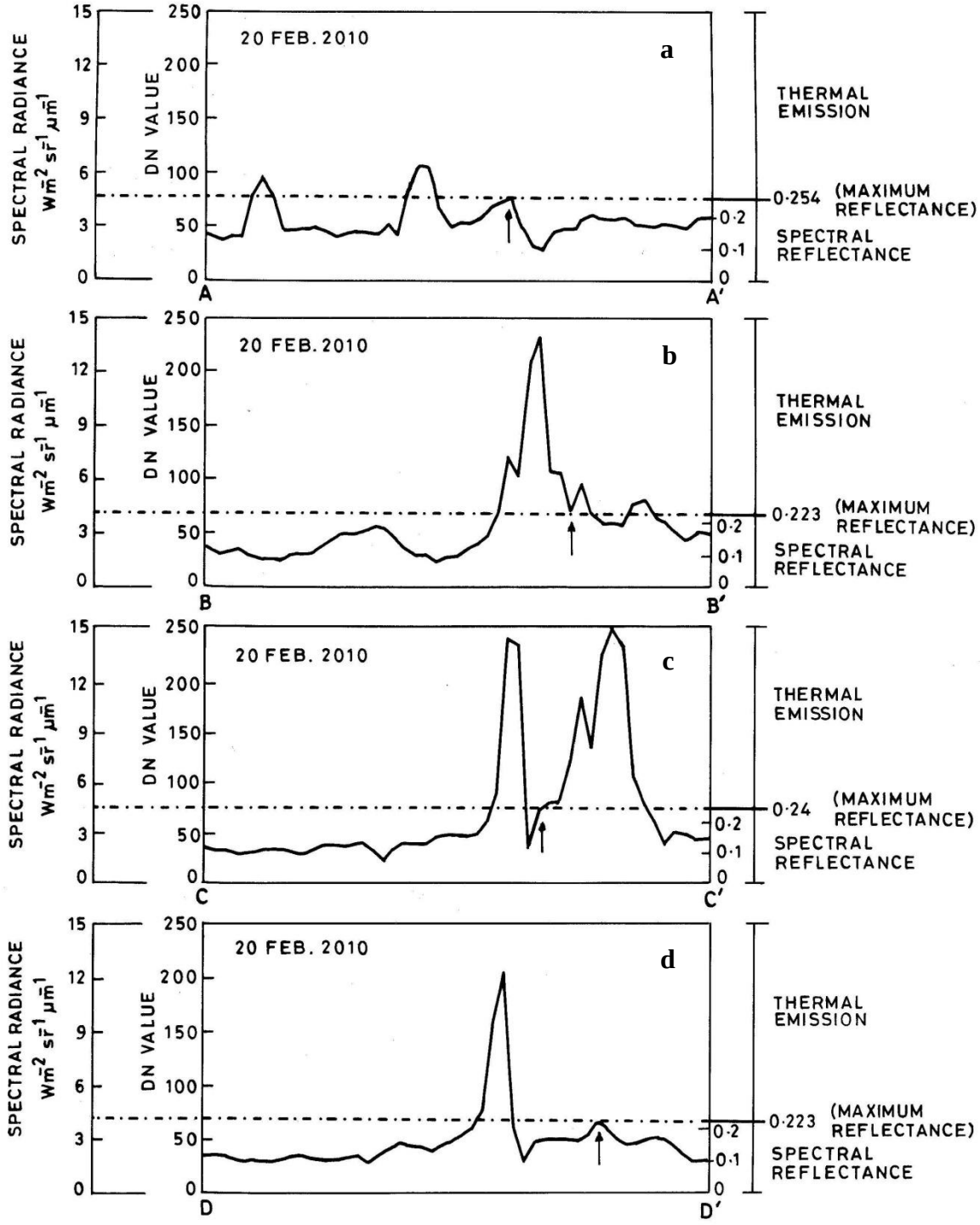

Figure 5.6(a)-(d) DN values, spectral radiance and maximum reflectance along profiles A-A', B-B', C-C' and D-D' extracted from Landsat TM-7 image dated 20 February 2010 for the JCF. The maximum reflectance of approximately 0.25 (or 25% reflectance) along the profiles corresponds to a spectral radiance of 4.762 $Wm^{-2}sr^{-1}mm^{-1}$ and appears as the threshold to separate the background reflective pixels vis-a`-vis the emissive fire pixels

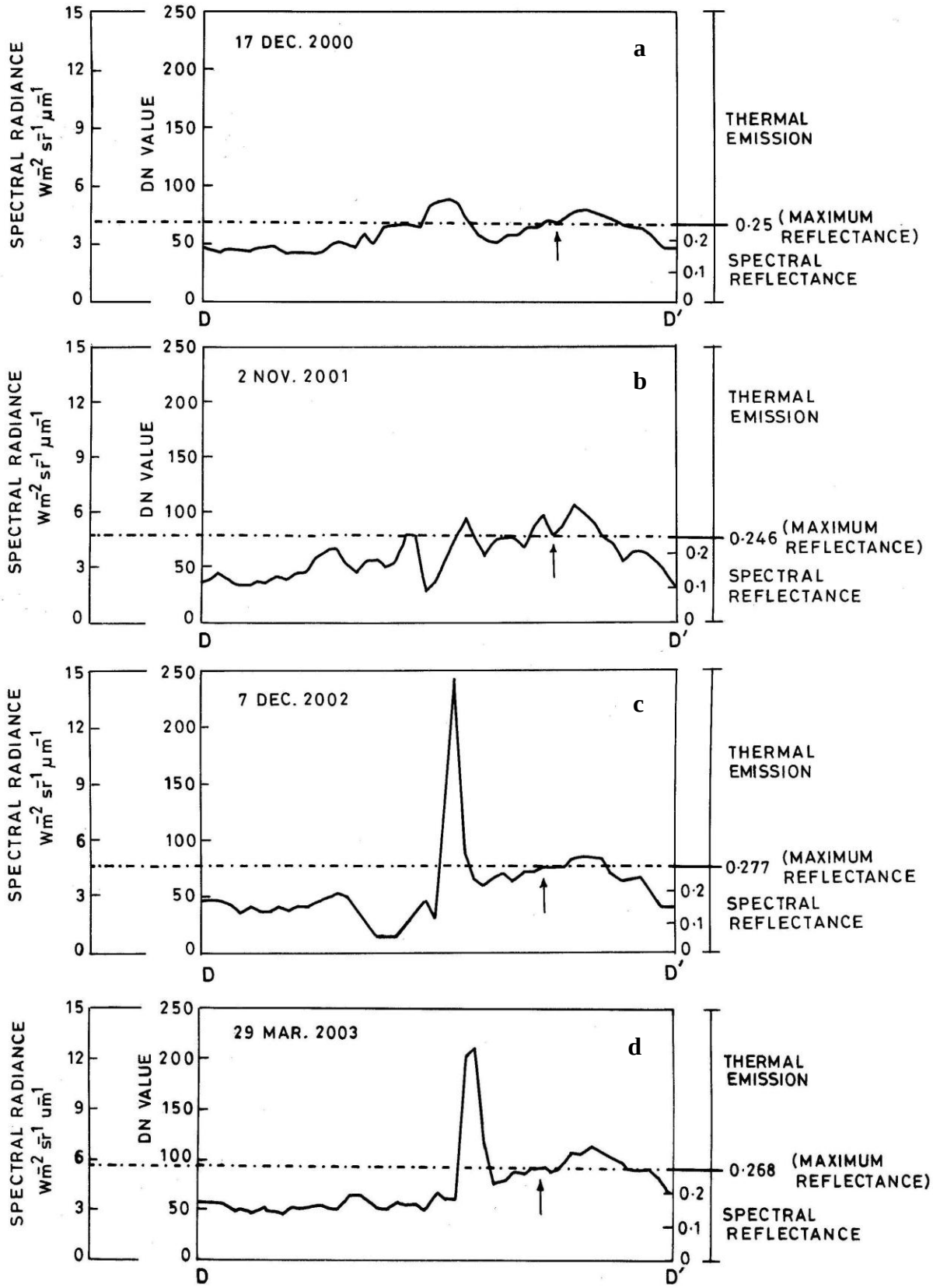
17 DEC. 2000
a
SPECTRAL RADIANCE
DN VALUE
THERMAL EMISSION
0·25 (MAXIMUM REFLECTANCE)
SPECTRAL REFLECTANCE
D
D′
2 NOV. 2001
b
0·246 (MAXIMUM REFLECTANCE)
7 DEC. 2002
c
0·277 (MAXIMUM REFLECTANCE
29 MAR. 2003
d
0·268 (MAXIMUM REFLECTANCE)

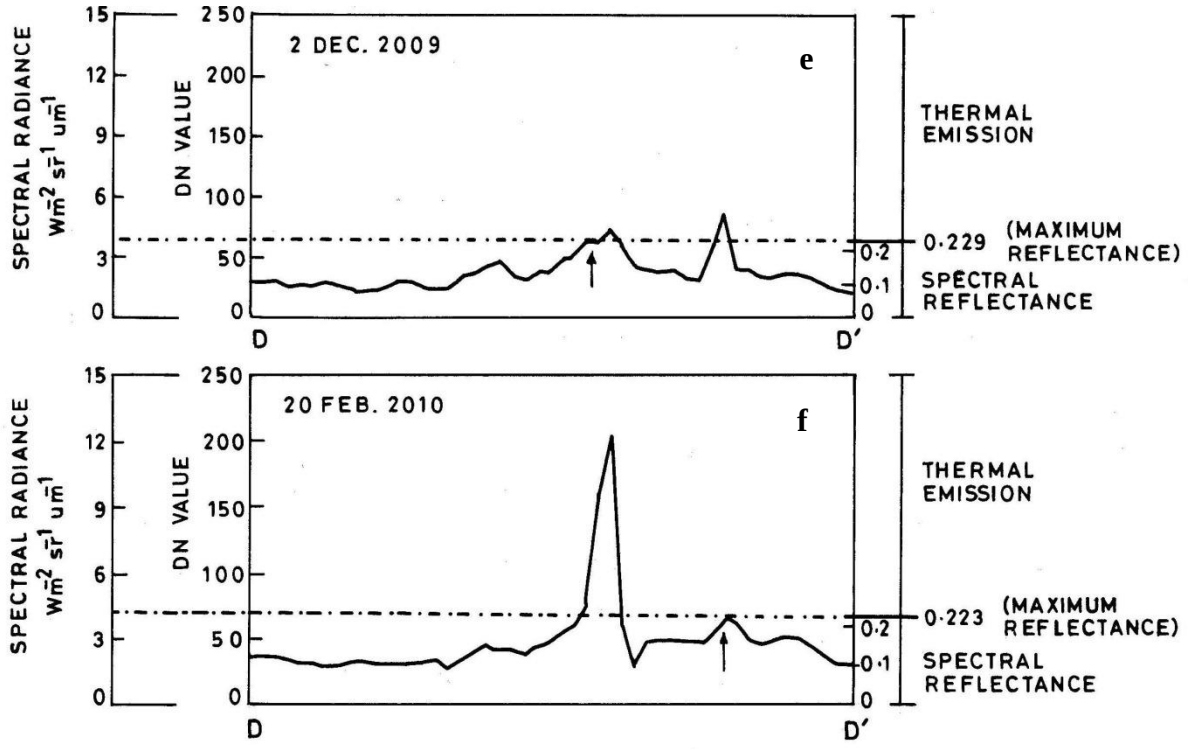

Figure 5.7(a)-(f) Comparison of spectral radiance, spectral reflectance and corresponding DN values in the same profile (profile D-D') on different temporal images. The maximum reflectance value of generally 0.25 (0.27 in some extreme cases) can be used as a threshold for isolating the pixels with definitely 'hot' (fire) material

Therefore, the profile lines used for comparison (Figure 5.9, E-E' and F-F' on the 17 Oct. 2000 and 10 Oct. 2006 images, respectively) had to be shifted by a corresponding amount to carry out a meaningful comparison. These profiles were selected at a relatively lower altitude of 1867 m, compared to another profile line (G-G') which was selected at a higher elevation of 2014 m.

Following the above method of data interpretation and analysis, the pixel values corresponding to maximum surface reflectance were 0.246 and 0.244 for the profiles E-E' and F-F', respectively (Figure 5.9(a) and (b)), and 0.226 for the profile G-G' (Figure 5.9(c)). Although there is considerable difference in the altitude of profiles E-E' and G-G', the corresponding difference in the maximum reflectance threshold of the pixels is only a negligible 2%.

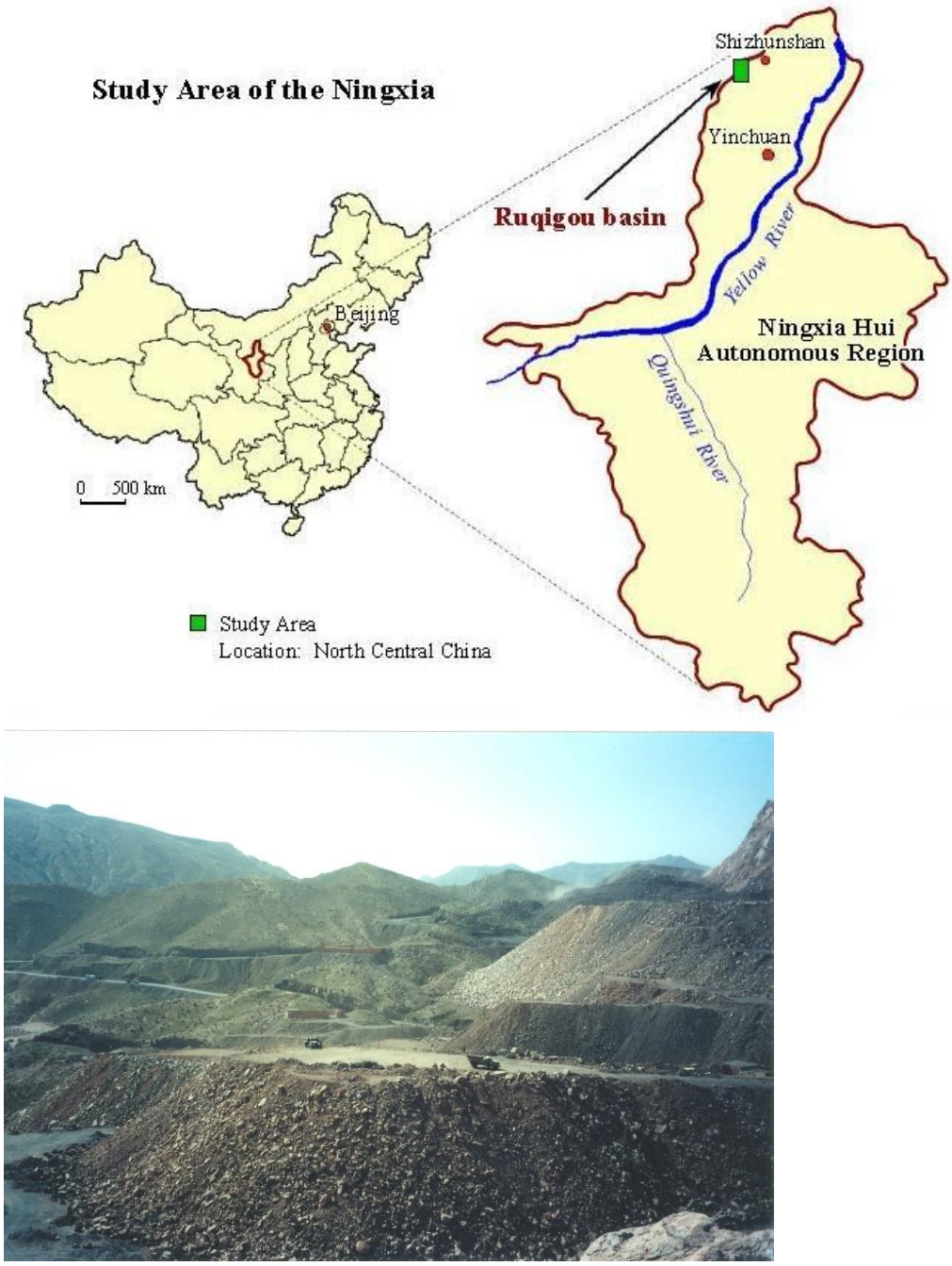

Figure 5.8 Location map of Ruqigou Coalfield (RCF), China, and field photograph showing overdumps and overall topography of Ruqigou coal field (by Anupma Prakash)

Peaks in the profiles corresponding to the maximum ground reflectance served as a basis for setting the threshold were analysed in terms of DN values, spectral radiance and reflectance for these two datasets (Figure 5.10). The maximum background reflectance for both the images was around 0.24-0.25 which is comparable to the maximum reflectance values determined for the JCF.

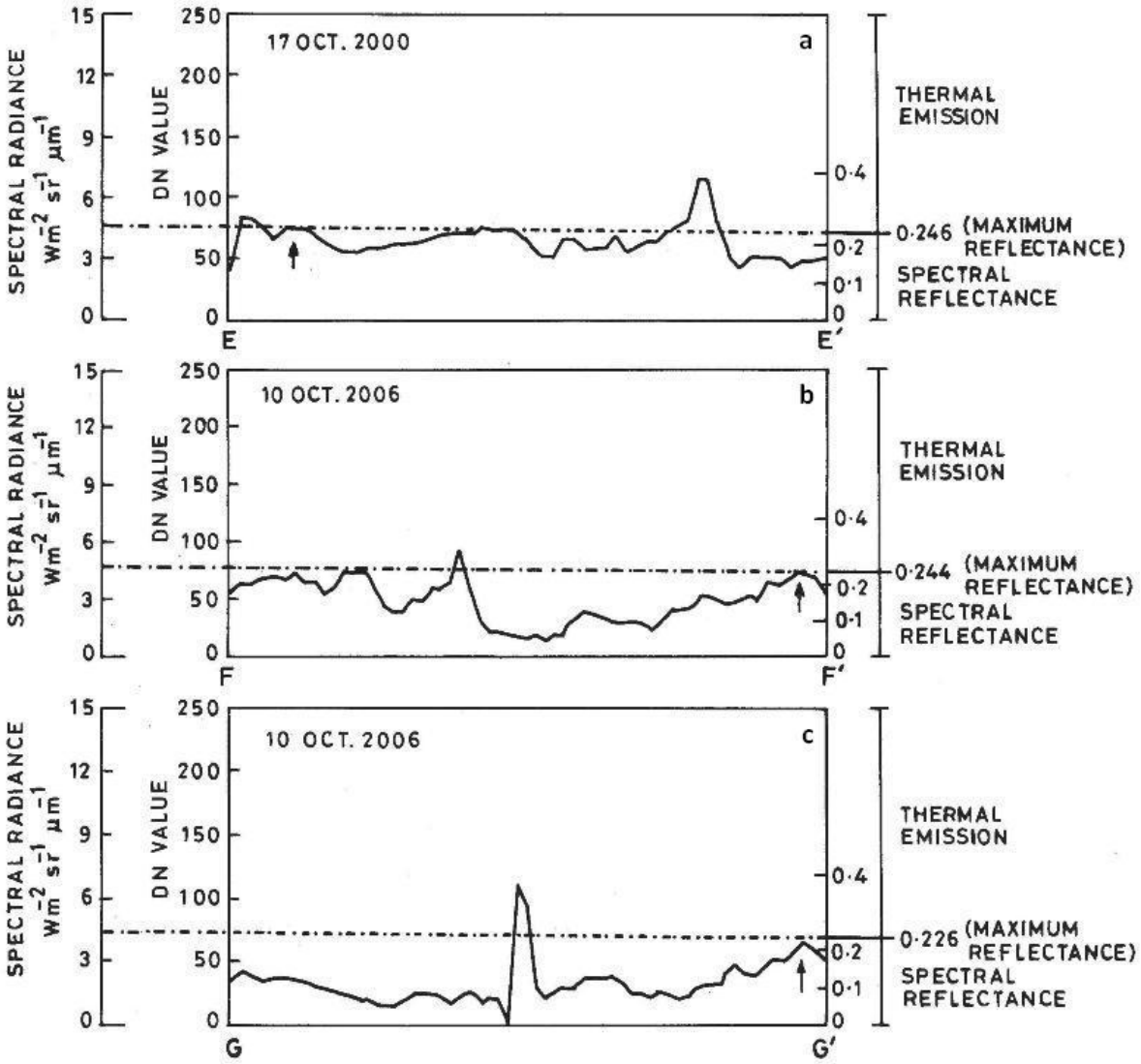

Figure 5.9(a)-(c) Comparison of percentage reflectance and corresponding DN values in profiles (E-E', F-F' and G-G') of two different images covering RCF.

5.7 CONCLUSION

A comparison of the threshold values observed in terms of DN value and maximum background reflectance percentage values for all datasets (including India and China) was carried out (Figure 5.10(a) and (b)). The threshold in terms of DN values varies from 62 to 93, whereas the same in terms of reflectance ranges from 0.23 to 0.27. Thus, as expected, there is a high variability when threshold is considered in terms of DN values; on the other hand, when the threshold is sought in terms of computed reflectance, there is a greater consistency and uniformity in various datasets irrespective of scene, topography, season or month.

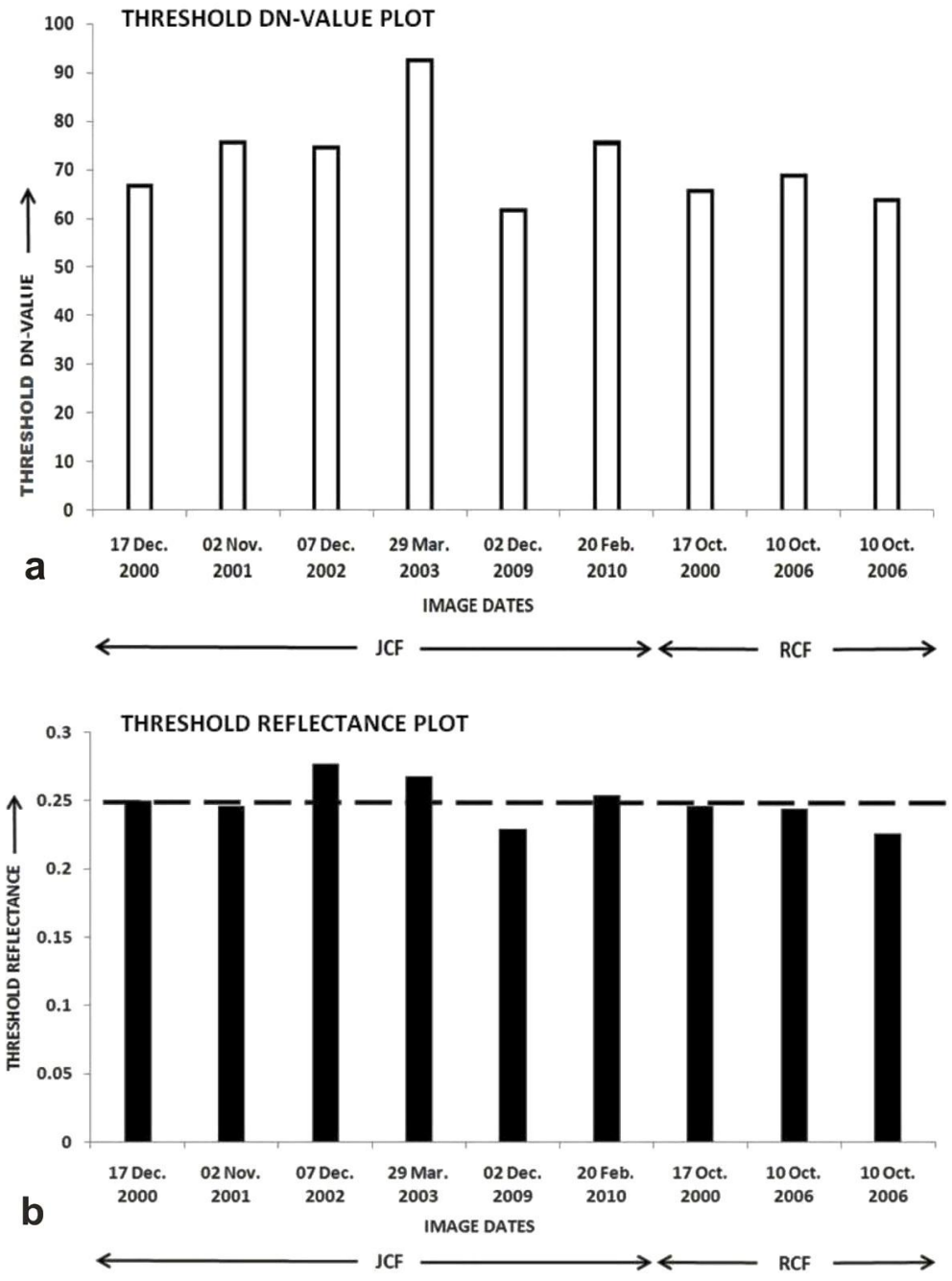

Figure 5.10(a)-(b) Collective comparison of the threshold values observed in terms of (a) DN value and (b) reflectance percentage for all the profiles selected on JCF and RCF datasets. Note that the maximum DN value of the reflective background rock material ranges from 62 to 93 in different temporal images, whereas the computed reflectance of the same target material ranges from 0.22 to 0.27, with the average being around 0.25. This indicates that the computed reflectance value provides a better way for uniform thresholding.

The results obtained from the above analysis clearly indicate that the maximum background reflectance computed in the coal field area is rather scene independent and ranges around 25%, although, in some cases, it can go up to 0.27. The 0.25-0.27 reflectance threshold appears to work well for tropical as well as temperate regions and may be considered as a reasonable threshold for isolating fire pixels using this type of SWIR data.

In this study, no corrections for atmosphere have been implemented for the simple reason that in the SWIR part of EM spectrum, the effect of atmosphere is quite minimal and we are working with data in an atmospheric window. Furthermore, relative reflectance values in spatial profiles to select highest reflectance value are considered as the threshold, practically, the effect of atmosphere would again tend to be evened out. Nevertheless, using this concept, a rigorous atmospheric correction can lead to numerical values of threshold that may be globally applicable.

Reflectance data can also vary with sun-earth satellite geometry and, as such, latitude, topographic slope and aspect are important. However, here maximum reflectance is considered as threshold, and, therefore, feel that this reflectance value will not increase any further with changes in local viewing geometry. Furthermore, taking this highest reflectance value as the threshold has one limitation that in some instances, possibly when the sun-earth-satellite geometry is not conducive, it is likely that the reflectance values from some fire areas are lower and may be missed. In this sense, this technique is a bit more conservative but arguably more reliable for fire delineation.

Despite its conservative nature, the maximum reflectance threshold technique for SWIR data described above provides a practical way to segregate pixels with definitely fire, has the advantage that it is based on physical processes controlling reflectance of typical material types found in coal mining areas and appears applicable in a wide range of geographic settings, and the method should be repeatable without introducing a user-bias.

CHAPTER 6

MAPPING OF COAL MINE SURFACE FIRE

6.1 INTRODUCTION

Coal is directly related to the production of energy. To confront the exponential demands of energy supply for industrial growth, the haphazard coal mining activities are being intensely carried out worldwide. Coal mining is closely associated with temporal variation in land use pattern that are affected by both anthropogenic and natural activities. Open cast mining, dumping of coal and frequent accumulation of mine dumps (overburden dumps) are some of the anthropogenic activities that causes frequent change in the land-use around a coal mining area. Unplanned mining activities and excavations in open casts unveil the burning coal seams. 'Surface-subsurface coal fires' are the typical characteristic of a coal mine area. Such features are sporadic in spatial extent and vary in dimension from few meters to tens of meters. Mapping of coal fire is the pre-requisite for coal fire related studies. To facilitate plan sustainable mining for industrial growth, temporal monitoring of coal fires has to be executed at regular interval.

The present chapter illustrates a brief overview of a novel methodology adopted for immediate localization of coal mine surface fires. The methodology first involves the analysis of spectral reflectance curve of different land cover classes recognized in the study area. Bands with maximum and minimum spectral reflectance have been selected to obtain ratio indices for different classes. Obtained Indices have been further interpreted to discriminate the coal and discussed the association of surface fire with exposed coal bed. In the present approach, two ratio indices namely; Normalized Difference Coal Index (NDCI) and Normalized Difference Coal Index (NDCfI) have been derived to systematically map the coal fires using Advance Spaceborne Thermal Emission and Reflection Radiometer (ASTER). The adopted methodology has been systematically implemented in JCF.

6.3 **THEORETICAL BACKGROUND AND CONCEPTUAL APPROACH**

Coal mining areas are generally characterized by seven major land cover classes such as vegetation, water bodies, settlement, barren land, coal, overburden dump and fire. Traditional field survey methods for mapping of spatial distribution of land cover classes are time consuming and acquired in a generalized manner for the whole area. Temperature measurement is also a difficult task as the areas are often inaccessible due to uncontrolled coal fires. Moreover, field surveys cannot be executed frequently and considered unfeasible from economic point of view. Satellite data have potential advantage over traditional field survey methods. Advanced mapping techniques using remote sensing methods provide useful inputs in analyzing coal mine related features.

Automatic classification techniques to discriminate the various land cover types have been effectively used in recent past (Prakash and Gupta, 1998b; Zha et al., 2003; Kenzer et al., 2007). However, mapping based on automatic classification techniques needs careful selection of the spectral signatures of the closely associated feature classes. Limited availability of the spectral channels operating in different regions of the electromagnetic spectrum also poses difficulty in retrieving signatures of different classes. Also, low spatial resolution of thermal infrared region (TIR) datasets and sensors response in short wave infrared region (SWIR) to both emission and reflection by fire also restrict thermal analysis of the coal fire. Localized high intensity surface fire and very low intensity surface fire in fresh mine dumps are closely located in the vicinity of open cast areas. Such dump fires are perceived automatically by TIR satellite datasets and often misinterpreted as ‘coal fire’ in coal mining area.

To deal with the aforesaid problems, systematic analysis of the spectral characteristics of different land cover classes in coal mine area has been carried out. In this respect, two spectral indices have been obtained using Advance Spaceborne Thermal Emission and Reflection Radiometer (ASTER) by applying simple band ratio technique and normalized difference method. ASTER has six and five channels operating in short-wave and thermal infrared region of the spectrum. These channels can be potentially applied in analyzing temperature related phenomenon (discussed in Chapter 2, Section 2.2). The approach presented here is rapidly practicable and less time consuming to delineate coal fire based on their variable spectral and textural characteristics (Table 6.1).

Table 6.1 Textural and spectral characteristics of the coal fires observed on the ASTER CIR composite

<table>
<tr><th rowspan="3">Land use / Land cover type</th><th colspan="6">Coal fires</th></tr>
<tr><th colspan="3">Dump fire</th><th colspan="3">Coal seam fire</th></tr>
<tr><th>Overburden dump fire</th><th colspan="2">Mined coal dump fire</th><th colspan="2">In situ coal seam fire</th><th>Buried subsurface coal seam fire</th></tr>
<tr><td rowspan="2">Textural characteristics</td><td>No or Small sporadic fire</td><td colspan="2">Scattered and irregular in nature. Lies in close association with freshly exposed in situ coal seam</td><td colspan="2">Linear / segregated fire</td><td>Clustered fire</td></tr>
<tr><td colspan="6">Appears as pale to bright yellow patches on 8-6-4 of ASTER color composites</td></tr>
<tr><td rowspan="2">Detectable sensors response in different spectral channel</td><td rowspan="2">High visible reflectance and no or very low thermal emission</td><td colspan="2">Low visible reflectance and low thermal emission</td><td colspan="2">Very low visible reflectance and high thermal emission</td><td>High surface reflectance and moderate to high thermal emission</td></tr>
<tr><td>No TIR + minor SWIR anomaly</td><td>Minor TIR anomaly</td><td>High SWIR anomaly</td><td>Saturation or high TIR anomaly</td><td>High TIR anomaly</td></tr>
</table>

6.4 **METHODOLOGY OVERVIEW**

An overview of the methodology scheme and data analysis followed in the present study is presented in Figure6.2. It involves acquisition of satellite data, processing, analysis (computation and thresholding of spectral indices) and interpretation of the results obtained from spatial distribution of coal fires. The datasets have been preprocessed as per the methodology and techniques discussed in Chapter 4, Section 4.5. Calibrated radiance data (VNIR and SWIR datasets) has been converted into spectral reflectance (ρ) by inputting required parameters (Table 4.8) in eq.4.6.

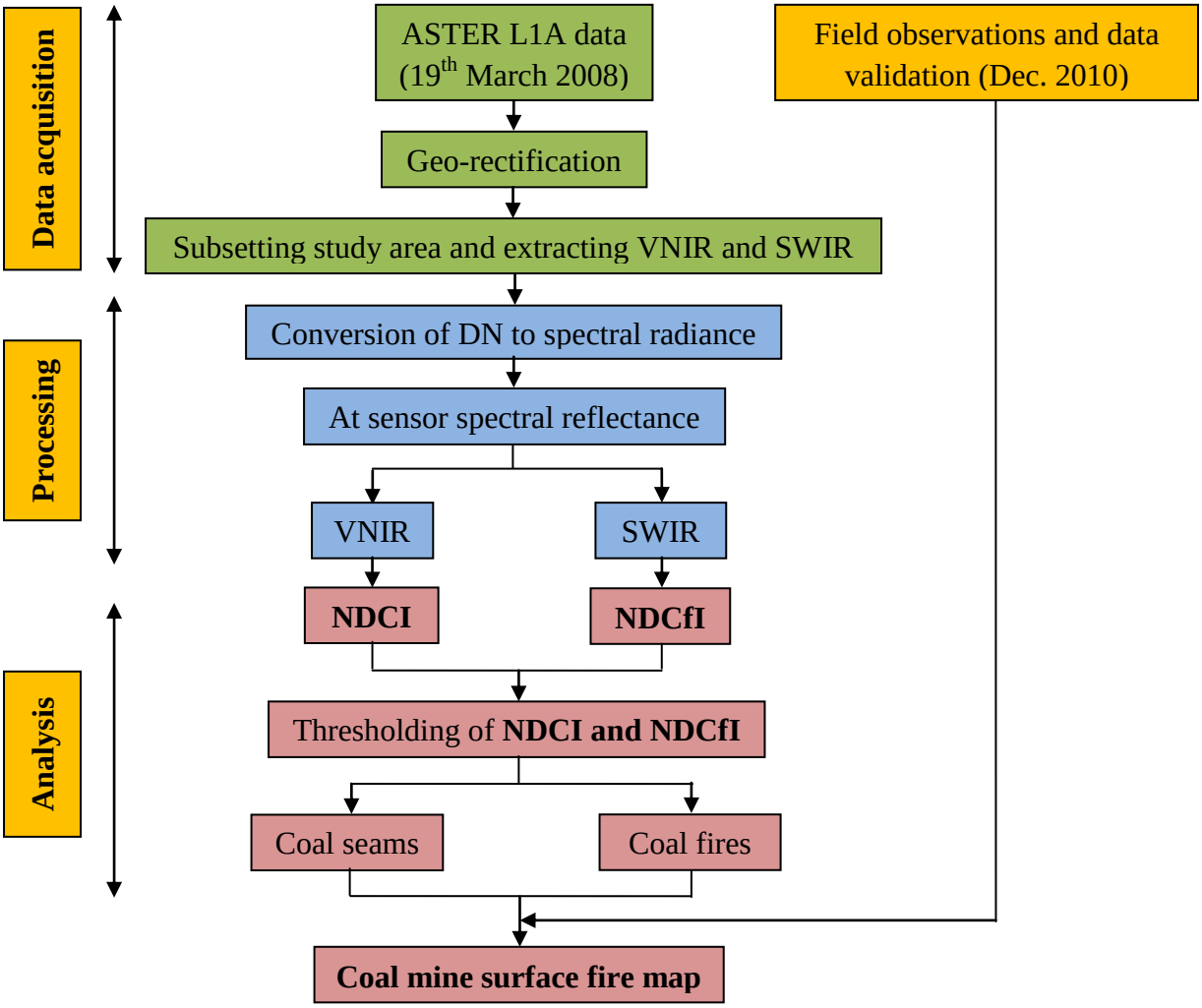

Figure 6.1 Schematic diagram showing the data processing and methodology adopted in the present work

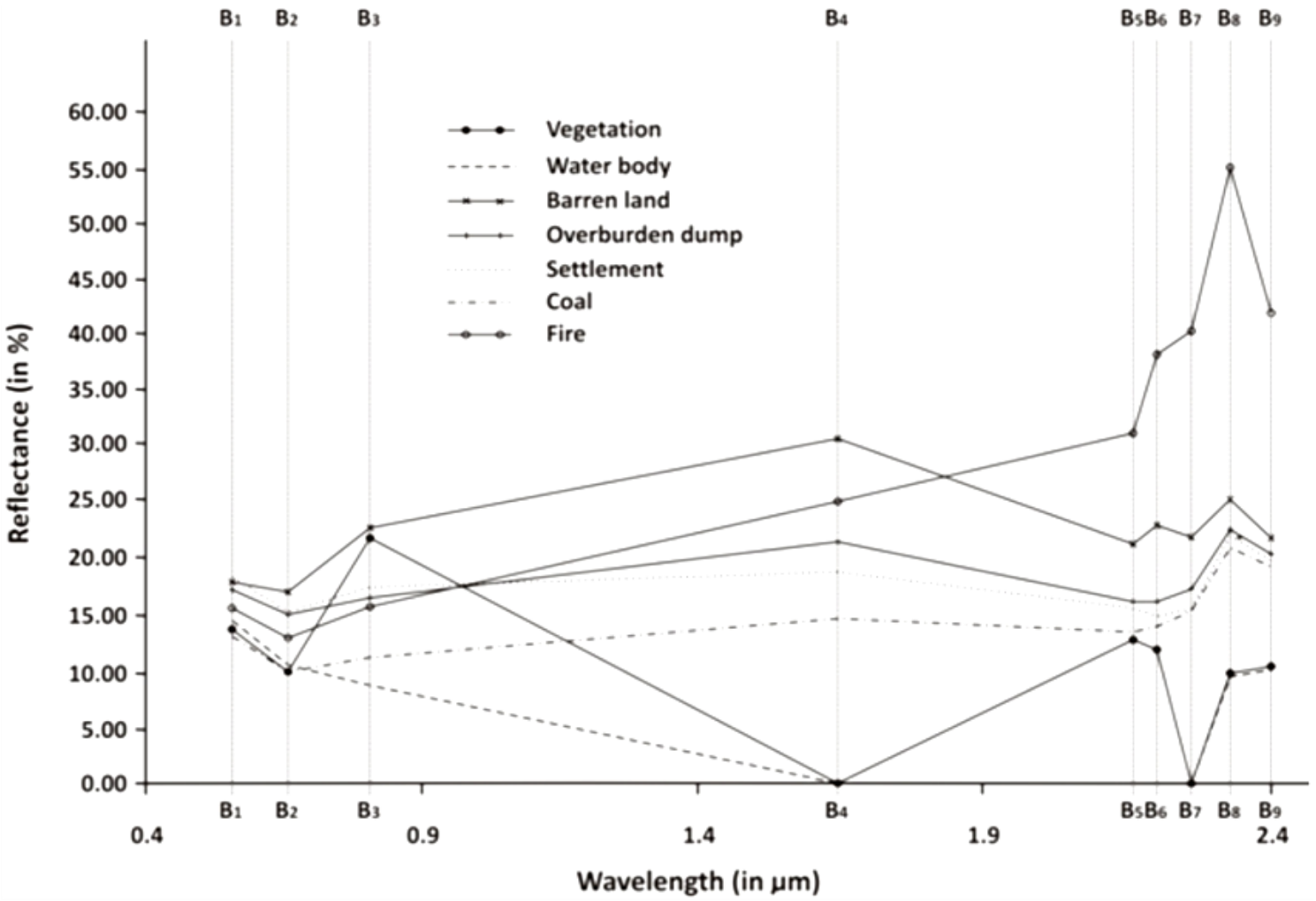

Figure 6.2 Spectral reflectance curves of common land cover classes recognized over CIR composite of ASTER data covering JCF, India

The methodology has been systematically implemented in JCF as test site. The area is almost flat with minor topographic variation and hence, more likely to have unaffected from topographic effects. Spectral characteristics of the different land cover classes in coal mine area have been carefully analyzed and their respective spectral reflectance curves have been plotted (Figure 6.2). Finally, spectral indices have been generated using simple normalized difference technique for coal fire related studies.

6.4 Computation of spectral indices

Normalized index is the ratio of difference and sum of maximum and minimum spectral reflectance of a particular feature class in specific spectral channels. Exposed coal seams, mine dumps, barren land, vegetation, water bodies and settlements are commonly observed in a coal mine area (Prakash and Gupta, 1998b). Normalized index to discriminate barren land/bareness (Zhao and Chen, 2005), built-up area (Zha et al., 2003), vegetation and water bodies (Gao, 1996) have been well studied using Landsat TM/ETM+ images. Excavated coal seams and fresh mined dumps are closely associated with surface fire. To demonstrate the association of surface fire with exposed coal bed, two indices have been proposed in the present study. The obtained indices have been precisely threshold by statistical analysis of their histogram for mapping of surface coal fires.

6.4.1 Normalized Difference Coal Index (NDCI)

Spectral reflectance of the coal observed in Figure 6.2 indicate that coal exhibits maximum drop in reflectance values from band 1 (ρB1) Band 2 (ρB2). However, a major difference in spectra of coal has also been observed in B8 to B7. But as B8 and B7 belongs to short wave infrared region (SWIR) of the spectrum that have significant contribution to reflectance and emission due to fire, these bands have not been taken into consideration for discriminating coal. Spectral characteristics of the vegetation and water bodies are closely associated with B1 and B2 (Figure 6.2). Both of these classes have been mixed up together with the pixels attributed to coal in the index obtained using B1 and B2. To separate the pixels attributed to the coal from the pixels assigned to vegetation and water, NDVI (B3 and B2) and NDWI (B1 and B4) have been calculated. Thresholds have been set between 0-1.0 to both NDVI and NDWI and pixels attributed to vegetation and water bodies have been segregated. To discriminate coal, finally a normalized difference index has been calculated using B1 and B2 and pixels attributed to the vegetation (Pv) and water bodies (Pw) have been precisely

masked from it (eq. 6.1). A threshold value has been set at 0.1-1.0 to the index (NDCI) and coal is precisely discriminated.

$$\mathbf{NDCI} = \left(\frac{\boldsymbol{\rho}\mathbf{B1} - \boldsymbol{\rho}\mathbf{B2}}{\boldsymbol{\rho}\mathbf{B1} + \boldsymbol{\rho}\mathbf{B2}}\right) - (\mathbf{Pv} + \mathbf{Pw}) \quad (6.1)$$

6.4.2 Normalized Difference Coal fire Index (NDCfI)

Mapping of coal fires are the fundamental requisite for coal fire related studies. Sensors response in SWIR and TIR have been potentially applied in recent past for delineating thermal anomalies and mapping of coal fires (Saraf et al., 1995; Prakash and Gupta, 1999a; Rosema et al., 1999; Chatterjee, 2006; Kuenzer et al., 2007c; Raju et al., 2012). Field surveys carried out in JCF reveal that the impracticable and haphazard mining activities in open casts exposed the uncontrolled subsurface coal seam fire to surface coal seam fire. Such subsurface coal seam fire that appeared as low intensity smoldering surface fire (Figure 3.13(b)) and high intensity exposed surface coal seam fire (Figure 3.13(c)) are highly localized in and around open cast areas. Both these fires are high intensity thermal phenomenon and can be potentially detected in ASTER 8-6-4 CIR composite based on their textural and spectral characteristics (Figure 6.3). It has been observed that the spectral reflectance value of the pixels attributed to the fire (hot object) exhibits maximum and minimum intensity response in B8 and B4, respectively, in short wave infrared region of the spectrum (Figure 6.2). To delineate the surface coal fire a normalized difference Coal fire Index (NDCfI) has been obtained using B8 and B4 (eq. 6.2). Frequency distribution curve of the obtained NDCfI (Figure 6.4(a)) has been carefully analyzed. Thresholds have been set at 0.137-0.208 (starting of the toe of the histogram) and 0.208-1.0 (major break in toe) for discriminating the low intensity surface fire and high intensity surface coal seam fire (Figure 6.4(b)).

$$\mathbf{NDCfI} = \left(\frac{\boldsymbol{\rho}\mathbf{B8} - \boldsymbol{\rho}\mathbf{B4}}{\boldsymbol{\rho}\mathbf{B8} + \boldsymbol{\rho}\mathbf{B4}}\right) \quad (6.2)$$

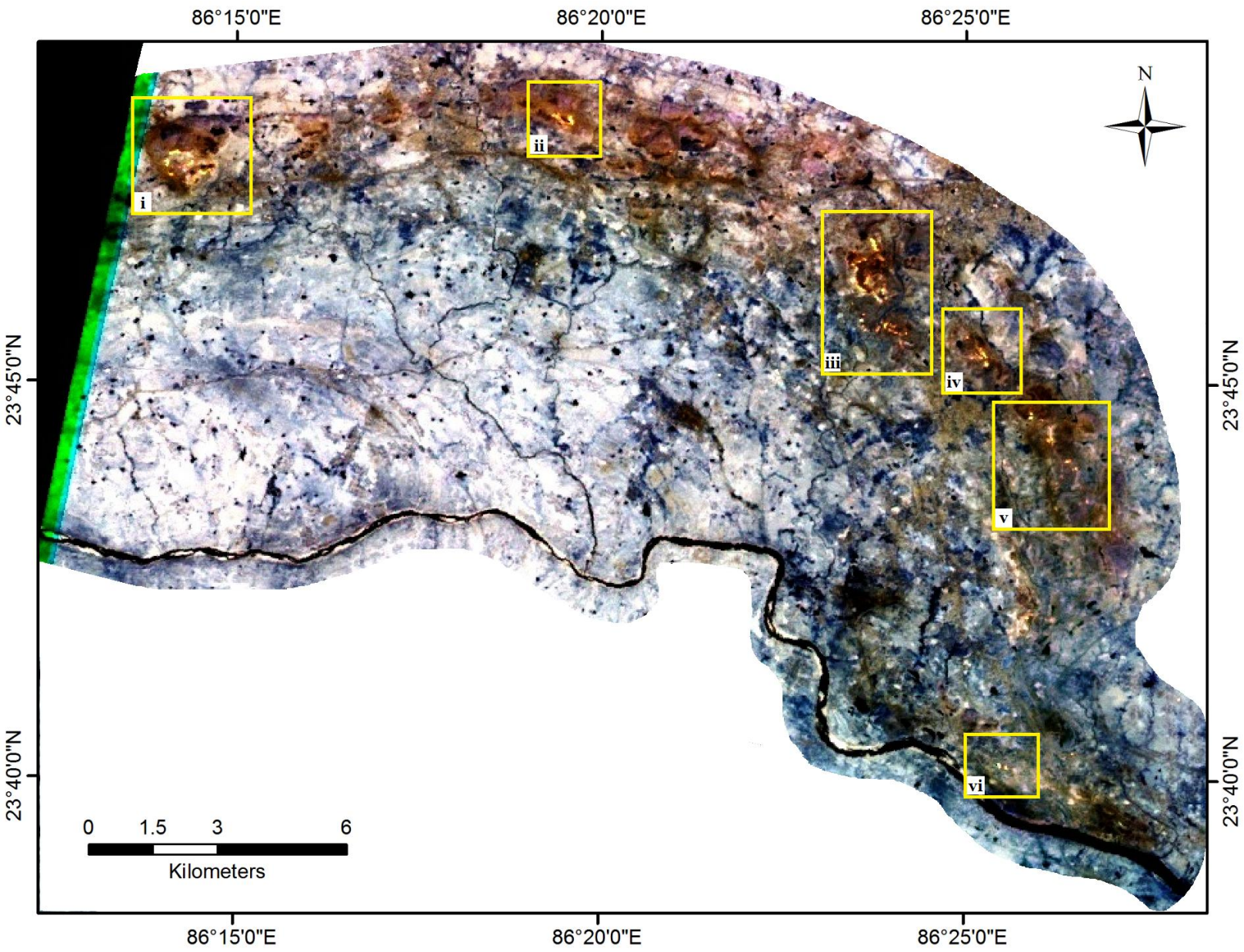
86°15'0"E
86°20'0"E
86°25'0"E
23°45'0"N
23°40'0"N
N
i
ii
iii
iv
v
vi
0 1.5 3 6
Kilometers

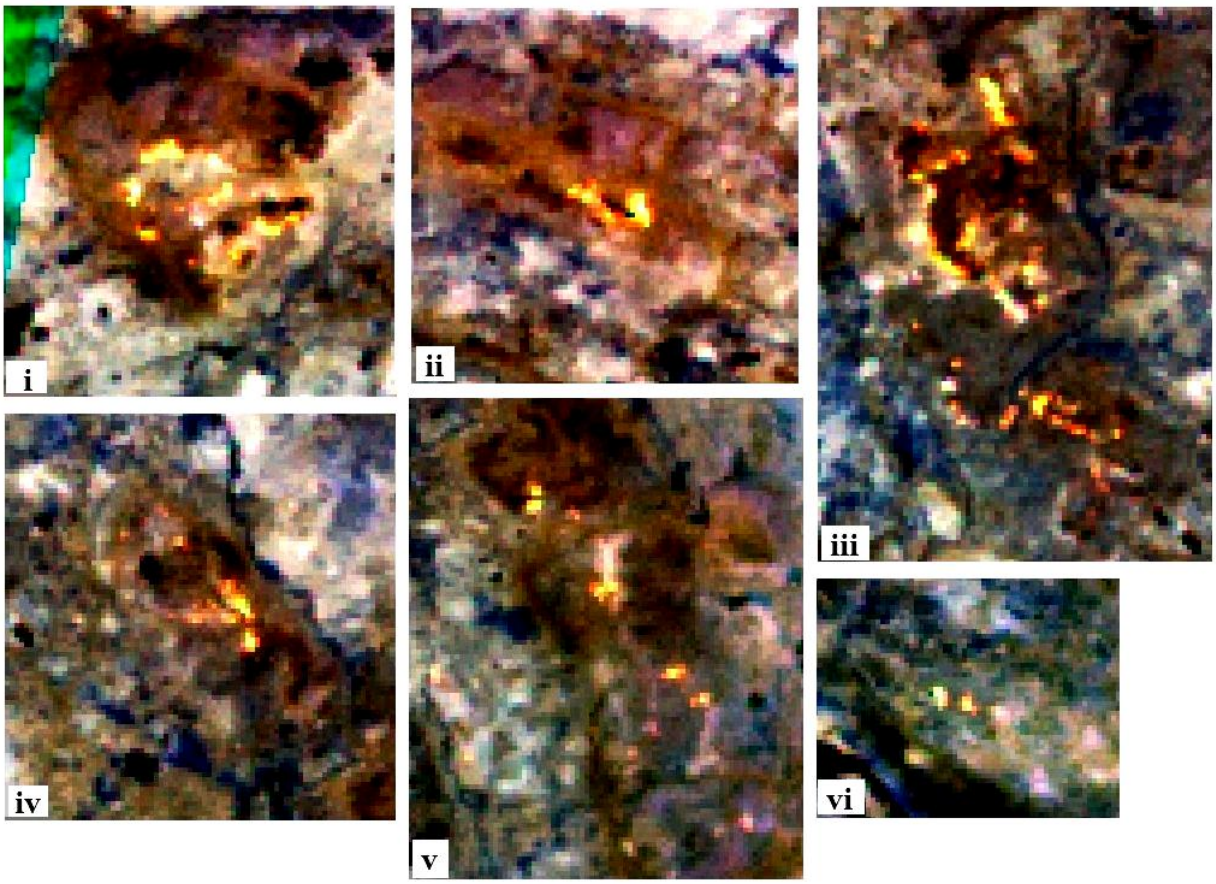

Figure 6.3 ASTER SWIR image of Jharia Coalfield, India showing surface coal fires sites that are appears as bright yellow patches on CIR composite on 8-6-4 band combinations.Key: (i) Shatabdi opencast, Barora (N 23° 47' 40.68"/E 86° 14' 46.68”), (ii) Sijua opencast (N 23° 48' 9.80"/E 86° 19' 28.05"), (iii) Kusunda (N 23° 46' 1.11"/E 86° 23' 53.83"), (iv) Bokapahari (N 23° 45' 10.25"/E 86° 25' 3.38"), (v) Kujama (N 23° 44' 2.38"/E 86° 26' 8.20"), and (vi) Sudamdih (N 23° 39' 14.7"/E 86° 26' 56.6")

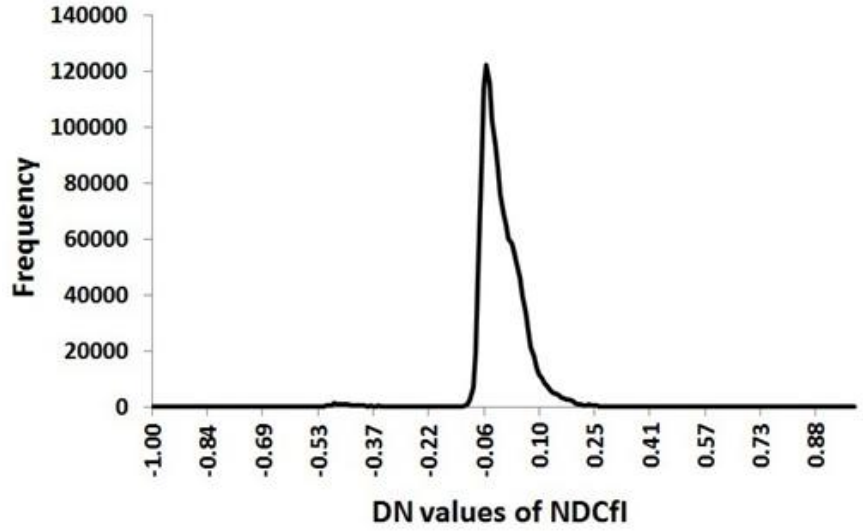

Figure 6.4(a) Frequency distribution curve of NDCfI

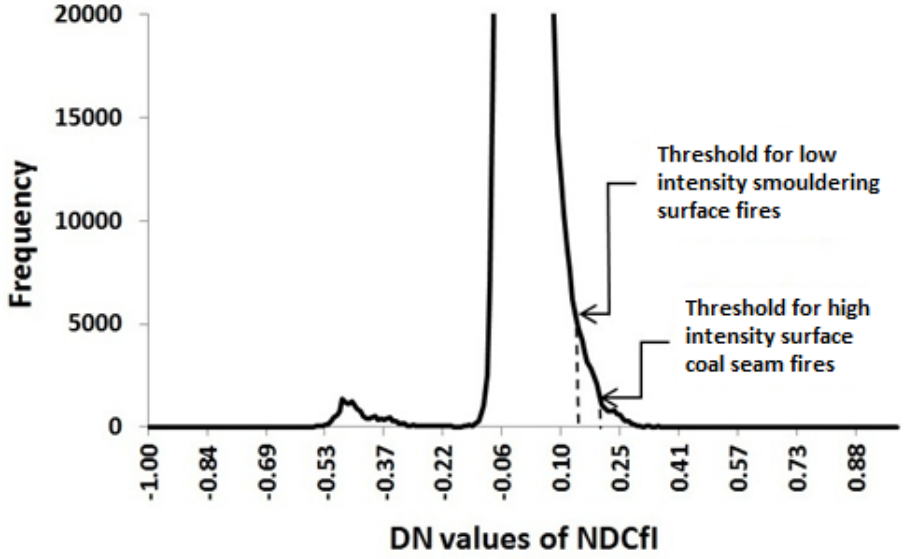

Figure 6.4(b) Zoomed portion of Figure 6.4(a). Thresholds have been set at 0.137-0.208 (starting from the toe of histogram) and 0.208-1.0 (major break in toe) for discriminating low intensity smoldering and high intensity surface coal seam fires, respectively

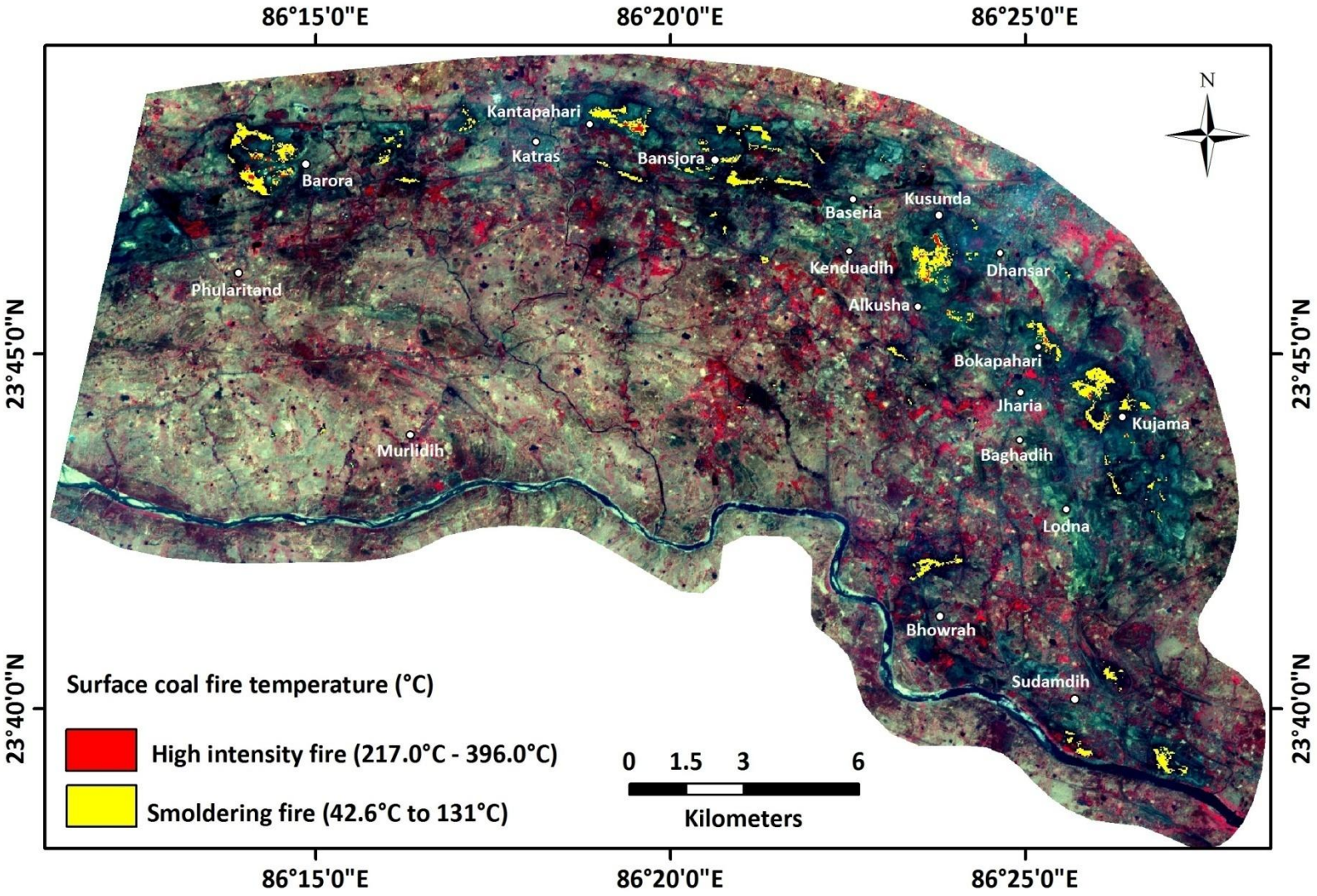

Figure 6.5 Surface coal fire map of JCF (2008) prepared from NDCfI. Low intensity smoldering (yellow) and high intensity coal seam fires are represented in yellow and red over 3-2-1 ASTER CIR composite. Surface temperature obtained during field based observations in February, 2010 area is also shown

Table 6.2 Error matrix generated for the land cover classes produced from ASTER ratio indices

Classified value	**Reference / Truth value**							**Total**	**User's Accuracy (%)**
Class name	**Surface fire**	**Vegetation**	**Water**	**Coal**	**Barren land**	**Overburden dump**	**Settlement**		
Surface fire	**12**	0	0	0	0	0	0	12	100
Vegetation	0	**14**	0	0	0	0	0	14	100
Water	0	0	**16**	2	0	0	0	18	88.9
Coal	0	0	0	**13**	0	0	1	14	92.8
Barren land	0	0	0	0	**12**	0	0	12	100
Overburden dump	3	0	0	0	0	**10**	1	14	71.4
Settlement	0	1	0	0	1	3	**9**	14	64.3
Total	15	15	16	15	13	13	11	**98**	
Producer's accuracy (%)	80	93.3	100	86.7	92.3	76.9	81.8		**87.7**

6.5 RESULTS AND INTERPRETATION

It has been observed that the precise thresholding of NDCI and NDCfI have distinctly segregated the coal seams associated with low intensity smoldering (yellow) and high surface intensity coal seam fires (red) in JCF (Figure 6.5). The obtained results reveal that the areas fall under the domains of Shatabdi opencast, Barora (N 23° 47' 40.68"/E 86° 14' 46.68"), Kantapahari (N 23° 48' 5.0"/E 86° 19' 6.0"), Sijua (Bansjora) opencast (N 23° 48' 9.80"/E 86° 19' 28.05"), Kusunda (N 23° 46' 1.11"/E 86° 23' 53.83"), Bokapahari (N 23° 45' 10.25"/E 86° 25' 3.38"), Kujama (N 23° 44' 2.38"/E 86° 26' 8.20"), Bhowra (N 23° 41' 58.4"/E 86° 23' 36.6") and Sudamdih (N 23° 39' 14.7"/E 86° 26' 56.6") are strictly under the high intensity surface fire. The fires are distributed mainly in eastern and SE part of the coal field with cumulative areal coverage of approximately 3.93 km^2. Field observations carried out in JCF shows that the surface temperatures of the smoldering and high intensity surface fires range from 42.6°C to 131°C and 217.0°C - 396.0°C, respectively (Table 3.5, see Chapter 3, Section 3.7.2). It has been observed that the low intensity surface fires (yellow) closely follow the pattern of excavated coal layers. These are nothing but very shallow to shallow subsurface fire with approximate spatial distribution of 3.7 km^2. Exposed burning coal seams with high radiant intensity are classified as high intensity fire (red) and occupy area coverage of 0.23 km^2.

6.6 VALIDATION AND ACCURACY ASSESSMENT

To obtain the ground truth information of different land cover classes, a field survey has been carried out around JCF using GPS and portable thermometer during February, 2011 (Table 6.2). Reliability of the results was validated by computing an error matrix. An error matrix was generated by comparing test pixels (reference values) in the classified image with their corresponding location in the field. As land cover classes in JCF are highly dynamic in nature, it would be difficult to use field verified ground reference locations for the test pixels. In the present approach, 98 evenly distributed reference points have been selected on the ASTER data using visual interpretation and user's knowledge about the area, and different land covers have been classified with an overall accuracy of 87.7 % (Table 6.2).

Spectral characteristics of overburden dump and settlements are closely associated with each other. Based on the accuracy assessment, it has been observed that the pixels attributed to overburden dump and settlement are difficult to discriminate. The user would only able to segregate these classes with 64.3 % and 71.4 % accuracy (user's accuracy) and only classify

76.9 % and 81.8 % of all the pixels attributed to overburden dump and settlement. All the pixels attributed to surface fire are effectively segregated by NDCfI. However, discrepancy appears in producer's accuracy due to close association of fire in freshly excavated dumps lying in the vicinity of opencasts. Similarly, only 86.7 % of the entire coal pixel are classified as coal due difficulty in discrimination between coal and water.

6.7 CONCLUSION

Industrial and economic growth has an exponential relationship with sustainable production of coal. To facilitate the plan sustainable mining and socio-economic management for industrial growth, temporal monitoring of coal fires has to be executed at regular interval. Coal fires have actively influenced the land-use pattern of coal mine area. Although, automated techniques for mapping land cover types and coal fires have been effectively used but still found to be time consuming and considered infrequent to apply temporally. In the present study, the spectral differences between different land cover types have been observed and two new ratio indices namely, 'Normalized Difference Coal Index (NDCI)' and 'Normalized Difference Coal fire Index (NDCfI)' have been made using ASTER data for accurate mapping and localization of surface fire in coal mine area. Obtained Indices have been further interpreted to discriminate the coal and demonstrate the association of surface fire with exposed coal bed. From thresholding of spectral indices it has been clearly observed that the surface fires (i.e., both low intensity smoldering and high intensity fire) are located all around JCF and closely follows the pattern of excavated coal seams. Eastern and south-eastern part of the JCF covering areas around Barora, Kantapahari, Sijua (Bansjora), Kusunda, Kujama and Bokapahari are mainly affected by surface coal fires. Although, the methodology adopted in the present study is conservative and robust in nature but could have been frequent apply for quick retrieval and precise monitoring of coal fire at specific temporal intervals.

CHAPTER 7

TEMPORAL MONITORING AND DYNAMICS OF COAL FIRE IN JCF

7.1 INTRODUCTION

Remote sensing techniques have been widely contributed in analyzing thermal phenomenon. It is cost effective, less time consuming and datasets available temporally for time series analysis. ASTER provides moderate spatial resolution data at high radiometric and temporal resolutions that holds great potential for effective mapping and monitoring of coal fires occurring worldwide (Wang, 2002; Tetzlaff, 2004; Martha et al., 2010). Utility of ASTER data for coal fire related studies have been discussed in details in the earlier chapters. But, even a moderate resolution satellite data like ASTER has certain limitation in monitoring thermal phenomenon like coal fires (Chapter 2, Section 2.3). Coal fires vary in dimension and occurring discrete patches over the surface. It can be only detected by the satellite sensor if its magnitude and intensity is large enough to enhance the per pixel radiant response than background. Large fires may cause the saturation of pixels. However, it is rarely possible to have such large fire in a coal mining area that can saturate ASTER TIR pixels. High radiometric and temporal resolution of ASTER TIR data also allows to detect even minor fluctuations in land surface temperature at regular interval. Such uniqueness facilitates the users to utilize ASTER data as obvious choice for mapping and monitoring of thermal phenomenon.

Coal fire is the trio of socio-economic and environmental problem. Jharia Coalfield (JCF) in India is one of the densest congregations of coal fires. Coal fires in JCF are highly dynamic in nature. Rigorous mining activities and uncontrolled coal seam fires cause temporal variation in land use pattern around JCF (Prakash and Gupta, 1998; Chatterjee et al., 2007; Singh and Singh, 2009; Martha et al., 2010). Dynamics of coal fires poses serious threat to the local resident. Hence, detailed study and monitoring dynamics of coal fire is absolutely required for planning of sustainable coal mining and associated geo-hazards. Temporal monitoring of coal fires can help to decipher the propagation or movement direction of the underground coal fires. This would further facilitate to plan proper mitigation measures for controlling coal fires and rehabilitation of local residents.

In the present chapter, the prevalent and existing thermal anomaly extraction technique has been employed for temporal monitoring and qualitative analysis of coal fires in JCF. Relative pros and cons of extraction technique in view of their suitability for detailed mapping of the coal fires have been discussed earlier (Chapter 2, Section 2.3.1). Here, three sets of ASTER data from 2000 to 2009 have been used and temporal fluctuations in the spatial extent of coal fires in JCF have been precisely measured. All datasets have been integrated together and analyzed on GIS framework. Coal fires have been visualized in association with their geographical attributes in meaningful way. GIS can serve as an excellent decision-making tool in a coal-mining operation and for planning fire fighting operations (Prakash and Gens, 2010). In the present approach, three consecutive temporal maps showing changes in fire location have been prepared and spatial dynamics of coal fire in JCF for different periods from 2000 to 2009 have been studied.

7.2 METHODOLOGY OVERVIEW AND DATA ANALYSIS

An overview of the methodology scheme followed in the present study is shown in figure 7.1. It involves acquisition, processing, analysis and interpretation of the satellite datasets for precise estimation of coal fire through time. Data from repetitive passes of ASTER (SWIR and TIR) spanning almost a decade have been used for the analysis (Table 4.3). In the present study, ASTER datasets of three consecutive years 2000, 2004 and 2009 have been used for delineating coal fire. ASTER SWIR data since April 2008 are not useable (https://lpdaac.usgs.gov). Hence, for detecting high intensity surface fire ASTER SWIR 2000, 2004 and 2008 data is used. Datasets have been preprocessed as per the methodology and techniques discussed in Chapter 4, Section 4.5. Calibrated radiance emitted from the 'hot ground features' in form of thermal anomalies have been effectively measured by the onboard satellite sensors. Measured radiant energy release has been subsequently used to obtain per pixel radiant temperature of the area from the Planck's function. Radiant temperature has been further utilized to compute pixel-wise temperature distributions of 'Land surface temperature (LST)' using ASTER band 13 emissivity derived from TES algorithm (Chapter 4, Section 4.5.3.1). Precise thresholding of the LST have been employed finally to delineate thermal anomaly and mapping of coal fires in JCF. In the present approach ASTER band 9 (SWIR) and band 13 (TIR) have been used for mapping of surface and subsurface coal fires in JCF.

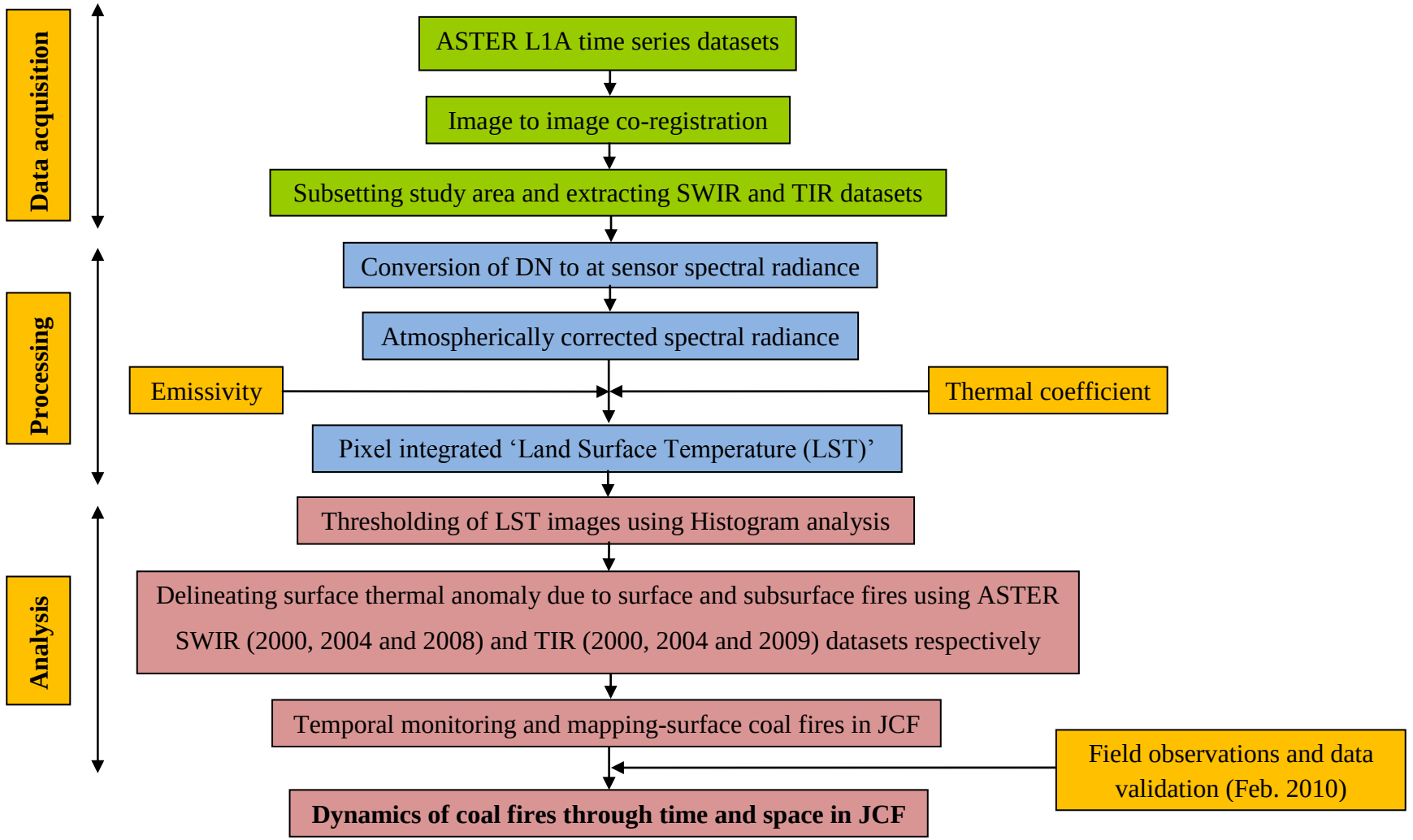

Figure 7.1 Schematic diagram showing the data processing and methodology adopted for mapping and monitoring of coal fires in JCF

7.3 DETECTING THERMAL ANOMALY AND TEMPERATURE DISTRIBUTION DUE TO COAL FIRE

Thresholding of sensors response for delineating thermal anomalies are the important aspect of thermal remote sensing. Several methods have been already carried out in recent past for thresholding of subtle surface thermal anomaly associated with underground coal seam fire using TIR data (Chapter 2, Section 2.3.1). In the present approach, the histogram showing temperature distribution curve of pixel integrated LST is carefully analyzed to set threshold for discriminating coal fire from non-fire area in JCF. Any value higher than selected threshold is attributed to the coal fires. These anomalous areas have been subsequently validated by field based observations carried out in JCF. Field observation has been also carried out at colliery level in JCF details of which have been discussed in Chapter 3, Section 3.7. In such a way, spatial distribution of surface-subsurface coal fire has been determined using SWIR and TIR datasets. Finally, a temperature distribution map for three year (2000, 2004 and 2009) is produced and potential variation in spatial extent of the surface-subsurface coal fire has been detected at temporal interval in JCF.

7.4 DETECTION OF COAL FIRES IN JCF THROUGH TIME

The present study has been carried out with an approach to evaluate the distribution of coal through time and space. For better observance at colliery level, whole JCF has been divided into three different blocks (block 1, 2 and 3) that have been subsequently subdivided into different colliery (Figure 7.2). Results obtained have been further studied and spatial distribution of the coal fire is assessed through 2000 to 2009 at colliery level.

7.4.1 Spatial and Temporal Distribution of Surface Coal Fire

Surface fires are relatively high temperature phenomenon of relatively local extent (Prakash and Gupta, 1999a). These can be fairly recognized on the basis of their variable spectral and textural characteristics as observed on the CIR composites of ASTER SWIR bands (Table 6.1). Different bands have different temperature sensitivity. Temperature sensitivity increases with the decrease in wavelength. Very high thermal phenomenon can be detectable with in bands operating within shorter wavelength region. ASTER SWIR band 9 operates in 2.36-2.43 μm range at normal gain setting and has the capability to detect pixel integrated temperature ranges between 66°C-222°C. In the present study, the pixels with highest radiance

response have been carefully analyzed in SWIR band 9 and no saturated pixel (pixel with DN value of 255) was identified. Hence, ASTER SWIR band 9 has been preferably chosen to map coal mine surface fires since 2000, 2004 to 2008 (Figure 7.3).

It has been observed that high intensity surface coal fires are the exposed shallow subsurface coal seam fire. In 2000, majority of the surface fire is located WSW and SE of Baghmara, Block II Project colliery, east Barora colliery (Shatabdi opencast), Gondudih quarry near Sijua and Kusunda collieries, all along Alkusha-Kusunda-Kustor quarry located SE of kenduadih and near Bhagatdih. Spatial extent of the fire in Block II Project colliery and east Barora colliery was increased from 2000 to 2004. In 2004, a new fire was sighted near east of Godhar (Kusunda block) covering an area of 0.01 km^2. Two highly intense zone of fire located near Bokapahari and NE of Lodna was significantly noticed from 2000 to 2004 in Bastacolla colliery (Figure 7.6, Table 7.1).

In 2008, intense mining activities in Katras and Kusunda collieries exposed the very shallow subsurface fires occurring beneath. Fire in WSW of Baghmara was vanished and existed only in SE of Baghmara (Block II Project colliery) during 2008. Two major fires were spotted near Kantapahari and north of Alkusha quarry in Katras colliery covering an area of 0.032 and 0.048 km^2, respectively. Surface fires have been also observed near Lodna-Tisra-Bhulanbarai area and NW of Bhowrah-Patherdih area in Lodna and Eastern Jharia collieries, respectively. Spatial extent of the surface fire area has been significantly increased in Kusunda colliery from 2000 to 2008. In East Barora colliery (Shatabdi opencast) surface fire is quite persistent and increased in spatial extent from 0.019 to 0.064 km^2 during 2000 to 2008 (Table 7.1).

7.4.2 Spatial and Temporal Distribution of Subsurface Coal Fire

ASTER TIR data can detect the minor difference in spectral response and has been potentially used for temporal monitoring of coal fires in JCF. In the present study, coal fire map for three subsequent years has been produced and the status of coal fires has been observed through time and space. ASTER derived coal fire map of the JCF during 2009 is shown in figure 7.4.

7.4.2.1 *Coal fire in Block 1*

In Block 1, fluctuations in spatial extent of fire have been observed in East Barora and Govindpur collieries from 0.677, 0.907 to 0.727 km^2 and 0.266, 0.474 and 0.294 km^2, respectively through 2000, 2004 to 2009 (Figure 7.5(a)-(b)). However, in Block II Project colliery, fire has been significantly decreased from 1.355 to 0.362 km^2. Area affected by fire in Block 1 has been slightly varied from 2.468 to 2.54 km^2 through 2000 to 2004 and decreased to 1.383 km^2 in 2008.

7.4.2.2 *Coal fire in Block 2*

In Block 2, coal fires are mainly noticed in Katras, Sijua and Kusunda collieries. In 2000, fire existed only in Sijua and Kusunda collieries covering an area of 0.492 and 0.244 km^2 which have been decreased to 0.129 and 0.049 km^2, respectively, in 2004 (Figure 7.5(c)-(e)). A significant increase in areal extent of fire has been noticed in 2008 where fire covers an area of 0.689 and 1.171 km^2 located all around Alkusha-Kusunda-Kustor area near SE of Kenduadih in Sijua and near Bhagatdih in Kusunda collieries, respectively. Kusunda colliery is the most affected by fire which has shown a significant increase from 0.496 to 1.171 km^2 through 2004 to 2009, respectively (Figure 7.5(c)-(e)).

7.4.2.3 *Coal fire in Block 3*

As mentioned, Block 3 is the most affected part of JCF. Intense mining activities have been precisely noticed and fire is quite persistent all around these Kustor, Lodna and Bastacolla collieries. However, fluctuations in spatial extent of fires have been noticed through 2000 to 2009 (Figure 7.5(f)-(h)). In Eastern Jharia colliery, spatial extent of fire has been significantly decreased in west of Bhowrah from 0.341 to 0.090 during 2000 to 2009. Block 3 has been significantly affected by the coal fire through 2000 to 2009 with a persistent spatial extent of 2.5 km^2 (Table 7.2).

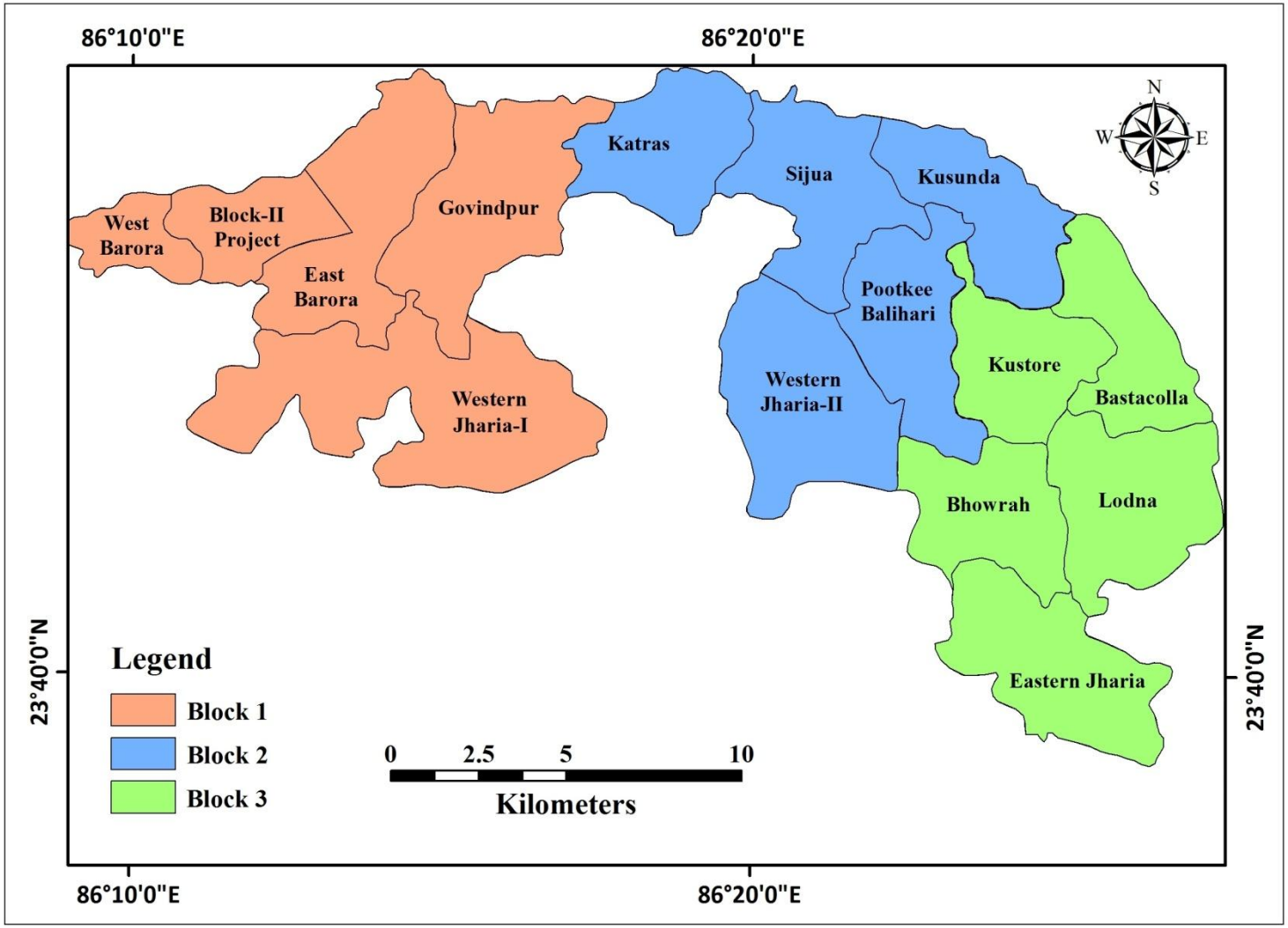

Figure 7.2 Subdivision of JCF into three different blocks (Block 1, 2 and 3) and their subsequently colliery

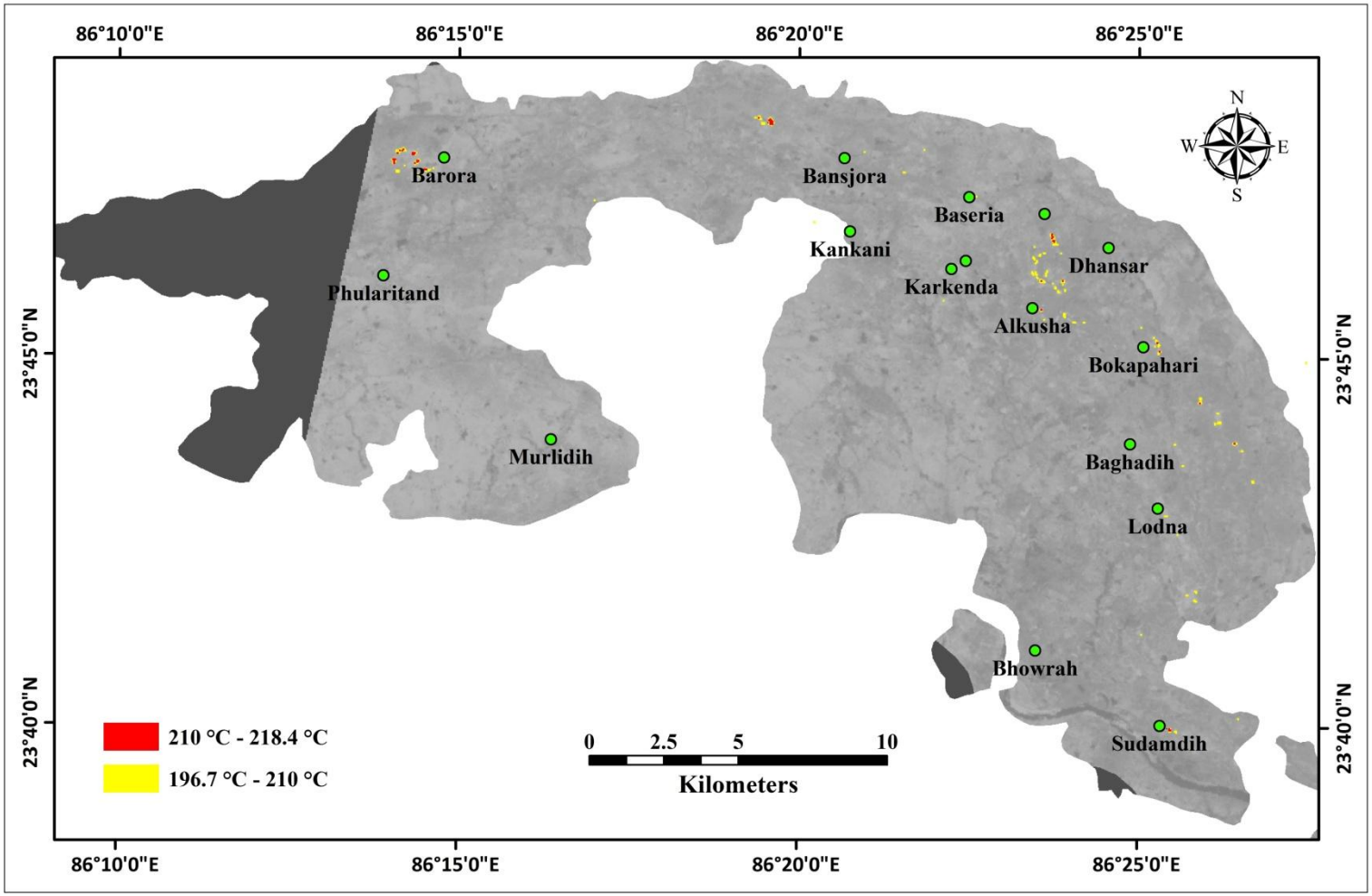

Figure 7.3 ASTER derived surface coal fire map showing spatial extent of high intensity coal mine fire in JCF during 2008. Colliery Result shows that the East Barora, Sijua, Kusunda, Kustor, Bastacolla, Lodna are the most affected collieries. Red and yellow represents the pixel integrated LST derived from ASTER 2008 data.

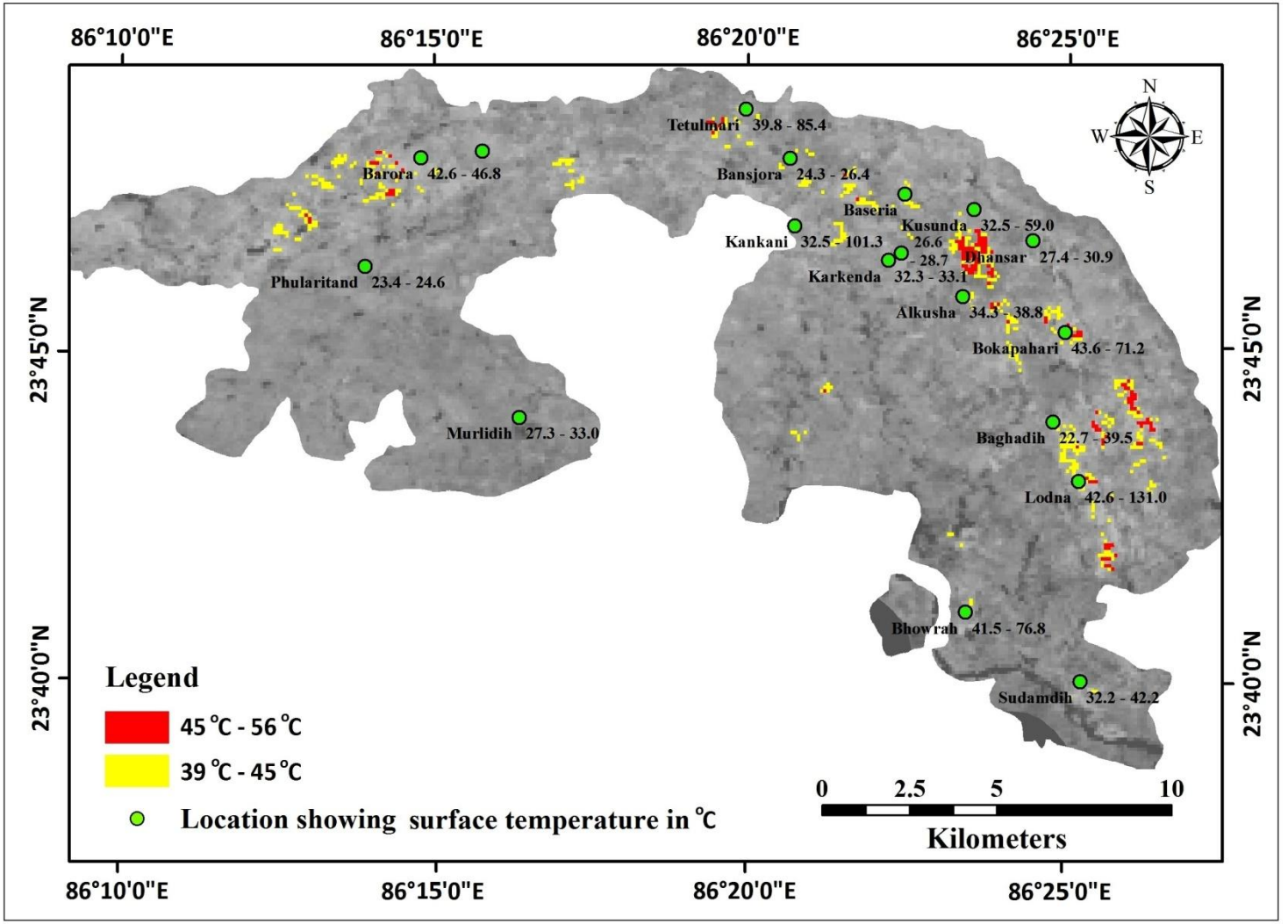

Figure 7.4 ASTER derived coal fire map of JCF (2009). Red and yellow represents the pixel integrated LST derived from ASTER 2009 band 13 data. Surface temperature obtained during field based observations in February, 2010 area is also shown**.**

7.5 DYNAMICS OF COAL FIRE THROUGH TIME AND SPACE

Results obtained from the coal fire mapping in JCF reveals that the surface fires are highly sporadic in nature and occurred as discrete patches in majority of the places (Figure 7.6). Surface fires in JCF exhibits minor fluctuations in magnitude from 2000 to 2008 at colliery level (Table 7.1). In 2008, two new surface fires have been noticed near Kantapahari, in Katras colliery and north of Alkusha quarry in Katras colliery. Fire in Gondudih quarry, near Sijua Bansjora in Sijua and Kusunda collieries has diminished after 2000. Spatial extent of the surface fire in JCF has been increased by 8.6% since 2000 to 2004 and then decreased by 14.66% from 2004 to 2008, respectively.

Majority of the area falls under the domains of Shatabdi opencast, Barora (N 23° 47' 40.68"/E 86° 14' 46.68"), Sijua opencast (N 23° 48' 9.80"/E 86° 19' 28.05"), Godhar colliery, Kusunda (N 23° 46' 1.11"/E 86° 23' 53.83"), Bokapahari (N 23° 45' 10.25"/E 86° 25' 3.38"), Kujama (N 23° 44' 2.38"/E 86° 26' 8.20") are strictly under intense fire with cumulative areal coverage of 5.93, 5.53 and 6.19 km^2 in 2000, 2004 and 2009, respectively, (Figure 7.7, Table 7.2). Since 2000 to 2004, a minor decrease (6.74%) in coal fire has been observed. However, 2009 is apparently marked by a substantial increase in coal fire area by 11.93%. In Block 1, fire area in all collieries has been decreased by 45.55% (1.157 km^2) from 2004 to 2009. A new fire site with a spatial extent of 1.171 km^2 has been noticed around Alkusha-Kusunda-Kustor area in Kusunda colliery. Katras, Sijua and Kusunda collieries of Block 2 are most affected and marked by a significant increase in fire area through 2004 to 2009. During the same period, an increase in fire area by 0.31 and 0.226 km^2 has been also noticed in Kustor and Bastacolla collieries of Block 3.

7.5.1 Structural Control of the Coal Fire Propagation

Jharia basin is structurally highly deformed. The area is marked by an intense system of faults and folded coal seams. Movement of the fire is estimated to be under structural control and has been well observed in the area around Kustor-Bastacolla-Lodna collieries. Coal fires are quite persistent in these three collieries. Temporal monitoring of coal fires (Figure 7.8) shows that the fire is significantly approaching toward Jharia township from NW to SE directions. Fire located east of Jharia (in Bastacolla colliery) and Jiyalgarh, Lodna (in Lodna colliery) is propagating into NNW and north direction toward Jharia, respectively, along the strike of the coal seam. Besides, fire located near Bokapahari and SE of Alkusha, near

Bhagatdih (in Kustor colliery) are propagating in south and SE direction heading toward Jharia (Figure 7.8).

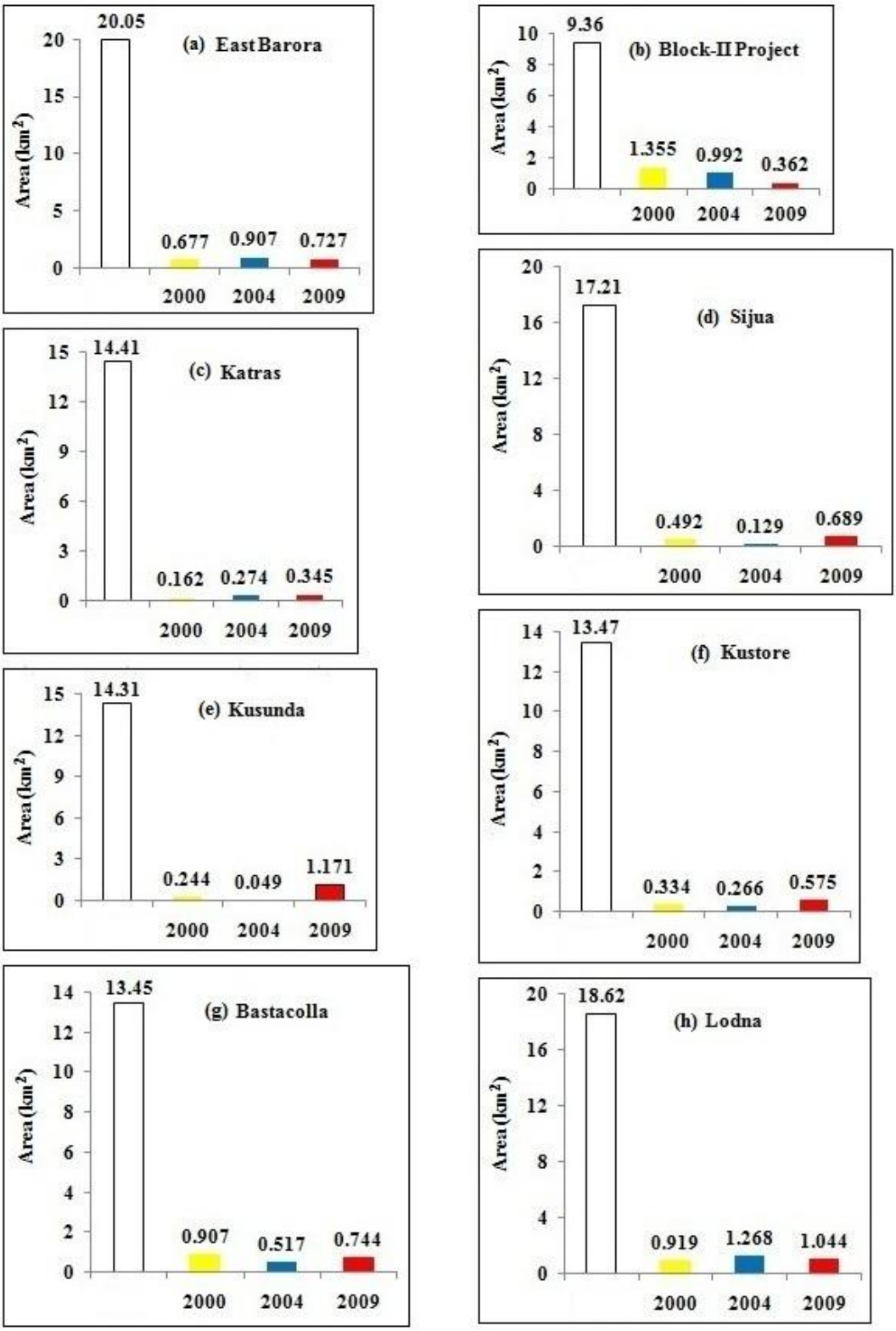

Figure 7.5 Fluctuation in spatial extent of coal fires in some important collieries of JCF from 2000 to 2009

Table 7.1 Spatial extent of surface coal fire in different blocks at colliery level in JCF from 2000 to 2008. 'NF' stands for 'no fire' in the colliery. Negative sign represent the decrease in surface fire area through time.

Spatial extent of surface coal fire in different blocks at colliery level from 2000 to 2008							
Block Name	**Colliery Name**	**Area of colliery (in km^2)**	**Surface fire area (in km^2)**			**Decrease / increase in the surface fire area from 2000 to 2004**	**Decrease / increase in the surface fire area from 2004 to 2008**
			2000	**2004**	**2008**		
Block 1	West Barora	5.81	NF	NF	0.000	NF	NF
	Block II Project	9.36	0.055	0.013	0.000	-0.042	-0.013
	East Barora	20.05	0.019	0.077	0.064	0.058	-0.013
	Govindpur	21.79	NF	0.012	NF	0.012	NF
	Western Jharia-I	33.7	NF	NF	NF	NF	NF
Total area under surface fire in Block 1		**90.72**	**0.074**	**0.090**	**0.064**	**0.016**	**-0.025**
Block 2	Katras	14.41	NF	0.002	0.032	0.002	0.030
	Sijua	17.21	0.009	0.014	0.005	0.005	-0.009
	Western Jharia-II	21.57	NF	0.003	NF	0.003	NF
	Pootkee Balihari	16.19	0.003	0.006	0.002	0.004	-0.005
	Kusunda	14.31	0.016	0.010	0.048	-0.007	0.039
Total area under surface fire in Block 2		**83.69**	**0.028**	**0.035**	**0.087**	**0.007**	**0.052**
Block 3	Kustor	13.47	0.062	0.095	0.053	0.033	-0.042
	Bastacolla	13.45	0.096	0.068	0.025	-0.028	-0.043
	Lodna	18.62	0.038	0.039	0.052	0.001	0.013
	Eastern Jharia	19.29	0.016	0.014	0.009	-0.003	-0.005
Total area under surface fire in Block 3		**64.84**	**0.212**	**0.216**	**0.140**	**0.004**	**-0.076**
Total area under surface fire in JCF		**239.25**	**0.314**	**0.341**	**0.291**	**0.027**	**-0.050**

Table 7.2 Spatial extent of coal fire in different blocks at colliery level in JCF from 2000 to 2009. 'NF' stands for 'no fire' in the colliery at respected year. Negative sign represent decrease in the coal fire area through time.

Spatial extent of coal fire estimated by ASTER TIR datasets in different blocks at colliery level from 2000 to 2009							
Block Name	**Colliery Name**	**Area of colliery (in km^2)**	**Coal fire area (in km^2)**			**Decrease / increase in the coal fire area from 2000 to 2004**	**Decrease / increase in the coal fire area from 2004 to 2009**
			2000	**2004**	**2009**		
Block 1	West Barora	5.81	0.170	0.151	0.000	-0.019	-0.151
	Block II Project	9.36	1.355	0.992	0.362	-0.363	-0.630
	East Barora	20.05	0.677	0.907	0.727	0.230	-0.180
	Govindpur	21.79	0.266	0.474	0.294	0.208	-0.180
	Western Jharia-I	33.7	NF	0.016	NF	0.016	NF
Total area under coal fire in Block 1		**90.72**	**2.468**	**2.540**	**1.383**	**0.072**	**-1.157**
Block 2	Katras	14.41	0.162	0.274	0.345	0.113	0.071
	Sijua	17.21	0.492	0.129	0.689	-0.364	0.561
	Western Jharia-II	21.57	0.023	0.022	0.106	-0.001	0.084
	Pootkee Balihari	16.19	0.040	0.022	0.041	-0.018	0.019
	Kusunda	14.31	0.244	0.049	1.171	-0.195	1.122
Total area under coal fire in Block 2		**83.69**	**0.961**	**0.496**	**2.352**	**-0.465**	**1.857**
Block 3	Kustor	13.47	0.334	0.266	0.575	-0.068	0.310
	Bastacolla	13.45	0.907	0.517	0.744	-0.389	0.226
	Lodna	18.62	0.919	1.268	1.044	0.350	-0.224
	Eastern Jharia	19.29	0.341	0.445	0.090	0.104	-0.355
Total area under coal fire in Block 3		**64.84**	**2.500**	**2.497**	**2.453**	**-0.003**	**-0.044**
Total area under coal fire in JCF		**239.25**	**5.93**	**5.53**	**6.19**	**-0.400**	**0.660**

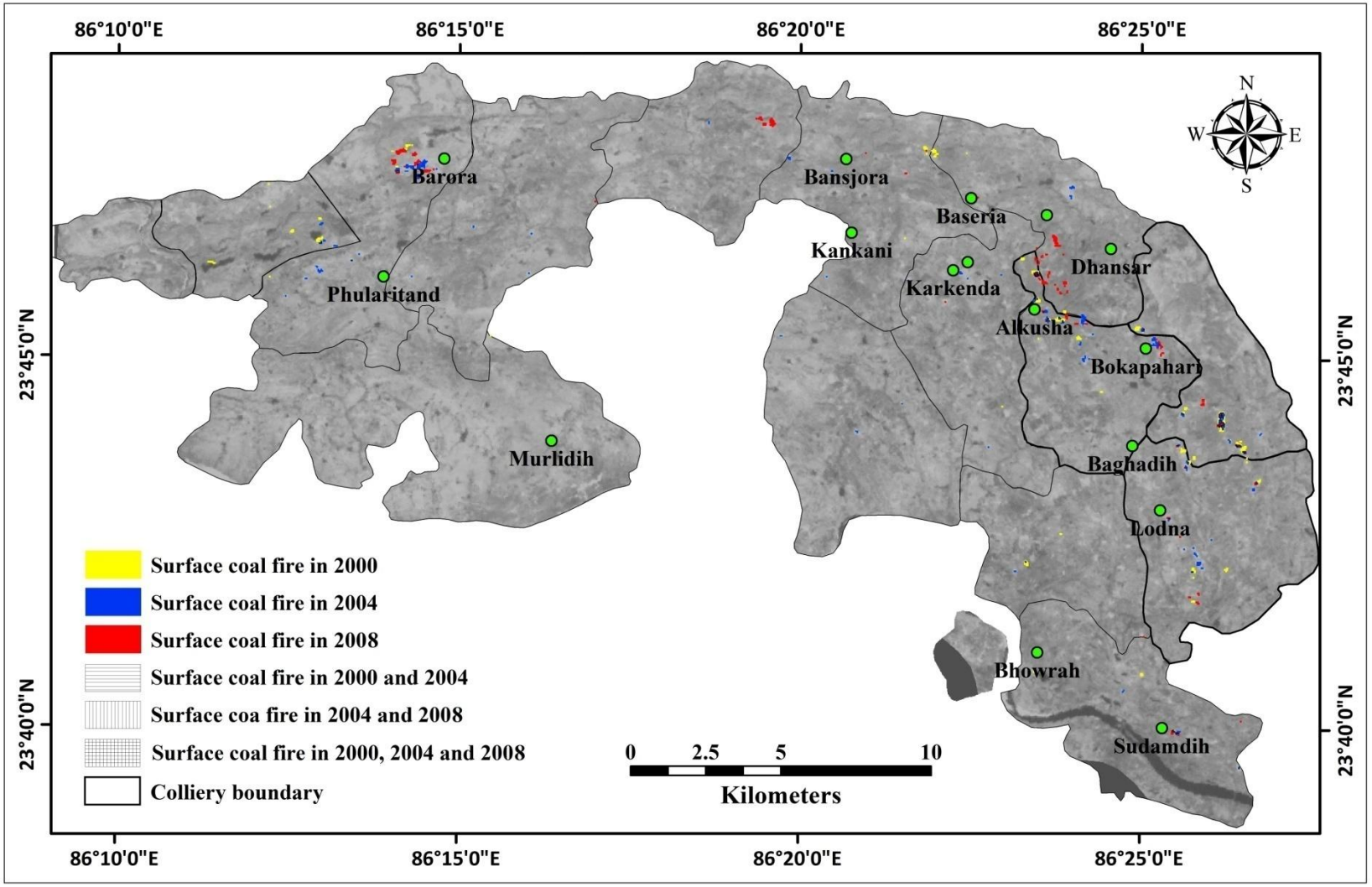

Figure 7.6 Colliery-wise distribution of spatial extent of coal mine surface coal fires in JCF during 2000 to 2008

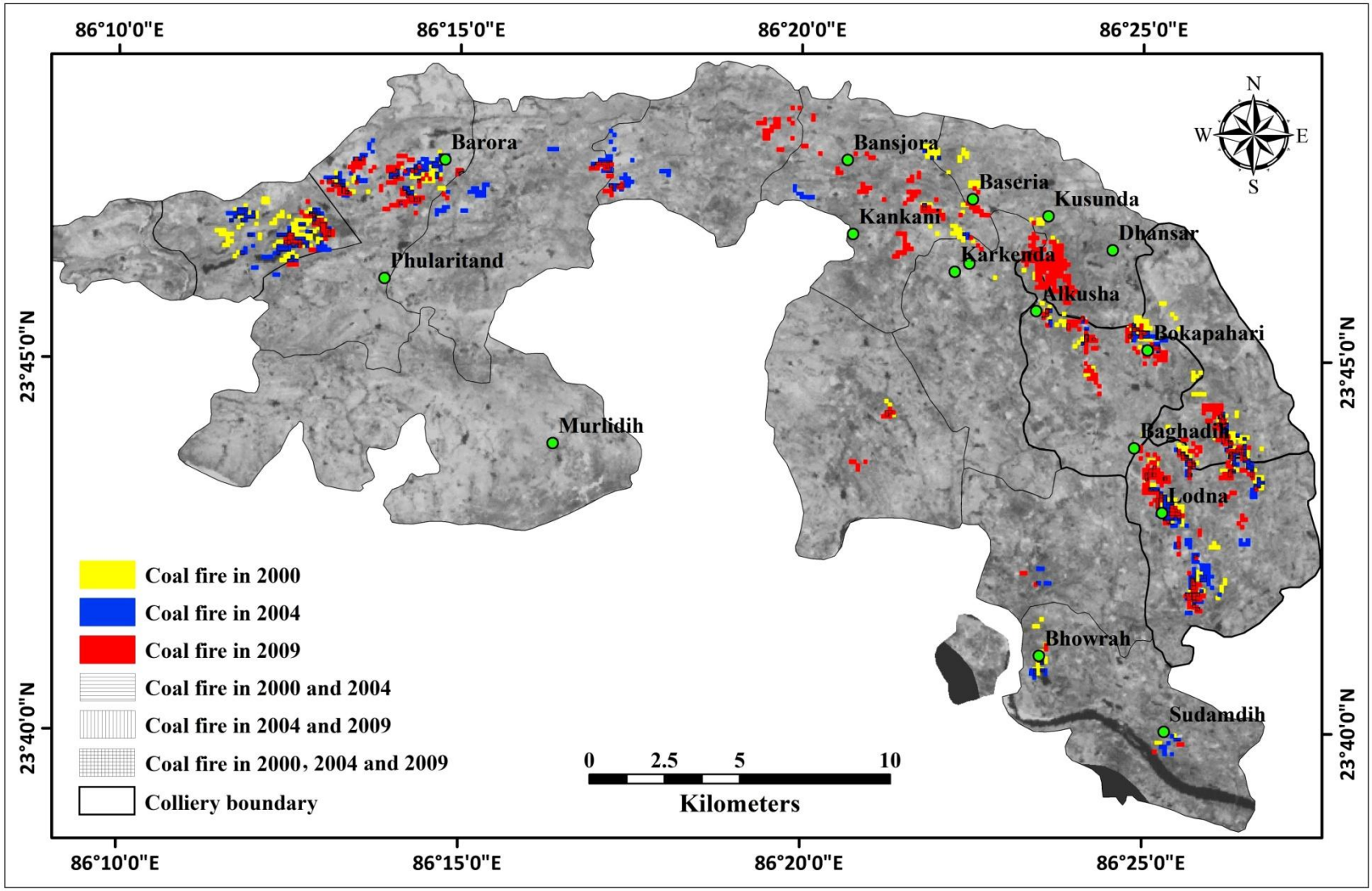

Figure 7.7 Colliery-wise distribution of spatial extent of coal fires in JCF during 2000 to 2008

7.6 CONCLUSION

Systematic investigation of actual scenario of coal fire is always been a critical issue for coal fire research community. Coal fires in JCF causes tones of coal loss by burning and actively contributed to the instability in the area from safety point of view. Systematic investigations of coal fires are essentially required to facilitate sustainable mining and safety management in Jharia, In the present approach, three sets of ASTER data have been used for quick retrieval of status of coal fires in JCF through time.

Coal fire in Jharia is highly dynamic in nature. It has been noticed that the magnitude of fire in JCF has been fluctuated with cumulative areal coverage of 5.93, 5.53 and 6.19 km^2 from 2000, 2004 to 2009, respectively (Figure 7.9(a)-(b)). Spatial extents of coal fires in JCF are quite persistent in Block 1 and 3 since 2000 to 2004. From 2004 to 2009, considerable decrease of 1.157 km^2 in the magnitude of fire has been noticed in the collieries (west and east Barora, Block II Project and Govindpur) located western most part (Block 1) of the JCF. It is observed that the west-central part (Block 2) of the JCF comprising Katras, Sijua, Western Jharia-II and Kusunda collieries are most affected and marked by a significant increase in fire area of 1.857 km^2 from 2004 to 2009. This remarkable increase in spatial extent fire is due to the appearance of new fire site located south of Kusunda and north of Alkusha in 2009. Since 2004, spatial extent of the fire exclusively in Kusunda colliery is increased by 1.122 km^2. Fire is quite persistent with minor increase in Kustor, Bastacolla and Lodna collieries located south and south-eastern part (Block 3) of the JCF.

Local heating and volume reduction due to the burning coal seam results in the development of fracture and crack system on the overlying bed rock. Aided together with the conjugate system of faults, excessive mining activity further exposes the coal seams to oxygen influx that accelerate the fire movement. Structural control of the dynamics of coal fire has been also evident in coal fire map of 2004 and 2009. Propagation of the fire has been well spotted in Kustor, Bastacolla and Lodna collieries. Coal fires were quite persistent in these three collieries and fire appears to be moving toward Jharia. In 2009, it has been observed that the fires located near east of Jharia (in Bastacolla colliery) and Jiyalgarh, Lodna (in Lodna colliery) are propagating in NNW and north direction toward Jharia, respectively. Besides, fires located near Bokapahari and SE of Alkusha (in Kustor colliery) are propagating in south and SE direction heading toward Jharia. Both these fire have been observed to be moving along the strike of coal

seam. Fire located SE of Alkusha (in Kustor colliery) may also under control of two NW-SE trending faults causing propagation of fire toward south and SE.

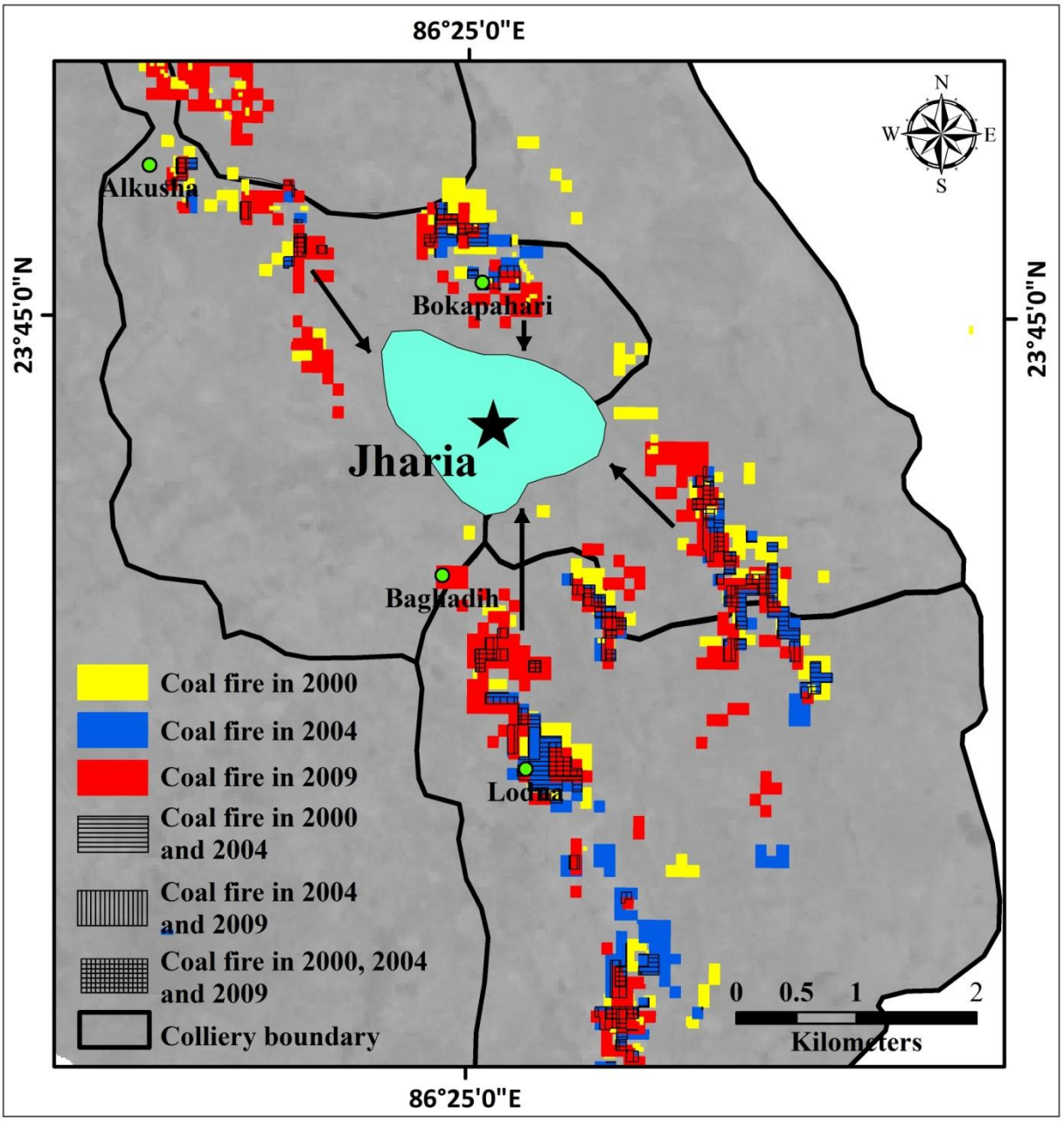

Figure 7.8 Dynamics of coal fire in Kusunda-Kustor-Bastacolla-Lodana collieries in JCF. Map shows that the fires located near east of Jharia (in Bastacolla colliery) and Jiyalgarh, Lodna (in Lodna colliery) are propagating in NNW and north direction toward Jharia, respectively. Besides, fires located near Bokapahari and SE of Alkusha (in Kustor colliery) are propagating in south and SE direction heading toward Jharia

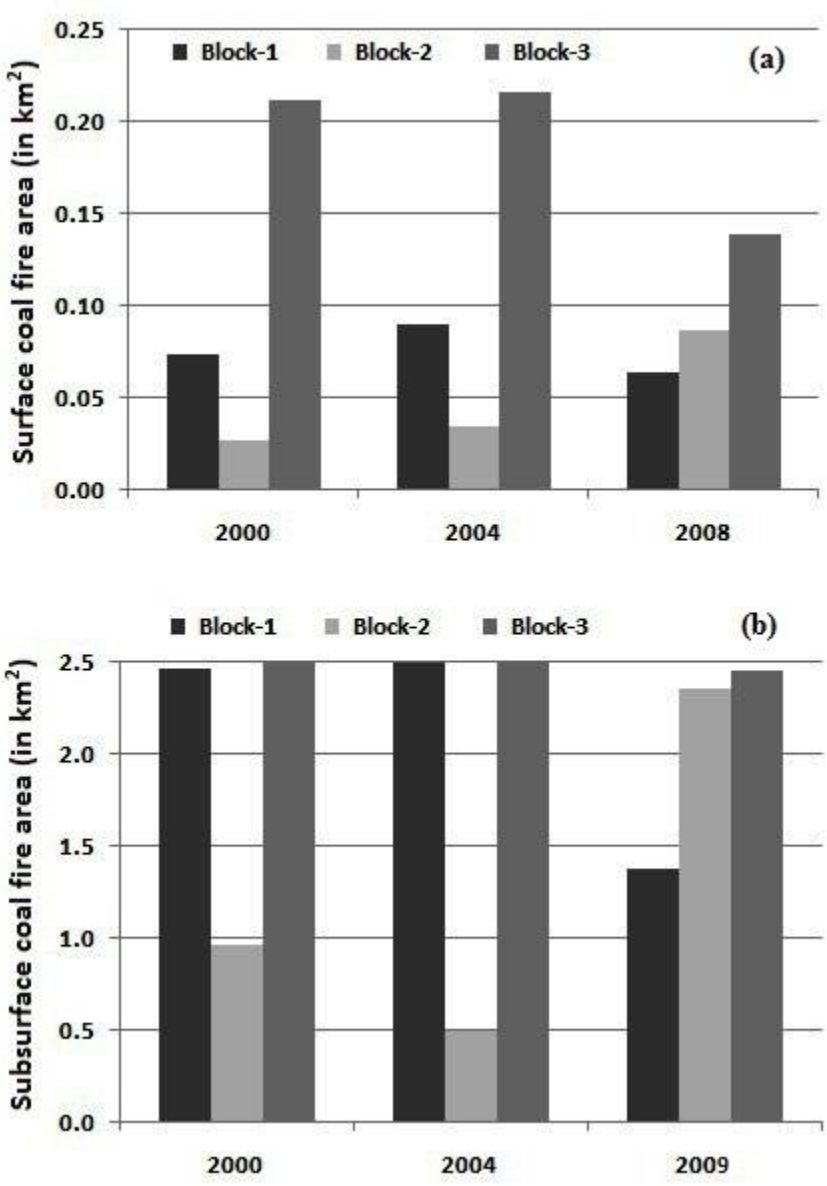

Figure 7.9(a)-(b) Fluctuation in the magnitude of surface and subsurface coal fire in JCF from 2000 to 2008 and 2000 to 2009, respectively

Problem of coal fire is still persisting in JCF. Local villages and inhabitants lying in the vicinity of Jharia township are on the verge of major devastation. Status of the fire is demanding some firm measures to control them. Although, the methodology adopted in the present study is conservative and robust in nature but it would provide precise evaluation and monitoring of coal fire through time and space.

CHAPTER 8

SUMMARY AND CONCLUSIONS

Indian coal mines, particularly the Jharia Coalfield is one of the most disaster prone industries which has witnessed numerous severe accidents leading to repeated loss of life and valuable energy resources. Because of holding high rank coal of sub-bituminous to bituminous range, this coalfield has now became one of the densest congregations of surface-subsurface coal fires in the world. To analyze these surface-subsurface coal fires, systematic studies have been carried out in the present research by developing suitable methods for mapping and monitoring of coal fires using remote sensing techniques. The attempts made here are mainly emphasized on developing a novel approach for thresholding and mapping of surface coal fires, and monitoring spatial dynamics of coal fires in JCF between 2000 and 2009. The datasets utilized in the present approach constitute time series L1G Landsat TM/ETM+ and L1A ASTER data. All datasets have been first pre-processed for necessary corrections using sensors calibration and then analyzed together with ancillary and field data as per the objectives of the present research.

Surface fires are common in coalfields. Such features are sporadic in nature and vary in spatial extent from few meters to tens of meters. These high intensity surface fires can be potentially detectable in SWIR bands. However in the absence of any specific method for thresholding of SWIR data, mapping of surface fires have not been targeted earlier. In the present approach, an innovative technique named 'The maximum solar reflection threshold' method has been proposed to segregate the pixels attributed to the surface fires. The method uses the highest spectral radiance that can be attributed to solar reflection as the conservative threshold to segregate the pixels emitted component from those with reflected component of the EM energy. The method has been applied on Landsat TM/ETM+ band 7 datasets to isolate the fire pixels. Investigating the maximum solar reflection on barren exposures in different coal mining areas indicated that a reflectance value of 0.23 to 0.25 was the most representative reflectance threshold in coal mining areas. A comparison of the threshold values observed in terms of DN value and maximum background reflectance percentage values for all datasets of different geographical setting (India and China) was carried out. The threshold in terms of DN values varies from 62 to 93, whereas the same in terms of reflectance ranges from 0.23 to 0.27. Thus, there is a high variability when threshold is considered in terms of DN values; on the

other hand, when the threshold is sought in terms of computed reflectance, there is a greater consistency and uniformity in various datasets irrespective of scene, topography, season or month. The results obtained from the analysis clearly indicate that the 0.25-0.27 reflectance threshold appears to work well for tropical as well as temperate regions and may be considered as a reasonable threshold for isolating fire pixels using this type of SWIR data.

Despite its conservative nature, the maximum reflectance threshold technique for SWIR data provides a practical way to segregate pixels with definitely fire, has the advantage that it is based on physical processes controlling reflectance of typical material types found in coal mining areas and appears applicable in a wide range of geographic settings, and the method should be repeatable without introducing a user-bias.

Surface coal mine fires are highly dynamic in nature and invariably associated with land use pattern around the coal mine area. To facilitate plan sustainable mining and socio-economic management, temporal monitoring of coal fires has to be executed at regular interval. In the present approach, a novel methodology have been introduced that may implemented frequently to access the status of surface coal fires. Methodology involves the formulation of two new ratio indices namely, 'Normalized Difference Coal Index (NDCI)' and 'Normalized Difference Coal fire Index (NDCfI)' based on the spectral differences between different land cover types derived using ASTER data. The methodology has been systematically implemented in JCF as test site for accurate mapping and localization of surface fire. The obtained Indices have been further interpreted to discriminate the coal and demonstrate the association of surface fire with exposed coal bed.

Precise thresholding of the NDCI and NDCfI distinctly segregate the coal seams associated with the pixels attributed to low intensity smoldering fires and high intensity coal seam surface fires. The outcome of the surface fires assessment map indicated that the surface fires closely follow the pattern of the excavated coal seams and distributed mainly in eastern and SE part of the coal field with cumulative areal coverage of approximately 3.93 km^2. Out of this cumulative coverage of 3.93 km^2, a major portion of approximately 3.7 km^2 is covered by low intensity smoldering surface fires. Field observations reveal that these low intensity smoldering fires are nothing but very shallow to shallow subsurface fire. Areas fall around the domain of Barora, Kantapahari, Sijua (Bansjora), Kusunda, Kujama and Bokapahari are strictly under high intensity surface coal fires represented by exposed burning coal seams and occupy spatial coverage of 0.23 km^2.

The obtained surface fire map closely represents the real scenario of surface coal fires in JCF. Although, the discussed methodology is conservative and robust in nature but could have been frequent apply for quick retrieval and precise monitoring of coal fire at specific temporal intervals. The methodology adopted will surely help in better categorization and localization of surface coal fires affected areas of the JCF.

Coal fires in JCF cause tons of coal loss every year in JCF. Fire once started can propagate along the coal seams. While moving, fires consume the underground coal seams and actively contribute instability in the area by sudden subsidence. Due to this reason, systematic investigation and quantification of actual scenario of coal seam is always been a critical issue for coal fire research community. Recent advancement in specifications and availability of satellite data at high temporal resolution allow to evaluate the spatial dynamics and trend of coal fire propagation. Such investigation can be assess by time series analysis that may help to execute sustainable mining activity in a coal mine area. Hence, in the present study, three sets of ASTER time series data have been used for evaluation of coal fires in JCF through time.

Coal fire maps of the three consecutive years suggested that the fires in Jharia are highly dynamic in nature. In JCF, areas around Shatabdi opencast, Barora, Sijua opencast, Godhar colliery, Kusunda, Bokapahari, Kujama and Lodna are strictly under intense fire with cumulative coverage of 5.93, 5.53 and 6.19 km^2 in 2000, 2004 and 2009, respectively. Since 2000 to 2004, a minor decrease (6.74%) in coal fire has been observed. However, 2009 coal fire area is apparently marked by a substantial increase of 11.93%.

It has been noticed that the magnitude of fire in JCF has been fluctuated with time from 2000 to 2009. Spatial extents of coal fires in JCF are quite persistent in Block 1 and 3 since 2000 to 2004. From 2004 to 2009, coal fires located in the western most part of the JCF has been significantly decreased by 1.157 km^2 in west and east Barora, Block II Project and Govindpur collieries located in Block 1. It is observed that the west-central part (Block 2) of the JCF comprising Katras, Sijua, Western Jharia-II and Kusunda collieries are most affected. During the same period i.e. from 2004 to 2009, a major fire site has appeared in south of Kusunda and north of Alkusha that significantly increases the spatial extent of coal fire in Block 2 by 1.857 km^2. Spatial extent of the fire in Block 3 is quite persistent through 2000 to 2009. However, a minor increase fire in Kustor, Bastacolla and Lodna collieries located south and south-eastern part (Block 3) of the JCF has been precisely noticed.

Using GIS, coal fire maps of three consecutive years (2000 to 2009) have been overlay together with structural data to assess the systematic analysis of coal fire propagation in JCF. Structural control of the coal fire dynamics has been well evaluated in Kustor, Bastacolla and Lodna collieries of JCF. Fire appears to be moving toward Jharia. In 2009, it has been observed that the fires located near east of Jharia (in Bastacolla colliery) and Jiyalgarh, Lodna (in Lodna colliery) are propagating in NNW and north direction toward Jharia, respectively. Besides, fires located near Bokapahari and SE of Alkusha (in Kustor colliery) are propagating in south and SE direction heading toward Jharia

ASTER derived results showed that the remote sensing is a relatively cost-effective and high-frequency tool to observed regional mapping and monitoring of coal fires. Satellite derived data of 2009 has been subsequently validated by the field observations carried out in JCF during February and December 2010. Field surveys suggested that the area exposed around East Barora, Katras, Sijua, Kusunda, Kustor, Bokapahari, Bastacolla and Lodna collieries are significantly affected by coal fire. Precise observation and recognition of coal fire help to support the investigation and results obtained from satellite data.

8.1 LIMITATION OF THE STUDY

(a) Thermal anomalies generated at the surface are the function of depth and spatial extent of fire. Heat generated by high intensity fire occurring at great depth may not high enough to produce thermal anomaly at the surface similarly small but high intensity surface fire can saturate the low spatial resolution TIR pixel. Thus, precise mapping of coal fires require careful selection of accurate threshold temperature 'value'. Thermal images of different seasons require different threshold to map coal fires. Statistical method of thresholding can effectively delineate the fire from non-fire area. However, better results can be obtained when threshold is set using field based informations.

(b) The proposed 'Maximum reflectance threshold' method is conservative and may lead to the missing out some small sub-pixel fires whose emitted spectral radiance is in the same range as the background solar reflected radiance.

(c) Mine dumps located in the vicinity of the large opencasts are affected by very low intensity smoldering fire. Such dump fires are perceived automatically by coarse resolution TIR satellite datasets, and often misinterpreted and mapped as 'coal fire' in

coal mining area. These ‘misinterpreted coal fires’ have to be carefully analyzed and must not be considered ‘actual coal fire’.

(d) SWIR bands have significant contribution of solar heat flux and, sensitive to both solar reflected radiation and blackbody radiation emitted by fire. Separate retrieval of the spectral response of solar heating and emission component recorded in SWIR channel is highly complicated. Radiant intensity response of SWIR data may produce unevenly distributed thermal data that would have resulted in uncertainty obtained in temperature image. Hence, SWIR data has not been significantly used for coal fire related studies.

(e) Land use pattern are invariably associated with coal mine activity and changes frequently due to intense mining. Rigorous mining activities expose the shallow subsurface fires to the surface. At places, surface-subsurface fires may control or sealed by several methods. Thus, date and season of the data acquired and field work should have been plan precisely for better validation of the results.

(f) Coal fire affected areas are often inaccessibly. Surface fire sites at places exhibits temperature of more than 400°C. Moreover, surface fires are also closely associated with the zone of subsidence. Due safety related issues, it would be highly dangerous to go closer to the fire zone for field based measurements. Hence, the field based measurements are mainly the close approximation of coal fires.

8.3 RECOMMENDATIONS AND SCOPE FOR FUTURE WORK

(a) Data obtain from field surveys are the essential component of the coal fire related studies. Without understanding of the actual scenario of the coal fires in field, precise evaluation and quantification of coal fires cannot be estimated. It would be advised to plan ground based observation at the locations where characteristics of coal fires can be fully explored.

(b) Coal fires are highly complex multivariable dependent system. With recent advancement in the available technologies, the coal fire related researches are needs to be progress with interdisciplinary approach. To better infer the dynamics of coal fires at subsurface level, the techniques of numerical modeling may have consider. Model of subsurface heat flow and temperature distribution due to coal fire can be simulated with suitable inputs from mechanical processes, geological data and thermal borehole log etc. Such information can accurately evaluate the dynamics of coal fires more close to

the reality. However, detailed study of coal fire using integrated approach is beyond the scope of remote sensing.

(c) Land subsidence zone are closely related to the thermal anomalies. Land subsidence studies have been well observed using DInSAR technique in many parts of the world. Hence, it would also be advisable to carry out land subsidence related studies in the JCF.

Problem of coal fire is still persisting in JCF. Local villages and inhabitants lying in the vicinity of Jharia township are on the verge of major devastation. Status of the fire is demanding some firm measures to control them. Maps and techniques proposed in the present research help in the better understanding of the coal fires and in disaster monitoring and management. The methodology adopted in the present study is conservative and robust in nature but it would provide precise evaluation and monitoring of coal fire through time and space. This may helps in planned sustainable mining for industrial growth and environmental remediation on a long term basis.

BIBLIOGRAPHY

[1] Abrams, M., Hook, S. and Ramachandran, B., 1999. ASTER user handbook, version 2 Jet Propulsion Laboratory, Pasadena, CA and EROS Data Center, Sioux Falls, SD.

[2] Ackersberg, R., 2003. Understanding self-ignition of coal, Internal unpublished project report, German Montan Technology and Federal Institute for Materials Research and Testing, Germany.

[3] Algorithm Theoretical Basis Document for ASTER L1 data processing (Ver. 3.0). Level-1 Data Working Group, ASTER Science Team, Japan. 1996.

[4] ASTER L1B Manual Ver. 3.0, 1996. Algorithm Theoretical Basis Document for ASTER Level-1 Data Processing (Ver. 3.0), Level-1 Data Working Group, ASTER Science Team, Japan, November 1, 1996.

[5] Barsi, J.A., Schott, J.R., Palluconi, F.D., and Hook, S.J., 2005. Validation of a Web-Based Atmospheric Correction Tool for Single Thermal Band Instruments. Earth Observing Systems X, edited by James J. Butler, Proceedings of SPIE Vol. 5882 (SPIE, Bellingham, WA, 2005).

[6] Bartolucci, L.A., Chnag, M., Anuta, P.E., and Graves, M.R., 1988. Atmospheric effects on Landsat TM thermal IR data. IEEE Transactions on Geoscience and Remote Sensing, 26, 171-175.

[7] BCCL, 2008. Master plan for dealing with fire, subsidence and rehabilitation in the leasehold of BCCL, March 2008, Bharat Coking Coal Limited.

[8] Bhattacharya, A., Reddy, C.S.S. and Dangwal, M., 1996. Coal mine fire inventory and monitoring in Jharia coal field, Bihar, India using thematic mapper thermal IR data. Proceedings of the Eleventh Thematic Conference and Workshops on Applied Geologic Remote Sensing, Las Vegas, USA, 27-29 February 1996 (Michigan, USA: ERIM), p. I-303-309.

[9] Bhattacharya, A. and Reddy, C.S.S., 1994. Underground and surface coal mine fire detection in India's Jharia coal field using airborne thermal infrared data. Asian-Pacific Remote Sensing Journal, Vol.7, No.1, pp.59-73.

[10] Bhattacharya, A., Reddy, C.S.S. and Mukherjee, T., 1991. Multi-tier remote sensing data analysis for coalfire mapping in Jharia coalfield of Bihar, India. In Proceedings of the 12th Asian Conference on Remote Sensing, 1991, Singapore (Singapore: National University of Singapore), pp. 22-1-22-6.

[11] Carras, J.N., Day, S.J., Saghafi, A., and Williams, D.J., 2009. Greenhouse gas emissions from low-temperature oxidation and spontaneous combustion at open-cut coal mines in Australia. International Journal of Coal Geology, 78 (2), 161–168.

[12] Cassells C.J.S., 1997. Thermal modelling of underground coal fires in northern China. PhD thesis, International Institute for Aerospace Survey and Earth Sciences (ITC), The Netherlands, ISBN 90-6164-234-5, ITC Dissertation No. 51, 183 pp.

[13] CGWB, 2009. Groundwater information booklet, Dhanbad district, Jharkhand. Central Groundwater Board, Ministry of Water Resources, Government of India, Mid Eastern Region, Patna, 2009.

[14] Chakraborty, C., Mandal, N., and Ghosh, S.K., 2003. Kinematics of the Gondwana basins of peninsular India. Tectonophysics 377 (2003) 299-324.

[15] Chander, G., Markham, B.L., and Helder, D.L., 2009. Summary of current radiometric calibration coefficients for Landsat MSS, TM, ETM+, and EO-1 ALI sensors. Remote Sensing of Environment. 113, 893-903.

[16] Chandra, D., 1992. Jharia Coalfield. Geological Society of India, Bangalore, India.

[17] Chatterjee, R.S., Wahiduzzaman, M., Shah, A., Raju, E.V.R., Lakhera, R.C., and Dadhwal, V.K., 2007. Dynamics of coal fire in Jharia Coalfield, Jharkhand, India during the 1990s as observed from space, Current Science, Vol. 92, p.61.

[18] Chatterjee, R.S., 2006. Coal fire mapping from satellite thermal IR data-A case example in Jharia Coalfield, Jharkhand, India. ISPRS Journal of Photogrammetry & Remote Sensing 60 (2006) 113-128.

[19] Chatterjee, R.S., Bannerjee, D., Roy, J. and Bhattacharya, A.K., 1994. Landsat TM data processing techniques for identifying and delineating environmental impacts of coal mining, ITC Journal, 2 (1994), 155-162.

[20] Chen, Y., Jing, L., Bo, Y., Shi, P. and Zhang, S. 2007. Detection of coal fire location and change based on multi-temporal thermal remotely sensed data and field measurements, International Journal of Remote Sensing, 28: 15, 3173-3179.

[21] CMPDIL, 1989. Geological map of the Jharia Coalfield, Central Mine, Planning and Design Institute, 1989.

[22] Coll, C., Caselles, V., Valor, E., Niclòs, R., Sánchez, J.M., Galve, J.M., and Mira, M., 2007. Temperature and emissivity separation from ASTER data for low spectral contrast surfaces. Remote Sensing of Environment 110: 162-175.

[23] Coll, C., Caselles, V., and Schmugge, T. J., 1994, Estimation of land surface emissivity differences in the split-window channels of AVHRR. Remote Sensing of Environment, 48, 127-134.

[24] Cracknell, A.P. and Mansor, S.B., 1992. Detection of subsurface coal fires using Landsat Thematic Mapper data. International Journal of Photogrammetry and Remote Sensing, v.29 (b7), pp.750-753.

[25] Deng, W., Wan, Y.Q. and Zhao, R.C., 2001. Detecting coal fires with a neural network to reduce the effect of solar radiation on Landsat Thematic Mapper thermal infrared images. International Journal of Remote Sensing, 22, 933-944.

[26] Dijk, P.M. van, Zhang, J., Wun, J., Kuenzer, C., and Wolf, K.-H., 2011. Assessment of the contribution of in-situ combustion of coal to greenhouse gas emission; based on a comparison of Chinese mining information to previous remote sensing estimates. International Journal of Coal Geology 86 (2011), 108-119.

[27] Dijk, P.M. van, Wang, H.Y., and Genderen, J.L. van, 2004. Earth observation knowledge transfer: the example of ITC's coalfire project. In: ISPRS 2004: proceedings of the XXth ISPRS congress: Geo-imagery bridging continents, 12-23 July 2004, Istanbul, Turkey. Comm. VI. pp. 176-180.

[28] Dijk, P.M. van, Prakash, A., Maathuis, B.H.P. and Zhang, X., 2003 Monitoring coal fires in North China: a remote sensing and GIS approach: abstract. In: Abstracts of the annual meeting of the American Associaton for the Advancement of Science, February 13-18 2003, Denver. 1 p.

[29] Dijk, P.M. van, 1996. Prototype monitoring system for the control of 'in-situ' coal fires in China. In: ITC research conference program, abstracts and session reports: February 15 and 16, 1996, pp. 73-74.

[30] Dozier, J. 1981. A method for satellite identification of surface temperature fields of subpixel resolution. Remote Sensing of Environment, 11, pp. 221-229.

[31] Eckmann, T.C., Roberts, D.A., and Still, C.J., 2009. Estimating subpixel fire sizes and temperatures from ASTER using multiple endmember spectral mixture analysis, International Journal of Remote Sensing, 30: 22, 5851-5864.

[32] Ellyett, C.D. and Fleming, A.W., 1974, Thermal infrared imagery of the Burning Mountain coal fire. Remote Sensing of Environment, 3, pp. 79-86.

[33] ENVI User's Guide, 2009. ENVI Version 4.7, August, 2009 Edition.

[34] Engle, M.A., Radke, L.F., Heffer, E.L., O'Keefe, J.M.K., Smeltzer, C.D., Hower, J.C., Hower,J.M., Prakash, A., Kolker, A., Eatwell, R.J., Schure, A. Ter, Queen, G., Aggen,

K.L., Stracher, G.B., Henke, K.R., Olea, R.A., and Román-Colón, Y., 2011. Quantifying greenhouse gas emissions from coal fires using airborne and ground-based methods. International Journal of Coal Geology 88 (2011), 147-151.

[35] Feng, K.K., Chakravorty, R.N., and Cochrane, T.S., 1973. Spontaneous combustion-a coal mining hazard. CIM Bulletin, 66, 75-84.

[36] Fisher, W. and Knuth, W., 1968. Detection and delineation of subsurface coal fires by aerial infrared scanning. Geological Society America, 115, pp. 67-68.

[37] Gangopadhyay, P.K., Van der Meer, F., Dijk, P.M. van, and Saha, K., 2012. Use of satellite-derived emissivity to detect coalfire-related surface temperature anomalies in Jharia coalfield, India, International Journal of Remote Sensing, 33:21, 6942-6955.

[38] Gangopadhyay, P.K., van Der Meer, F., and Dijk, P.M. van, 2008. Atmospheric modelling using FASCOD to identify CO_2 absorption bands and their suitability analysis in variable concentrations for remote sensing applications. Journal of Quantitative Spectroscopy and Radiative Transfer 109, 670-683.

[39] Gangopadhyay, P.K., 2007. Application of remote sensing in coal-fire studies and coal fire related emissions, in:Stracher, G.B., (Ed.), Geology of Coal Fires: Case Studies from Around the World. Geological Society of America Reviews in Engineering Geology, v. XVIII, pp. 239-248, doi: 10.1130/2007.4118 (16).

[40] Gangopadhyay, P.K., Lahiri-Dutt, K. and Saha, K., 2006, Application of remote sensing to identify coalfires in the Raniganj Coalbelt, India. International Journal of Applied Earth Observation and Geoinformation, 8, pp. 188–195.

[41] Gangopadhyay, P.K., and Lahiri, Dutt, K., 2005. Detecting Coal fires with Remote Sensing: A Comparative Study of Selected Countries, Resource Management in Asia-Pacific Working Paper No. 58, Resource Management in Asia-Pacific Program, Research School of Pacific and Asian Studies, The Australian National University, Canberra, ISSN-1444-187X.

[42] Gangopadhyay, P.K., Maathuis, B. and Dijk, P.M. van, 2005. ASTER derived emissivity and coal fire related surface temperature anomaly: a case study in Wuda, North China. International Journal of Remote Sensing, 26, pp. 5555–5751.

[43] Gao, Bo-Cai., 1996. NDWI-a normalized difference water index for remote sensing of vegetation liquid water from space. Remote Sensing of Environment, 58(3), 257-266.

[44] Gao, Y., Mas, J.F., Maathus, B.H.P., Zhang, X. and Dijk, P.M. van, 2006. Comparison of pixel-based and object-oriented image classification approaches-a case study in a

coal fire area, Wuda, Inner Mongolia, China. International Journal of Remote Sensing, pp. 4093-4055.

[45] Gautam, R.S., Singh, Dharmendra, Mittal, A., 2008. An efficient contextual algoirthm to detect subsurface fires with NOAA/AVHRR data. IEEE transactions on geo-science and remote sensing 46 (7), 2005-2015.

[46] Genderen, J.L. van and Guan, H.Y., 1997. Environmental Monitoring of Spontaneous Combustion in the North China Coalfields, pp. 5, pp. 24.

[47] Genderen, J.L. van, Cassells, C.J.S. and Zhang, X.M., 1996. The synergistic use of remotely sensed data for the detection of underground fires. International Archives of Photogrammetry and Remote Sensing, Vienna, 9–19 July 1996 (Vienna, Austria: XVIII International Congress for Photogrammetry and Remote Sensing), vol. XXXI, Part B7, pp. 722–727.

[48] Geological Survey of India (GSI), 2004, Coal resource scenario of India (as on 01/01/2004). Available online at: http://www.gsi.gov.in/indiacol.pdf.

[49] Ghosh, S.K., and Mukhopadhyay, A., 1985. Tectonic history of the Jharia basin-an intracratonic Gondwana basin in eastern India. Quarterly Journal of the Geological, Mining and Metallurgical Society of India 57, 33-58.

[50] Gielisch, H. and Kuenzer, C., 2003. Innovative Technologies for Exploration, Extinction and Monitoring of Coal Fires in North China, Work Package 2220-Structural Pattern of the Coal Deposits (Wuda, Rujigou, Gulaben); Analysis of Linear Pattern (Air Photos, Satellite Images), Coal fire research, A sino-german initiative.

[51] Gillespie, A., Rokugawa, S., Matsunaga, T., Cothern, J.S., Hook, S. and Kahle, A.B., 1998. A Temperature and Emissivity Separation Algorithm for Advanced Spaceborne Thermal Emission and Reflection Radiometer (ASTER) Images, IEEE Transactions on Geoscience and Remote Sensing, Vol. 36, No. 4, July 1998.

[52] Gillespie, A., Rokugawa, S., Hook, S.J., Matsunaga, T., and Kahle, A.B., 1999. Temperature/emissivity separation algorithm theoretical basis document, version 2.4, Jet Propulsion Laboratory, Pasadena, CA, Aug. 16, 1996, http://asterweb.jpl.nasa.gov/asterhome/atbd/ATBD-AST-03.doc.

[53] Guan, H., 1989. Applications of remote sensing techniques in coal geology. Acta Geologica Sinica, 2, 253-269.

[54] Guha, A and Kumar, K.V., 2012. Structural controls on coal fire distributions-Remote sensing based investigation in the Raniganj coalfield, West Bengal. Journal of the Geological Society of India, May 2012, Volume 79, Issue 5, pp 467-475.

[55] Guha, A., Kumar, K.V. and Kamaraju, M.V.V., 2008. A satellite-based study of coal fires and open-cast mining activity in Raniganj coalfield, West Bengal, Curr. Sci., v.95, pp.1603–1607.

[56] Gupta, R.P., 2003. Remote Sensing Geology, 2nd Edition, Springer. 656 p., ISBN-13: 978-3540431855.

[57] Gupta, R.P., and Prakash, A., 1998. Reflection aureoles associated with thermal anomalies due to subsurface mine fires in the Jharia Coalfield, India. International Journal of Remote Sensing, 19 (14), 2619-2622.

[58] Huang, J.J., Bruining, J., and Wolf, K.-H., 2000. Modeling of gas flow and temperature fields in underground coal fires. Fire Safety Journal 36, 477-489.

[59] Huang, Y., Huang, H., Chen, W., and Li, Y., 1991. Remote sensing approaches for underground coal fire detection. Proceedings of the International Conference on Reducing of Geological Hazards, 20-25 October, Beijing, pp. 634-641.

[60] Indian Chamber of Commerce (ICC), 2012. The Indian coal sector: Challenges and future outlook, Indian Chamber of Commerce, 2012.

[61] Karmakar, B., GhoshM T., Ojha, K., Pathak, A. K., and Devraju, J., 2013. Effects of chemical composition and petrography of coal for coalbed methane evaluation with special reference to in-situ gas content. 10th Biennial International Conference & Exposition, Kochi 2013.

[62] Knuth, W.M., Fisher, W.J.R. and Stingelin, R.W., 1968. Detection, Delineation and Monitoring of Subsurface Coal Fires by Aerial Infrared Scanning, pp. 877-881 (Pennsylvania, PA: Geographer HRB-Singer, Inc.).

[63] Kolker, A., Engle, M., Stracher, G., Hower, J., Prakash, A., Radke, L., ter Schure, A., and Heffern, E., 2009. Emissions from coal fires and their impact on the environment: U.S. Geological Survey Fact Sheet, 2009-3084, 4p.

[64] Kuenzer, C., Hecker, C., Zhang, J., Wessling, S., Wagner, W., 2008. The potential of multi-diurnal MODIS thermal bands data for coal fire detection. International Journal of Remote Sensing 29, 923–944. doi:10.1080/01431160701352147.

[65] Kuenzer, C., Zhang, J., Li, J., Voigt, S., Mehl, H., and Wagner, W., 2007c. Detection of unknown coal fires: synergy of automated coal fire risk area delineation and improved thermal anomaly extraction, International Journal of Remote Sensing, 28(20), 4561–4585.

[66] Kuenzer, C., Zhang, J., Voigt, S., and Wagner, W., 2007b. Remotely sensed land-cover changes in the Wuda and Rujigou–Gulaben coal mining areas China. In: Stracher, G.B.

(Ed.), Geology of Coal Fires: Case Studies from Around the World: Geological Society of America Reviews in Engineering Geology, v. XVIII, pp. 219–228. doi:10.1130/2007.4118 (14).

[67] Kuenzer, C., Zhang, J., Tetzlaff, A., Voigt, S., Dijk, P.M. van, Wagner, W. and Mehl, H., 2007a. Uncontrolled coal fires and their environmental impacts: Investigating two arid mining environments in north-central China. Applied Geography, 27, pp. 42-62.

[68] Kuenzer, C., Zhang, J.A. and Hirner, A., 2005. Multitemporal coal fire dynamics-combining thermal remote sensing analysis and temperature field mappings to assess coal fire development in Wuda coal mining area. In Proceedings of the 9th International Symposium on Physical Measurements and Signatures in Remote Sensing, ISPMSRS, 7–19 October 2005 Beijing, pp. 805-807.

[69] Kuenzer, C., Strunz, G., Voigt, S. and Wagner, W., 2004. Multitemporal Landcover Investigations in a Semi-arid Mining Environment: Coal Fire Areas in Northern China. In Proceedings of the Conference of the EARSeL Special Interest Group on Land use and Land Cover, Dubrovnik, May 2004, pp. 31-37.

[70] Li-Ding, C., 1999. Environmental problems in a coal mining area affected by coal fires-a case study in Ruqigou Coalfield, Ningxia, China. Environmental Sciences, 11, pp. 23-32.

[71] Lillesand, T. M. and Kiefer, R. W., 2000. Remote Sensing and Image Interpretation, pp. 361, pp. 335-336, pp.533-535.

[72] Mansor, S.B., Cracknell, A.P., Shilin, B.V., and Gornyi, V.I., 1994. Monitoring of underground coal fires using thermal infrared data, International Journal of Remote Sensing 15(8), pp. 1675-1685.

[73] Martha, T.R., Guha, A., Kumar, K.V., Kamaraju, M.V.V., and Raju, E.V.R., 2010. Recent coal-fire and land-use status of Jharia Coalfield, India from satellite data. International Journal of Remote Sensing, 31 (12), 3243-3262.

[74] Martha, T.R, Bhattacharya, A. and Kumar, K.V., 2005. Coalfire detection and monitoring in Raniganj coalfield, India-A remote sensing approach. Curr. Sci., pp.21-24.

[75] Michalski, S.R., 2004. The Jharia mine fire control technical assistance project: an analysis. International Journal of Coal Geology 59 (2004) 83-90.

[76] Michalski, S.R., Custer, E.S., and Munshi, P.L., 1997. Investigation of the Jharia Coalfield Mine Fires-India. Vision 2000, 14th Annual Meeting of the American Society for Surface Miuing and Reclamation Austin, Texas, May 10-16, 1997.

[77] MINENVIS, 2001. Newsletter of the ENVIS Nodal Centre on Environmental Problems of Mining Areas, Centre of Mining Environment, Indian School of Mines, Dhanbad-826 004, Number 29 & 30, June & Sept. 2001.

[78] Mishra, R.K., Roy, P.N.S., Pandey, J., Khalkho. A., and Singh, V.K., 2014. Study of coal fire dynamics of Jharia coalfield using satellite data, International Journal of Geomatics and Geosciences, ISSN 0976-4380, Volume 4, No. 3, 2014.

[79] Mishra, R.K., Bahuguna, P.P., Singh, V.K., 2011. Detection of coal mine fire in Jharia Coal Field using Landsat-7 ETM+ data. International Journal of Coal Geology, 86 (2011) 73-78.

[80] Mukherjee, T.K., Bandopadhyay, T.K. and Pande, S.K., 1991. Detection and delineation of depth of subsurface coalmine fires based on an airborne multispectral scanner survey in a part of the Jharia coalfield, India. Photogrammetric Engineering and Remote Sensing, 57, pp. 1203-1207.

[81] Munshi, P.L. 1995. Experience of dealing with fires in Jharia Coalfield-Introduction to Diagnostic Technique. P. 82-90. National Seminar on Mine Fires. (Varanasi, Feb. 24-25, 1995). Dept. of Mining Engineering, Institute of Technology, Banaras Hindu University.

[82] NRSA, 1996. Coal Mine Fire Mapping Using Aerial Pre-Dawn Thermal IR Data in Jharia Coalileld, Dhanbad District, Bihar. Geosciences Group, National Remote Sensing Agency, Dept. Of Space, Govt. of India, Hyderabad, May 1996.

[83] Pandey J, Mishra R.K., Khalkho A, Singh, R.V.K., and Singh, V.K., 2011. Thermographic Technique-A versatile tool for assessment and monitoring of coal mine fire Jharia coalfields, Mine Tech, 32(3), pp 33-41.

[84] Paul, S. and Chatterjee, R., 2011. Mapping of cleats and fractures as an indicator of in-situ stress orientation, Jharia coalfield, India. International Journal of Coal Geology 88 (2011) 113–122.

[85] Peng, W.X., Genderen, J.L. van, Kang, G.F., Guan, H.Y. and Tan, Y.J., 1997. Estimating the depth of underground coal fires using data integration Techniques, Terra Nova, vol. 9, pp. 180-183.

[86] Prakash, A., Gens, R., Prasad, S, Raju, A. and Gupta, R.P., 2013. Coal Fires in the Jharia Coalfield, India. Book chapter in 'Coal and Peat Fires: A Global Perspective, Volume 2: Photographs and Multimedia Tours', Glenn B. Stracher, Anupma Prakash, Ellina V. Sokol, Elsevier Publ., 2013, pp. 153-177, ISBN No. 978-0-444-59412-9.

[87] Prakash, A. and Gens, R., 2010. Remote sensing of coal fires, in: Stracher, G.B, Prakash, A. and Sokol E.V., (Eds.), Coal and peat fires: A global perspective, Volume 1, Coal - combustion and geology. Elsevier, Oxford, pp. 231-253.

[88] Prakash, A., and Berthelote, A.R., 2007. Subsurface coal-mine fires: Laboratory simulation, numerical modeling, and depth estimation. The Geological Society of America Reviews in Engineering Geology, Volume XVIII.

[89] Prakash, A. and Vekerdy, Z., 2004. Design and implementation of a dedicated prototype GIS for coal fire investigations in North China. In: International journal of coal geology, 59(2004)1-2, pp. 107-119.

[90] Prakash, A., Fielding, E. J., Gens, R., Van Genderen, J. L., and Evans, D. L., 2001. Data fusion for investigating land subsidence and coalfire hazards in a coal mining area. International Journal of Remote Sensing, 22, 921-932.

[91] Prakash, A., Gens, R. and Vekerdy Z., 1999b. Monitoring coal fires using multi-temporal night-time thermal images in a coalfield in North-west China. International Journal of Remote Sensing, 20 (14), 2883-2888.

[92] Prakash, A., and Gupta, R.P., 1999a. Surface fires in Jharia Coalfield, India - their distribution and estimation of area and temperature from TM data. International Journal of Remote Sensing, 20(10), 1935-1946.

[93] Prakash, A., and Gupta, R.P., 1998. Land-use mapping and change detection in a coal mining area - a case study of the Jharia Coalfield, India. International Journal of Remote Sensing, 19 (3), 391-410.

[94] Prakash, A., Gupta, R. P., and Saraf, A. K., 1997. A Landsat TM based comparative study of surface and subsurface fires in the Jharia Coalfield, India. International Journal of Remote Sensing, 18, 2463-2469.

[95] Prakash, A., 1996. Remote Sensing-GIS Based Geoenvironmental Studies in Jharia Coalfield, India, With Special Reference to Coalmine Fires, PhD. Thesis, 1996.

[96] Prakash, A., Saraf, A.K., Gupta, R.P., Dutta, M. and Sundaram, R.M., 1995b. Surface thermal anomalies associated with underground fires in Jharia Coal Mine, India. International Journal of Remote Sensing, 16(12), 2105-2109.

[97] Prakash, A., Sastry, R. G. S., Gupta, R. P., and Saraf, A. K., 1995a. Estimating the depth of buried hot feature from thermal IR remote sensing data: a conceptual approach. International Journal of Remote Sensing, 16, 2503-2510.

[98] Quattrochi, D.A., Prakash, A., Evena, M., Wright, R., and Hall, D.K., 2009. Thermal Remote Sensing: Theory, Sensors, and Applications. in Manual of Remote Sensing 1.1:

Earth Observing Platforms & Sensors, volume ed. Mark Jackson, ASPRS, 550 p. ISBN: 1-57083-086-X.

[99] Rabchexsky, G.A., 1972. Determination from available satellite and aircraft imagery of the applicability of remote sensing techniques to the detection of fires burning in abandoned coal mines and unmined coal deposits located in North Central Wyoming and Southern Montana. In U.S. Department of Interior, Bureau of Mines, Prepared by Allied Research Associates Inc., Contract No. SO 211087, Final Report No. 8G86-F, 21 pp.

[100] Raju, A., Gupta, R.P., and Prakash, A., 2012. Delineation of coalfield surface fires by thresholding Landsat TM-7 day-time image data, Geocarto International, vol. 28, issue 4, pp. 343-363.

[101] Reddy, C.S.S., Srivastav, S.K. and Bhattacharya, A., 1993, Application of thematic mapper short wavelength infrared data for the detection and monitoring of high temperature related geoenvironmental features, International Journal of Remote Sensing, Vol. 14, pp.3125- 3132.

[102] Rosema, A., Guan, H., van Genderen, J.L., Veld, H., Vekerdy, Z., Ten Katen, A.M., and Prakash, A., 1999. Manual of coal fire detection and monitoring. Report of the Project 'Development and implementation of a coal fire monitoring and fighting system in China'. Netherlands Institute of Applied Geoscience, Utrecht, NITG 99-221-C, ISBN 90-6743-640-2, 245 pp.

[103] Rosema, A., Van Genderen, J. L., and Schalke, H.J.W.G., 1995, Environmental monitoring of coal fires in north China. Project Identification Mission Report, BCRS 93-29, ISBN 90 5411 1054, 24 p.

[104] Saraf, A.K., Prakash, A., Sengupta, S. and Gupta, R.P., 1995. Landsat-TM data for estimating ground temperature and depth of sub-surface coal fire in the Jharia coalfield, India. International Journal of Remote Sensing, 16, pp. 2111-2124.

[105] Schmal, D., 1987. A model for the spontaneous heating of stored coal. PhD thesis, Delft University of Technology.

[106] Schmugge, T., French, A., Ritchie, J. C., Rango, A., and Pelgrum, H., 2002. Temperature and emissivity separation from multispectral thermal infrared observations. Remote Sensing of Environment 79:189-198.

[107] Sengupta, N., 1980. A revision of the Geology of the Jharia Coalfield with particular reference to distribution of coal seams. Ph.D. Thesis, Indian School of Mines, Dhanbad.

[108] Singh, R.V.K., 2013. Spontaneous heating and fire in coal mines. Procedia Engineering 62 (2013) 78-90.

[109] Singh, R.V.K. and Singh, V. K., 2009. Status of Mine Fire of Jharia Coalfield and Suggestions for Prevention and Control, National Seminar on Reinventing Jharia Coalfield, MGMI, Dhanbad Chapter, Aug. 2009.

[110] Sinha, P.R., 1986, Mine fires in Indian coalfields. Energy, 1-12, pp. 1147-1154.

[111] Stracher, G.B., Prakash, A., Schroeder, P., McCormack, J., Jhang, X., van Dijk, P.M. and Blake, D., 2005. New mineral occurrences and mineralization processes: Wuda coal-fire gas vents of Inner Mongolia, American Mineralogist, Volume 90, pages 1729.1739, 2005.

[112] Stracher, G.B. and Taylor T.P., 2004. Coal fires burning out of control around the world: thermodynamic recipe for environmental catastrophe. International Journal of Coal Geology. 59, 7-18.

[113] Tetzlaff, A., Zhukov, B., Hirner, A., Kuenzer, C., and Voigt, S., 2005. Coal fire quantification and detection using the DLR experimental bi-spectral infrared detection (BIRD) small satellite. Small Satellites for Earth Observation - Selected Proceedings of the 5th International Symposium of the International Academy of Astronautics, Berlin 4-8, 2005, H.-P. Röser, R. Sandau, A. Valenzuela (eds.), ISBN: 3-11-018851-1, V, pp. 255-262.

[114] Tetzlaff, A., 2004, Coal fire quantification using Aster, ETM and BIRD satellite instrument data. Ph.D thesis at the Ludwig Maximilians University Munich, Germany, 155 pp.

[115] Thome, K., Biggar, S., and Slater, P., 2001. Effects of assumed solar spectral irradiance on intercomparisons of earth-observing sensors. In Sensors, Systems, and Next-Generation Satellites. (Proceedings of SPIE Vol. 4540, pp 260-269, H. Fujisada, J. Lurie, and K. Weber, Eds., December 2001).

[116] Thome, K., Palluconi,F., Takashima,T. and Masuda,K., 1998. Atmospheric correction of ASTER, IEEE Transactions on Geoscience and Remote Sensing, 36, 1199-1211.

[117] USGS LP DAAC (Land Processes Distributed Active Archive Centre) archive (https://lpdaac.usgs.gov/data_access)

[118] Vekerdy, Z., and Genderen, J.L. van, 1999b. CoalMan–information system for the monitoring of subsurface coal fires and the management of fire fighting in coal mining areas. Proceedings of the Geoinformatics: Beyond 2000, 9-11 March 1999, IIRS, India (India: IIRS), pp. 179-184.

[119] Vekerdy, Z., Prakash, A., and Gens, R., 1999a. Data integration for the study and visualisation of subsurface coal fires. Proceedings of the 13th International Conference on Applied Remote Sensing, 1-3 March 1999, Vancouver, Canada, pp.II, 150-51.

[120] Voigt, S., Tetzlaff, A., Zhang, J., Künzer, C. Zhukov, B., Strunz, G., Oertel, D. Roth, A., Dijk, P.M. van, and Mehl, H., 2004. Integrating satellite remote sensing techniques for detection and analysis of uncontrolled coal seam fires in North China, International Journal of Coal Geology, 59 (1-2), 121-136.

[121] Walker, S., 1999. Uncontrolled fires in coal and coal wastes. International Energy Agency, IEA on coal Research, UK.

[122] Wang, C., 2002. Detection of coal fires in Xinjiang (China) using remote sensing techniques. Unpublished Masters Thesis, International Institute for Geo-Information Science and Earth Observation, Enschede, The Netherlands.

[123] Wessling, S., Kuenzer, C., Kessels, W., and Wuttke, M.W., 2008b. Numerical modeling for analyzing thermal surface anomalies induced by underground coal fires. International Journal of Coal Geology74, 175-184.

[124] Wessling, S., Kessels,W., Schmidt, M., and Krause, U., 2008a. Investigating dynamic underground coal fires by means of numerical simulation. Geophys. J. Int. 172 (1), 439-455. doi:10.1111/j.1365-246X.2007.03568.x.

[125] Whitehouse, A.E. and Mulyana, A.A.S., 2004. Coal fires in Indonesia. International Journal of Coal Geology. 59, 91-97.

[126] Wolf, K.-H., and Bruining, H., 2007. Modelling the interaction between underground coal fires and their roof rocks.Fuel 86, 2761-2777.

[127] Yang, B., Chen, Y., Li, J., Gong, A., Kuenzer, C. and Zhang, J., 2005. Simple normalization of multi-temporal thermal IR data and applied research on the monitoring of typical coal fires in Northern China. In Proceedings of the Geoscience and Remote Sensing Symposium, IGARSS 25-29 July 2005, Volume 8, pp. 5725–5728.

[128] Yaobao, M., 2010. Research on Hyperspectral Quantitative Remote Sensing Detection of the Rujigou Coal Fire Area in Ningxia, Remote Sensing For Land & Resources, Issue 3, Page 69-75.

[129] Zha, Y., Gao, J. and Ni, S., 2003. Use of normalized difference built-up index in automatically mapping urban areas from TM imagery. International Journal of Remote Sensing, 24(3), 583-594.

[130] Zhang, J., Kuenzer, C., Tetzlaff, A., Oertel, D., Zhukov, B. and Wagner, W. 2007b. Thermal characteristics of coal fires 2: Results of measurements on simulated coal fires. Journal of Applied Geophysics 63 (3), 135-147.

[131] Zhang, J. and Kuenzer, C., 2007a. Thermal surface characteristics of coal fires 1: Results of in- situ measurements. Journal of Applied Geophysics 63 (3-4), 117–134.

[132] Zhang, J., Wagner, W., Prakash, A., Mehl, H., and Voigt, S., 2004. Detecting coal fires using remote sensing techniques. International Journal of Remote Sensing, 25: 16, 3193-3220.

[133] Zhang, X., Kroonenberg S.B. and de Boer, C.B. 2004b. Dating of coal fires in Xinjiang, north-west China. doi: 10.1111/j.1365-3121.2004.00532.x. Terra Nova, Vol 16, No. 2, 68–74.

[134] Zhang, X., Zhang, J., Kuenzer, C., Voigt, S. and Wagner, W., 2004a. Capability evaluation of 3-5mm and 8-12, 5mm airborne thermal data for underground coalfire detection. In International Journal of Remote Sensing, 25, pp. 2245-2258.

[135] Zhang, X., Kroonenberg, S.B. and Genderen, J.L. van, 2003. Spatial analysis of thermal anomalies from airborne multispectral data. Int. J. Remote Sensing, 24, 3727–3742.

[136] Zhang, X., Cassells, C.J.S. and Genderen, J.L. van, 1999. Multi-sensor data fusion for the detection of underground coal fires. Geol. Mijnb., 77, 117–127.

[137] Zhang, X., 1998. Coal Fires In Northwest China, Detection, Monitoring, and Prediction Using Remote Sensing Data. Unpublished PhD Thesis, International Institute for Geo-Information Science and Earth Observation, Enschede, The Netherlands.

[138] Zhang X., Genderen J.L. van and Kroonenberg S.B., 1997. A method to evaluate the capability of landsat-5 TM band 6 data for sub-pixel coal fire detection. International Journal of Remote Sensing 18: 3279-3288.

[139] Zhao, H.M. and Chen, X. L., 2005. Use of normalized difference bareness index in quickly mapping bare areas from TM/ETM+, Geoscience and Remote Sensing Symposium, 3 (25-29), 1666-1668.

PUBLICATIONS

[1] **Ashwani Raju**, Ravi P. Gupta & Anupma Prakash, 2013: Delineation of coalfield surface fires by thresholding Landsat TM-7 day-time image data, Geocarto International, vol. 28, issue. 4, pp. 343-363.

[2] Anupma Prakash, Rudiger Gens, Sheochandra Prasad, **Ashwani Raju**, Ravi P. Gupta, 2013: Coal Fires in the Jharia Coalfield, India, book chapter in 'Coal and Peat Fires: A Global Perspective, Volume 2: Photographs and Multimedia Tours', Glenn B. Stracher, Anupma Prakash, Ellina V. Sokol, Elsevier, 2013.